Quantum State Transfer in Spin Chains

Analia E. Zwick

Presentado ante la Facultad de Matemática, Astronomía y Física

como parte de los requerimientos para acceder al grado de

Doctor en Física

de la

Universidad Nacional de Córdoba

Director: Dr. Omar Osenda

ii

A Gon,

por TODO.

Y por mucho mas.

Pacs

Palabras claves

Resumen

El procesamiento de la información cuántica ha sido un área intensamente estudiada durante los últimos años. Uno de los principales desafíos a sortear en las posibles implementaciones de dicha tecnología es la manipulación de la información cuántica con suficiente precisión para poder prevenir errores. En particular, esto es importante para poder transferir información entre los distintos elementos de una computadora cuántica. Con este motivo, las cadenas de espines cuánticos han sido propuestas como canales para la transmisión de estados. En esta tesis, estudiamos la confiabilidad y robustez de estos canales cuánticos frente a la acción de posibles perturbaciones, presentes en una eventual implementación experimental.

Contents

Contents

Resumen

El procesamiento de la información cuántica ha sido un área extensamente estudiada durante los últimos años. Uno de los principales desafíos a sortear en las posibles implementaciones de dicha tecnología es la manipulación de la información cuántica con suficiente precisión para poder prevenir errores. En particular, esto es importante para poder transferir información entre los distintos elementos de una computadora cuántica. Con este motivo, las cadenas de espines cuánticos han sido propuestas como canales para la transmisión de estados. A partir de dicha propuesta, estos sistemas han sido estudiados a fin de mejorar su rendimiento para la transmisión de estados. Uno de los principales objetivos es encontrar sistemas donde sea posible transferir estados sin ningún tipo de control durante la transferencia o con sólo mínimos requerimientos para de esta manera evitar la introducción de errores. Pero aún en estos sistemas, perturbaciones estáticas producidas por imperfecciones en la fabricación del canal modifican las interacciones entre los espines. Por otro lado, la interacción con el medio ambiente también puede degradar la calidad de la transferencia.

Es por esto que consideramos que una buena caracterización sobre la confiabilidad y robustez de estos canales cuánticos debe hacerse considerando la acción de dichas perturbaciones, presentes en una eventual implementación. Este es el tema de investigación de esta tesis.

Primero, introducimos las ideas básicas sobre información cuántica y los elementos necesarios para realizar y caracterizar la transferencia de estados en cadenas de espines. A continuación, estudiamos las propiedades de cadenas de espines con acoples homogéneos en los cuales controlamos los acoples de los espines de ambos extremos y determinamos las condiciones óptimas para transmitir estados rápidamente y con gran fidelidad. Luego, estudiamos cadenas de espines donde cada acoplamiento ha sido diseñado exclusivamente para lograr una transmisión perfecta. Consideramos a estos sistemas bajo la influencia de desorden estático y determinamos las propiedades que los hacen robustos para la transferencia. Por último, comparamos a ambos tipos de cadenas de espines, con los acoples de los bordes controlados y con los acoples completamente diseñados, bajo la acción de diferentes tipos de desorden estático y

Resumen

determinamos que cadenas, y bajo que condiciones, son las mas robustas para la transferencia de estados.

Abstract

Quantum information processing has been extensively studied during the past years. One of the main challenges of actual physical implementations has been the manipulation of the quantum information with sufficient accuracy to prevent errors. In particular it is important to be able to transfer quantum information between different elements of a quantum computer. In this respect, spin chain systems have been proposed as quantum channels for the transmission of quantum states, where the spins-$\frac{1}{2}$ act as the quantum bits. From this proposal, these systems have been studied to improve their performance for the transmission of states. One of the main goals is to find systems where states can be transferred without any control during the transfer procedure or with only minimal control requirements to thereby prevent the introduction of errors. But even in these systems, static perturbations, due to imperfections in the manufacture of the channel, modify the interactions between the spins. Furthermore, the interaction with the environment can also degrade the quality of the transfer.

That is why we consider that a complete characterization of the reliability and robustness of these quantum channels should take into account the action of such perturbations, present in a possible implementation. This is the research topic of this thesis.

First, we introduce the basic ideas about quantum information and the necessary elements to achieve and to characterize the transfer of spin states in chains. Then we study the properties of boundary-controlled unmodulated spin chains and we determinate the optimal conditions to transfer a quantum state quickly and with high fidelity. Afterwards, we study spin chains where each coupling, has been specifically designed to achieve a perfect transmission. We consider these systems under the influence of static disorder and we determine the properties that make them robust for the transfer. Finally, we compare these two classes of qubit chains, boundary-controlled and fully engineered spin chains, against different models of static disorder and we determine under which conditions they are most robust for state transfer.

Abstract

Agradecimientos

Tengo tanta tanta gente a la que agradecer... a Gon, a la hermosa y genial familia que tengo, a los amigos, amigos, amigos y AMIGOS! a los colegas y compañeros tanto del GTMC como del FaMAF, a... la lista es interminable! son tantos los que me dieron vida y sonrisas día tras día para estar hoy donde estoy, que seguramente sería injusta con muchos al tratar de hacer un agradecimiento explícito.... Así que, a todos aquellos que de una u otra manera contribuyeron a que hoy este culminando este trabajo:
GRACIAS!!!!!

Agradezco también a las instituciones que me brindaron el espacio físico para el desarrollo de este trabajo, al FaMAF y a TU Dortmund, y a las que me brindaron el apoyo económico, el CONICET y el DAAD.

Y en especial quiero agradecer a los que están directamente relacionadas con la investigación presentada en esta tesis: mi director Omar Osenda y codirectores-colegas Joachim Stolze y Gonzalo A. Alvarez. Ellos han sido un pilar fundamental en mi formación como física. Me han enseñado y dado muchísimo. Y siempre con mucha paciencia, predisposición, motivación y alegría. De cada uno he aprendido distintas, fascinantes y enriquecedoras formas de ver, pensar y sentir la física; y con todas ellas he crecido. He disfrutado a pleno esta experiencia y crecimiento, así que una vez mas
GRACIAS POR TODO!!!

1 Introduction

'I can't believe that!' said Alice.
'Can't you?' the Queen said in a pitying tone.
'Try again: draw a long breath, and shut your eyes.'
Alice laughed. 'There's no use trying,' she said;
'one cannot believe impossible things.
''I daresay you haven't had much practice,' said the Queen.
'When I was your age, I always did it for half-an-hour a day.
Why, sometimes I've believed as many as six impossible things before
breakfast.'

Lewis Carroll, Through the Looking Glass

We live in the digital communication era. The fast development of new technologies has brought deep socio-cultural changes in the whole world. In just few years, it has been possible to go from enormous and extremely expensive calculation machines to portable computers, mobile phones, extraordinary devices applied to medicine and a huge variety of electronic tools which are really accessible and already part of our daily lives. Now, people are constantly using digital devices to communicate, connect and interact with each other, to access detailed information on any topic from anywhere on the world.

All of this is the product of the prompt and constant miniaturization of the electronic technology which allows more and more storage capability, faster interchange and processing of digital information.

The trend of this size reduction of the electronic components (as the transistors in integrated circuits) follows Moore's law predicted by Gordon Moore strikingly in 1965 [74]. It implies that in really few years the smaller electronic components will leave the classical realm to enter in the quantum one such as it is shown in Fig. 1.0.1. And, it is here, where comes the *quantum computer*, referring to any device that processes information in a *quantum physical system*. But, to develop effectively quantum processors, we need first to rethink the way to manipulate the information there since the behavior, described by the classical or quantum physical laws, changes drastically. This change entails amazing and profitable consequences, but also huge challenges related with the control and implementations.
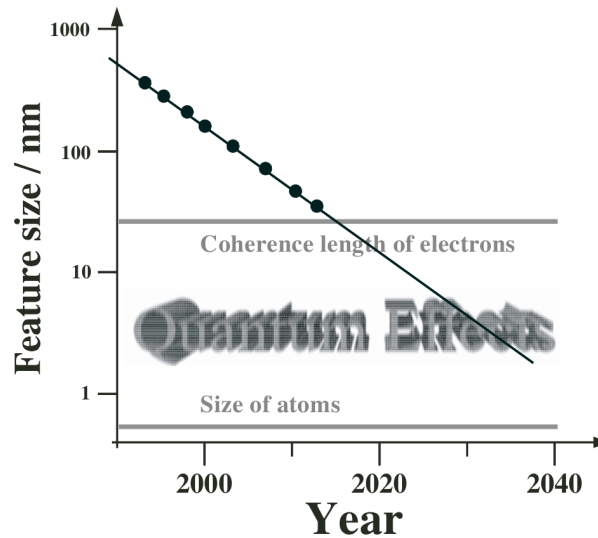
Figure 1.0.1: Predicted evolution of feature size in microelectronic circuits. The data source is international semiconductor association road map (Stolze and Suter 2008 [99]).

One of the great potentialities of a quantum computer is its capability to do parallel processing. This feature can decrease exponentially the calculation time normally required in a classical computer. That means, quantum computers can solve problems that classical computers can not in a practical time!! One relevant example is the factorization of large numbers (see Fig. 1.0.2) which seriously compromises the actual system of information cryptography. Another one, is the quantum simulation, an idea stated by Richard Feynman in 1982 [44], which is of great relevance in many scientific studies.

Knowing these potentialities from the eighties, why do we not have already personal quantum computers? The drawback was already stated at the beginning of these ideas

> *"I want to build a billion tiny factories, models of each other, which are manufacturing simultaneously... The principles of physics, as far as I can see, do not speak against the possibility of maneuvering things atom by atom. It is not an attempt to violate any laws; it is something, in principle, that can be done; but in practice, it has not been done because we are too big."*

Richard P. Feynman (1959 fragment of a talk [43]) - 1965 Nobel prize in Physics.

A quantum system are particles described by *states* of a *Hilbert space*, whose dimension grows exponentially with the number of particles that compose it. System interactions are described by a *Hamiltonian* defined by a set of unitary operators, that in this context are usually called *quantum gates*; and the system dynamics is given by Schrödinger equations. From all this, a quantum computer is made of. Thus, to perform a given computation or task there, we must design the system interactions, as well as programming it, to obtain the desired Hamiltonian that under the dynamical process will yield the awaited result.

Therefore, to build a quantum computer, it is indispensable to control with high accuracy the interactions and dynamical behavior of a large number of microscopic quantum physical systems. The main impediment to achieve this is the vulnerability of quantum systems against perturbations which cause the loss of quantum information (*ie.*, decoherence/dissipation [118]). Disturbances on the system have, mainly, a twofold origin. One is the interaction of the particles with their surrounding environment which is normally a larger physical system with several degrees of freedom, and the other one is the noise from imperfections introduced in the engineering design process. For this reason, finding systems that allow to manipulate quantum information without any dynamical control during the procedure to achieve the desired computation or task, or with only minimal additional requirements is important for making quantum computation feasible. But not only that, they must be robust and stable against eventual and unvoided perturbations.
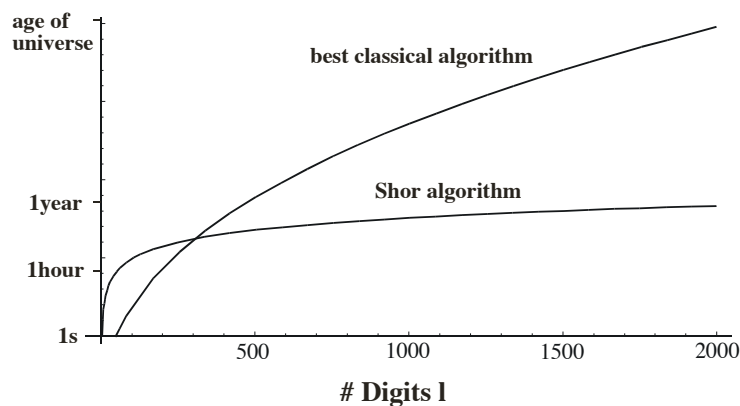

Figure 1.0.2: Comparison between the time complexity required for classical factorization algorithm and quantum algorithm (Stolze and Suter 2008 [99]).

One of the main building blocks to build a scalable and powerful quantum computer, is the ability to communicate between their different components, such as quantum processors, memories or registers. This communication is essential to transfer information, and also, to distribute and generate entangled states of spatially distant particles, *ie.* having non-local correlation between different parts. Entanglement [6] is another amazing and powerful aspect of the quantum systems which allows, inter alia, quantum teleportation [14, 17] and quantum dense coding [13]. From these ideas and the necessity of communication, emerge the concept of *quantum channels*, linear systems through which two parties communicate and transmit information from one place to another.

A promising class of systems in condensed matter to serve as reliable quantum channels are the *spin chains* [15, 82, 18, 80, 61, 85, 25, 16]. Information transfer along spin chains is possible even without any designing of interactions between spins, but they do it with a reliable fidelity only for up to really few spins [15]. However, the transfer through longer chains can be considerably improved by designing the Hamiltonian [1, 109, 55, 47, 87] or by performing local or global gates or applying external fields that allow to manipulate the dynamical process [45, 46, 22, 21, 91, 57, 72, 111]. For example, by an adequate engineering of the spin coupling strength interactions, the information is, after some time, perfectly transferred through chains of any length [1, 29, 30, 60, 61, 62]. Since systems of this last kind do not require any dynamical control, they are supposed to be more isolated from the environment, *ie.* more protected from decoherence; they thus seem to be a great option to implement experimentally as channels for transmission. But, on the other hand, designing each of the interactions between the spins require a hardly possible accuracy, opening the possibility for many random static imperfections to seriously damage the information [28, 62, 93]. This demonstrates that it is extremely important to consider several aspect before deciding which channel is best for information transfer.

In this thesis we precisely investigate the reliability and robustness of some promising systems as quantum channels, focusing on the decisive task of transmitting quantum information. Some initial questions from where our research emerges are: Which are the best channels to transfer quantum information with minimal control and requirements? How do perturbations affect them? Which are the necessary conditions to achieve and improve the transfer? Which channels for transmission are most robust against perturbations? The intention of this investigation is to shed light on these questions through a theoretical work going one step further to reduce the gap between what is

conceivable theoretically and what is possible experimentally.

1.1 Thesis outline and research contributions

All of the subjects aforementioned and many others, are part of the emergent fields of quantum information and quantum computation. The basics of these theories will be presented in the following **chapter 2**, we review some basic concepts of quantum mechanics too. We will raise briefly only those aspects that we use later in the writing. More detail about these topics can be found in [99, 77, 48, 12, 52, 89].

Then, in the following chapters we focus on our research contributions.

In **chapter 3**, first of all, we look for the intrinsic physical properties that allow to improve the state transfer along a spin chain system. In an attempt to minimize the requirements of control or tailoring interactions, and to avoid the introduction of errors and consequent loss of information, we consider a boundary controlled coupling in a homogeneous spin channel to analyze the localization of the eigenstates of the system and their bipartite entanglement. We distinguish regimes well characterized by the strength of the boundary coupling. We analyze the dynamical behavior of the transfer of one state between the channel ends by calculating the localization of the chain state. The effects observed allow us to distinguish interesting behaviors and regimes for state transfer, both closely related with the eigenstate localization. Then, we consider symmetrical boundary-controlled couplings to implement a protocol of state and entanglement transfer. We find an optimal regime for transmission given by an optimal boundary coupling which we determine for any chain length. This regime is efficient in the transmission because it transfers the state relatively fast with a high fidelity.

In **chapter 4**, we consider different fully engineered spin chains to perform perfect state transfer, without requiring any dynamical control. We characterize them by their energy spectrum. Then we obtain their corresponding spin couplings, by solving the inverse eigenvalue problem. Afterwards, we analyze their performance in the state transfer by calculating numerically the fidelity of the transfer. Following on, we consider random static perturbations in the spin coupling strengths and we evaluate how they affect the fidelity of transfer. We show how some of these chains are strongly affected by the perturbations; and last, we analyze and determine which general properties of the chains make them more robust against static perturbations and timing errors.

In **chapter 5** we compare the performance for state transfer of the most robust system for perfect state transfer, characterized in the previous chapter, with boundary controlled systems such as those considered in Chap. **3**. We find similarities between both kinds of systems, stressing that the latter are more feasible for a practical implementation than the former, since they do not demand a huge control or engineering design. We calculate and analyze the transfer fidelity under two different models of static disorder. We conclude that to determinate which systems are more robust it is necessary to contemplate the kind and strength of perturbation. However, we show that in most situations the transmission performance of boundary-controlled spin chains renders the full engineering of the couplings of a spin chain unnecessary in order to obtain quantum state transmission with high fidelity under static perturbations.

Finally, the conclusion and outlook are in **chapter 6**, where we discuss about our current research, including some preliminary results.

The research done involves both analytical and numerical calculation. For the latter ones, I have developed all the necessary codes with Fortran.

Most of the results were published [119, 120, 121] and others are included in an article in preparation. These works were developed in the Universidad Nacional de Córdoba under the direction of my advisor Omar Osenda, and in the Technische Universität Dortmund, during my research stays there, under the co-direction and collaboration of Joachim Stolze and Gonzalo A. Alvarez.

2 Quantum Information Theory

"What're quantum mechanics?"
"I don't know. People who repair quantums, I suppose."
Terry Pratchett, Eric

Information is physical and its storage, transmission and processing can only be done by physical means. Digital information is coded in a binary system represented by 0 and 1, which is called bit. In electronic devices, these two possible values are distinguished by voltages (electrical potential difference), assigning low voltage to the state 0 and high voltage to 1. Since the voltage is a continuous variable, a criterion to distinguish low and high voltage must to be chosen depending on the device design.

In a similar way, two distinguishable states are chosen at the quantum scale to represent a **qubit**, the unit of quantum information. In the quantum realm, there are physical properties which take only discrete values. So, the more typical qubits are the spin-$\frac{1}{2}$ of some particles such as electrons (the spin can be up or down, *ie.* 0 or 1), or the photon polarization (it can be vertical or horizontal).

At this point, nothing seem to be different from the classical representation. The main difference between classical and quantum information emerges with the particularity of the quantum states of being a superposition of these distinguishable and discrete values! They are not necessarily 0 or 1, they can use simultaneously both possibilities.

Feynman [44], Deutsch [35], inter alia, realized that the quantum mechanics have features to exploit in terms of information, such as, the superposition of states which give the possibility to do calculation in parallel that allows to increase amazingly the calculation power. This brought about, suddenly and with a great repercussion, all the disciplines, theoretical and experimental, related with a quantum theory of information.

2.1 The basics of quantum computation and quantum mechanics

Qubit and quantum states

The quantum states are described by vectors in a Hilbert space. In this way, the states of a qubit lie in the Hilbert space $\mathcal{H}$ of two-dimensional vectors, and can be expressed as superpositions of the two orthogonal computational states $|0\rangle = \begin{pmatrix} 1 \\ 0 \end{pmatrix}$ and $|1\rangle = \begin{pmatrix} 0 \\ 1 \end{pmatrix}$:

$$|\psi\rangle = \alpha|0\rangle + \beta|1\rangle, \tag{2.1.1}$$

where α and β are complex numbers which satisfy $|\alpha|^2 + |\beta|^2 = 1$. In a geometrical representation, a classical bit lies in two points, while the qubit lies in the so called Bloch sphere (see Fig. 2.1.1). Despite that the information is codified in a superposition of states, to any measurement, the qubit behaves like $|0\rangle$ or $|1\rangle$ with probability $|\alpha|^2$ or $|\beta|^2$.
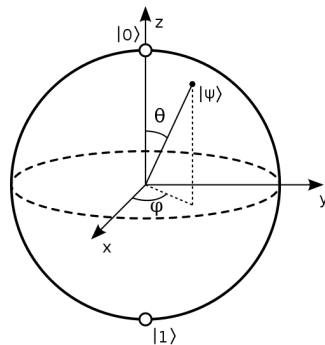
Figure 2.1.1: The Bloch sphere is a representation of a qubit state $|\psi\rangle = \alpha|0\rangle + \beta|1\rangle$ where $\alpha = cos\frac{\theta}{2}$ and $\beta = e^{i\phi}sin\frac{\theta}{2}$.

This graphic qubit representation is useful to to visualize and distinguish *mixed* and *pure* states: A quantum state, with a vector $\overrightarrow{V}$ in the Bloch sphere, is pure when $\left|\overrightarrow{V}\right| = 1$ and mixed, when $\left|\overrightarrow{V}\right| < 1$.

The general representation of a state is by its *density matrix* ρ[1]. In these terms, a state is pure when $\rho = \rho^2$, otherwise it is mixed. Since the Pauli

---

[1] *Density matrix properties:*$\rho = \rho^\dagger$ *is self-adjoin, so ρ has real eigenvalues, $\rho > 0$ is positive-definite, $Tr\rho = 1$.*

matrices[2] $\overrightarrow{\sigma} = \{\sigma^x, \sigma^y, \sigma^z\}$, together with the identity $\mathbb{I}$, are a basis for the matrix 2×2 space; the density matrix ρ_q of a qubit can be expressed as

$$\rho_q = \frac{1}{2}\left(\mathbb{I} + \overrightarrow{V} \cdot \overrightarrow{\sigma}\right).$$
(2.1.2)

Two states can be totally unambiguously only if they are orthogonal to each other [77]. A measure used to characterize the similarity between two states, namely ρ and σ, is the *fidelity*[3] [104, 59, 77]

$$F(\rho, \sigma) = \left(Tr\sqrt{\sqrt{\sigma}\rho\sqrt{\sigma}},\right)^2,$$
(2.1.3)

which is a real function with values between $[0, 1]$, meaning $F = 1$ when both states are equal, $\rho = \sigma$. In case that both states are pure, $\rho = |\psi\rangle\langle\psi|$ and $\sigma = |\phi\rangle\langle\phi|$, the fidelity is the projection between them

$$|\langle\psi|\phi\rangle|^2.$$
(2.1.4)

Hamiltonian and time evolution of a quantum state

The interactions between spins are described in terms of spin operators, the Pauli matrices. The *Hamiltonian* of the system is the operator that includes all of the interactions that affect the system, *ie.* interactions between the spins and external interactions such as the action of external magnetic fields. Since the state of a system of N spins is represented by vectors in a Hilbert space of dimension 2^N; the matrix representation of the Hamiltonian is of dimension $2^N \times 2^N$. The Hamiltonian's eigenvalues E_i, are the energies of the system, and the eigenstates $|\Psi_i\rangle$ are the stationary states that satisfy

$$H|\Psi_i\rangle = E_i|\Psi_i\rangle.$$
(2.1.5)

The total state of the system, $|\psi\rangle$, evolves in time under the interaction of the Hamiltonian follows the Schrödinger equation

---

[2]Also called Pauli operator: $\sigma^x = \begin{pmatrix} 0 & 1 \\ 1 & 0 \end{pmatrix}, \sigma^y = i\begin{pmatrix} 0 & -1 \\ 1 & 0 \end{pmatrix}, \sigma^z = \begin{pmatrix} 1 & 0 \\ 0 & -1 \end{pmatrix}$. Some properties of Pauli matrix: $Tr\sigma = 0$, $det\sigma = -1$, $\left[\sigma^i, \sigma^j\right] = 2i\sigma^k \in_{ijk}$.

[3]In some sources, the fidelity is also defined without the square.

$$i\hbar\frac{d|\psi(t)\rangle}{dt} = H|\psi(t)\rangle, \tag{2.1.6}$$

where $\hbar$ is the Planck constant[4]. Therefore, given an initial state of the system, $|\psi(t=0)\rangle$ we obtain the state for any time solving

$$|\psi(t)\rangle \;=\; e^{-i\frac{Ht}{\hbar}}|\psi(0)\rangle, \tag{2.1.7}$$

where $e^{-i\frac{Ht}{\hbar}}$ is the time evolution operator that usually is expressed in terms of its spectral decomposition

$$e^{-i\frac{Ht}{\hbar}} \;=\; \sum_i e^{-i\frac{E_i t}{\hbar}}|\Psi_i\rangle\langle\Psi_i|. \tag{2.1.8}$$

Quantum gates

Quantum gates acting on qubits are unitary operations $\mathbb{U}$[5]. Any quantum algorithm and computation can be expressed in terms of quantum gates of one and two qubits. The action of quantum gates on single qubits may be perceived as rotations in the Bloch sphere. Such rotations can be experimentally implemented [105], for example, by radio frequency pulses acting on nuclear spins in presence of a static magnetic field or by wave plates acting on polarized photons.

Implementation of a quantum computer

After defining the basic elements of quantum computing, qubits and quantum gates, the following step is the implementation of a quantum computer device. The requirements for a successful implementation of a quantum computer are known as DiVincenzo's criteria [37]:

1. *A scalable physical system with well characterized qubits*
   Well defined qubits are the two level systems, *ie.* systems with two eigenstates of a quantum operator, such as the electron spin. Other option to define qubits are two specific levels of a larger group of eigenenergies.

2. *The ability to initialize the state of the qubits to a simple fiducial state, such as $|00...0>$*

---

[4]in the following we consider as $\hbar = 1$
[5]$\mathbb{U}\mathbb{U}^\dagger = \mathbb{U}^\dagger\mathbb{U} = 1$

A pure state of an N-body system is, by no means, trivially attainable. Most usually, the initial state to be prepared can be approximately obtained by lowering the temperature of the system, using laser cooling or other similar tools. Another way to initialize the state is by applying non-demolition measurements. In NMR, effective pure states can be initialized at relative high temperatures.

3. *Long relevant decoherence times, much longer than the gate operation time*
   This refers to the need to have stable states for relative long times to avoid the energy decay or the losses of the quantum coherence due to the inevitable interaction with the environment.

4. *A universal set of quantum gates*
   This refers to the ability to implement quantum gates on one-and two-qubit. It has been shown that with a finite set of one-and two-qubits gates, it is possible to implement any unitary operation of N qubits efficiently. So, any Hamiltonian evolution of a system of N qubits can be obtained applying successively just one and two qubits gates. Examples of this are the implementations of the quantum factorization algorithm (or Shor's algorithm) and Grover's search algorithm.

5. *A qubit-specific measurement capability.*

Figure 2.1.2: A quantum computer follows the Schrödinger equation. The Schrödinger cat commemorates the *gedanken* experiment to prove the superposition principle.

2.1.1 The Potential and Power of Quantum Computing

Quantum parallelism

While the information codified in n-classical bits is stored in a string of 0 and 1 (such as $x = \overbrace{00110...10}^{n}$), the information codified in n-qubits is stored in a superposition of the 2^n quantum orthogonal states[6]. Then, a logical operation acting on the quantum superposition allows to perform 2^n operations in parallel. To obtain such results in classical computers, it is necessary to repeat the same operation on each one of the 2^n possible strings. Quantum parallelism make the quantum computer faster and highly efficient compared to classical computers, see graphic representation in Fig. 2.1.3.
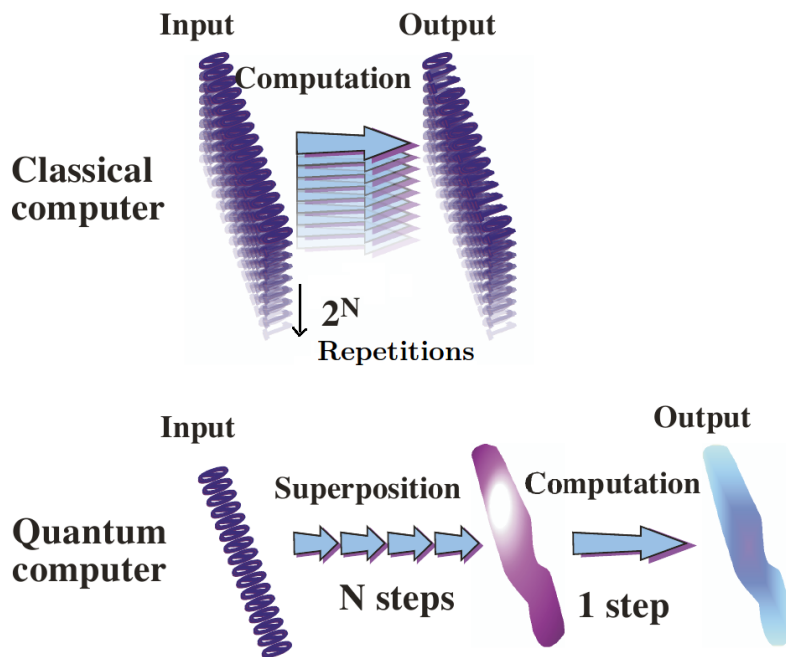

Figure 2.1.3: The quantum parallelism is a potential advantage of quantum algorithms over the classicals (Stolze and Suter 2008 [99]).

---

[6]Superposition of the 2^n quantum orthogonal states: $|\psi\rangle = \sum\limits_{x=00..0}^{11...1} a_x |x\rangle$ where $|x\rangle = |x_1 x_2...x_n\rangle$ and a_x is a complex number with $\sum\limits_{x} |a_x|^2 = 1$.

Entanglement

It is the most wonderful and counter-intuitive feature of quantum states. Some times, particles interact creating a lasting bond beyond the physical distance. Because of these non-local correlations, they can no longer be described independently of each other and we called them *entangled particles*. Measurements done only on one of these particles can not give any information on the global state of the system, and what is more, it changes inevitably and instantaneously the other particle's states.

This amazing tool allows in quantum computer science, the possibility to develop unbreakable protocols for communication. If any eavesdropper intercepts a message, he destroys it even without accessing to the information, thus making obvious his presence. The entanglement is also the key component to do teleportation [14, 17] and quantum dense coding [13].

Let us give a formal description and definition of entanglement. Consider a *bipartite* state (*ie.* it has two parts) $|\psi\rangle_{AB}$ in the Hilbert space $\mathcal{H}_A \otimes \mathcal{H}_B$, where $|\psi\rangle_A \in \mathcal{H}_A$ and $|\psi\rangle_B \in \mathcal{H}_B$. The state $|\psi\rangle_{AB}$ is *entangled* if it cannot be expressed as a product state:

$$|\psi\rangle_{AB} \;\; = \;\; |\psi\rangle_A \otimes |\psi\rangle_B \qquad (2.1.9)$$

and the reduced density matrices $\rho_A = |\psi\rangle_{AA}\langle\psi|$ $\rho_B = |\psi\rangle_{BB}\langle\psi|$ represent mixed states. In the other case, $|\psi\rangle_{AB}$ is *separable* and the ρ_A and ρ_B are pure.

An example for a pure separable state of two qubits is $|\psi\rangle = |00\rangle$, for entangled states we can mention the four Bell states:

$$\begin{aligned} |\phi^\pm\rangle &= \tfrac{1}{\sqrt{2}}(|00\rangle \pm |11\rangle) \\ |\psi^\pm\rangle &= \tfrac{1}{\sqrt{2}}(|01\rangle \pm |10\rangle) \end{aligned} \qquad (2.1.10)$$

The Bell states have the particularity to be maximally mixed when they are reduced to a single part state, since, for example,

$$\rho_A = Tr_B|\psi^+\rangle\langle^+\psi| = \frac{1}{2}\begin{pmatrix} 1 & 0 \\ 0 & 1 \end{pmatrix} = \frac{1}{2}\mathbb{I}. \qquad (2.1.11)$$

The bipartite entanglement between two qubits can be calculated using the Concurrence [110]. The Concurrence of two qubits in an arbitrary state characterized by the density matrix ρ is given by

$$C(\rho) = max\{0, \lambda_1 - \lambda_2 - \lambda_3 - \lambda_4\}, \qquad (2.1.12)$$

where the λ_i are the square roots of the eigenvalues, in decreasing order, of the non-Hermitian matrix $\rho\widetilde{\rho}$. The spin-flipped state $\widetilde{\rho}$ is defined as

$$\widetilde{\rho} = (\sigma^y \otimes \sigma^y)\rho^*(\sigma^y \otimes \sigma^y), \qquad (2.1.13)$$

were ρ^* is the complex conjugate of ρ and it is taken in the computational basis $\{|00\rangle, |01\rangle\, |10\rangle, |11\rangle\}$. The concurrence takes values between 0 and 1, where 0 means that the state is disentangled whereas 1 means a maximally entangled state.

2.2 Quantum communication

Transmission of the quantum information between distant parts is a main requirement to develop a quantum computer, since it is impossible transport quantum information on a classical channel [107]. Hence arises the challenge to find appropriate and reliable methods and channels for the communication of quantum information.

When a long distance communication is required, photons happen to be the best candidate to carry the information [52].

Communication over short distance is of great importance for connecting up all the necessary components (quantum processors, registers or memories) to make a powerful quantum computer. To design these solid-state quantum networks, condensed matter systems have been explored. As we mentioned, spin chains are promising to act as channel or wires for quantum state transmission [15].

2.2.1 Quantum state transfer with spin chain channels

S. Bose [15] was the first to propose spin chains as a channel for quantum state transfer in the context of quantum information processing. Nevertheless, an early antecedent can be found already in the seventies, in the work of Shore and co-workers, see for example [31]. Some experiments showing the basic principles of quantum transmission, such as the recovering of the initial state after some time, and with some probability, were reported in Refs.[40, 32].
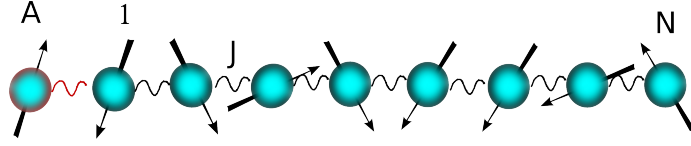
Figure 2.2.1: Spin chain of N qubits with homogeneous interactions J. The external qubit A is used to encode and initialize state in the spin on site 1. The qubit A interacts only initially with the first spin to pass a state which will be transferred along the channel. The protocol of the transmission is explained in [15].

Many physical systems can be described as two-level systems, i.e. in some regime the relevant physics properties can be described using only two energy levels and the corresponding "wave functions". The electronic spin, i.e. the electronic intrinsic angular momentum is the most celebrated case. Since two level systems are described, as corresponds to their discrete spectrum, in a two dimensional Hilbert space, the complete mathematical structure of this space is at disposal. In particular, any Hamiltonian of two level systems can be written in terms of the operator basis of the Hilbert space: the Pauli matrices and the identity matrix. For this reason, composite systems, formed by two level systems, whose Hamiltonian is written in terms of these matrices are usually termed "spin systems".

A Hamiltonian that includes interactions between all the spins in a chain is known as the general *Heisenberg* Hamiltonian

$$H_{XYZ} = -\frac{1}{2}\sum_{\substack{i,j \\ j>i}} \sum_{\nu=x,y,z} J_{ij}^{\nu}\sigma_i^{\nu}\sigma_j^{\nu} \tag{2.2.1}$$

where $\vec{\sigma_{\mathbf{i}}} = (\sigma_i^x,\sigma_i^y,\sigma_i^z)$ are the Pauli matrices on the site i, N is the chain length, $\vec{J}_{ij} = (J_{ij}^x, J_{ij}^y, J_{ij}^z)$ is the exchange interaction coupling between the spins located at sites i and j. An external magnetic field acting on the spins can be represented by adding the term $\frac{1}{2}\sum_{i=1}^{N} b_i^z \sigma_i^z$, to (2.2.1), where b_i^z is the external-field interaction coupling.

The properties and characteristics of a system with Hamitonian (2.2.1) depend, basically, on the couplings $J_{ij}^{x,y,z}$. A system with

- $J^x = J^y = J^z$ is called *isotropic* Heisenberg Hamiltonian H_{XYZ}

- $J^x = J^y \neq J^z$ is the *anisotropic* XXZ Hamiltonian H_{XXZ}

- $J^z = 0$ is the *XY* Hamiltonian H_{XY}

- $J^z = 0$, and $J^x = J^y$, is the *XY* Hamiltonian H_{XX}

- $J^z = J^x = 0$ is the Ising Hamiltonian.

Protocol of transmission

The steps to follow to transfer information along spin channels are: To encode the information in the quantum state of a spin and put it in one extreme of the spin chain. Let the system evolve in time under its Hamiltonian . After time t, read out the state at the other extreme of the chain.

Time scales and transfer speed

Which is the appropriate time to read out the transferred state, is particular to each system. The information travels within the chain as a spin wave. The propagation from one extreme of the spin chain to the other takes place at time

$$t_M. \tag{2.2.2}$$

This time is associated with the sometimes called mesoscopic echo time $2t_M$ [90]. For a chain supporting spin waves as elementary excitations, e.g. the uniformly coupled XX or Heisenberg chains, t_M is fixed by the maximum group velocity of the spin waves [83, 84, 40, 15]. The group velocity of excitations with dispersion relation $E(k)$ (where E is the energy and the k denotes the wave number) is given by $v_g = \frac{dE}{dk}$.

In what follows of the thesis, we consider as a reference the known value t_M^h for a homogeneous spin-chain with XY or Heisenberg interactions. In that systems, constructive interference at site N occurs at time [40]

$$t_M^h \sim \frac{N}{2J} \tag{2.2.3}$$

related with what is often called the *quantum speed limit* [114, 67, 65, 75].

Dispersion and efficiency of the transmission

In general, the constructive interference of the spin-wave at the echo time does not contain the same information as that the initial state. In most of the spin

channels the spin-wave is dispersed and therefore we usually judge, that the transfer is not perfect. That happens, for example, with the transmission in homogeneous chains of several spins; and far from having a perfect transfer, the efficiency of the transmission decrease notably with the length of the channel. An efficient and reliable transfer happens only in very short chains (around only 10 spins [15]). To improve the transmission quality, different schemes and protocols of transmission have been proposed. Many of them focus on systems that have the particularity to transfer without any external dynamical control. This absence of external control is desirable to avoid perturbations on the system that could damage the information.

The schemes and proposals significantly improve the quality of the state transfer, and can be classified in three different approaches:

(i) Designing the channel's interactions. Even perfect state transfer is achieved by an appropriate engineering of all the coupling interactions between the spins [1, 29, 30, 20, 19, 61, 62]

(ii) Applying external fields or control gates on the channel, or only on both extremes of the channel, to encode and extract the information [21, 22, 23, 47]

(iii) Multi-rails setups [18, 20, 97].

From an experimental point of view, all of these approaches must face some challenges to avoid the loss of information. Proposals of the type (i) can require great accuracy to design each interaction, while those of style (ii) can require an amazing precision to apply the necessary local operations.

2.2.2 Implementations and experiments

Every proposal for physical qubits that allows to couple them permanently can be used to develop spin chains. In solid-state systems, there are proposals to implement qubit chains using superconducting nanocircuits, such as charge qubits [92, 101], Josephson junctions [103] or flux qubits [69, 70]. The advances in semiconductor technology allow to couple quantum dots, so there are proposals using chains of charged quantum dots [79, 85, 80] or alternatively, excitons in quantum dots [98, 33]. Spin chains can be also simulated with cold atoms confined in optical lattices [39, 38, 56, 66] or with nuclear spin systems in NMR [71, 5]. Very few of these systems have been implemented experimentally, for example using small numbers of spins in liquid-state NMR [71, 78, 116, 117, 5] and slightly larger numbers of them in solid-state NMR

[26, 94]. Nitrogen vacancy centers in diamond [113, 27, 76] is another promising system that is under scrutiny for its potential.

In the following subsections we briefly describe the process of state transfer through unmodulated spin chains, including the first protocol for state transmission along unmodulated spin chains [15]; later on, we will pay some attention to the pioneering work on perfect state transfer by modulated spin-chains [1, 29, 30].

2.2.3 State transfer through unmodulated spin-chains

2.2.3.1 Heisenberg interactions

Bose considered as spin channel a homogeneous[7] ferromagnetic chain with isotropic nearest-neighbor Heisenberg interactions in an external magnetic field, with Hamiltonian

$$H_{XXX} = -\frac{1}{2} \sum_{i=1}^{N-1} J(\vec{\sigma}_i \cdot \vec{\sigma}_{i+1}) - \frac{1}{2} \sum_{i=1}^{N} b_i^z \sigma_i^z. \qquad (2.2.4)$$

This channel will be used to transfer the spin state located at one extreme of the chain to the other one. The protocol to carry out this transmission through the spin chain can be summarized in the following steps:

1. Initialize the spin chain in the state $|\mathbf{0}\rangle = |0_1 0_2 ... 0_N\rangle$

2. Prepare the state to be transferred in the first site $|\psi_1\rangle = \alpha|0_1\rangle + \beta|1_1\rangle$.

3. Let the system evolve under its Hamiltonian for a time t:

$$|\psi(t)\rangle = e^{-iHt/\hbar}(|\psi_1\rangle \otimes |0_2 0_3 ... 0_N\rangle) = e^{-iHt/\hbar}|\psi_0\rangle.$$

4. At time t_M, the initial state is transferred (at least partially) to the other extreme of the chain. Take $|\psi(t_M)\rangle$.

5. Check the *fidelity* of the transfer, *ie.* compare the state $|\psi(t_M)\rangle$ with $|\psi_0\rangle$.

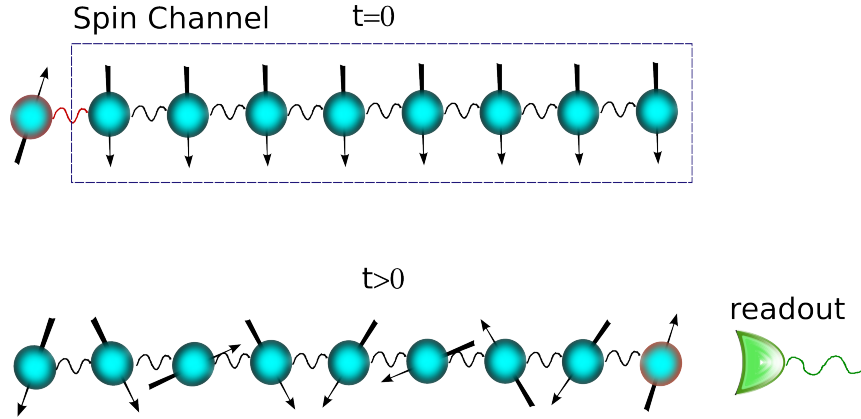[7]Throughout the thesis, we refer to homogeneous and unmodulated as synonymous

Figure 2.2.2: Protocol of the state transmission through spin chains described in [15].

The Hamiltonian (2.2.4) commutes with the total spin magnetization along the z-axis, $\left[H_{XYZ}, \sum_{i=1}^{N}\sigma_i^z\right] = 0$, *ie.* the number of excited spins is conserved (this point will be explained with more detail in the section 2.2.3.2). Since the initial state of the total system

$$|\Psi(t=0)\rangle = |\psi_1\rangle \otimes |0_20_3...0_N\rangle = \alpha|\mathbf{0}\rangle + \beta|\mathbf{1}\rangle \tag{2.2.5}$$

is a superposition of the eigenstate $|\mathbf{0}\rangle = |0_10_2...0_N\rangle$ and the state $|\mathbf{1}\rangle = |1_10_2...0_N\rangle$, the component $|\mathbf{0}\rangle$ is conserved and the component $|\mathbf{1}\rangle$ evolves within the one excitation subspace spanned by the basis states $|\mathbf{i}\rangle = |0...01_i0...0\rangle$.

The state of the system at a given evolution time t is

$$|\Psi(t)\rangle = e^{-iHt/\hbar}|\Psi_0\rangle = \alpha|\mathbf{0}\rangle + \beta\sum_{i=1}^{N} f_i(t)|\mathbf{i}\rangle, \tag{2.2.6}$$

where $f_i(t) = \langle\mathbf{i}|e^{-iHt/\hbar}|\mathbf{1}\rangle$.

Fidelity

To measure the effectiveness of state transfer between sites 1 and N, we determine the fidelity

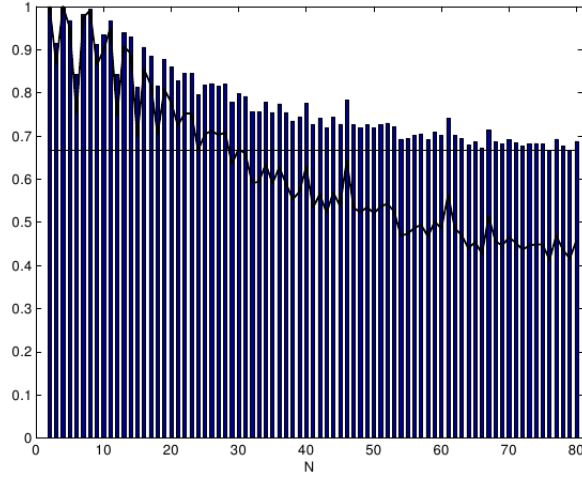$$\mathcal{F}(t) = \langle\psi_1|\rho_N(t)|\psi_1\rangle \tag{2.2.7}$$

Figure 2.2.3: Maximum fidelity F of quantum communication achieved in a Heisenberg spin-chain in a time interval $[0, 4000/J]$ as a function of the chain length N from 2 to 80. The time t at which this maximum is achieved varies with N. The straight line at $F = \frac{2}{3}$ shows the highest fidelity for classical transmission of a quantum state. (Bose 2003 [15])

averaged over all possible initial states $|\psi_1\rangle$ distributed uniformly over the Bloch sphere, which is given by [15]

$$F(t) = \frac{|f_N(t)|\cos\gamma}{3} + \frac{|f_N(t)|^2}{6} + \frac{1}{2}, \qquad (2.2.8)$$

where $\gamma = \arg|f_N(t)|$. Because the phase γ can be controlled by the external field once the state is transferred, b_i is chosen such that γ is multiple of 2π and therefore, $\cos\gamma = 1$. When a perfect transmission of the state happens, $F = 1$, on the contrary when nothing is transferred, $F = \frac{1}{2}$ (*ie. $f_N = 0$*).

In his work [15], S. Bose showed some numerical simulations summarized in Fig. 2.2.3 for the system (2.2.11). Perfect state transfer happen only for $N = 2$ or $N = 4$. For longer chains, the fidelity of state transmission decreases progressively with the increase in the size of the chain, N. A transfer with a fidelity higher than 0.9 is possible only for some values of N smaller than 17. Also shown in Fig. 2.2.3 is the maximum classical fidelity transmission $F = \frac{2}{3}$ [58]. That value of the fidelity is exceeded in quantum chains up to N=80 spins.

2.2.3.2 XY interactions

A linear spin chain with nearest-neighbor homogeneous XY-interactions is described by the following Hamiltonian

$$H_{XY} = -\frac{1}{2}\sum_{i=1}^{N-1} J(\sigma_i^x \sigma_{i+1}^x + \sigma_i^y \sigma_{i+1}^y). \tag{2.2.9}$$

Since this Hamitonian has also the particularity to commute with the total magnetization along the z-axis, $\left[H_{XY}, \sum_{i=1}^{N} \sigma_i^z\right] = 0$, the Hamiltonian H_{XY}, of dimension $2^N \times 2^N$, has a block structure where each block corresponds to a fixed number of excitations. These blocks have associated subspaces that are invariant under time evolution, as a result the number of excited spins is conserved. This feature allows to deal with this kind of systems in a much easier way, theoretically and numerically, since the problem can be decomposed into separate Hilbert spaces with dimensions smaller than 2^N. For example, if we are interested in the transmission of a state with one excited spin from one end of the chain to the other, we need to take into account only the one excitation subspace, spanned by the basis states $|\mathbf{i}\rangle = |0...01_i0...0\rangle$, where the complete dynamics take place. In the one excitation basis, the Hamiltonian H is represented by a $N \times N$ matrix

$$H_{XY} = - \begin{pmatrix} 0 & J & 0 & \dots & 0 \\ J & 0 & J & \dots & 0 \\ 0 & J & 0 & \dots & 0 \\ \vdots & \vdots & \vdots & \ddots & J \\ 0 & 0 & 0 & J & 0 \end{pmatrix}. \tag{2.2.10}$$

As an example of the performance for state transfer of the system with homogeneous couplings, we consider the same protocol of transmission described above in 2.2.3.1. In Figs. 2.2.4 and 2.2.5 we show our numerical calculation of the fidelity $\mathcal{F}$ of the state transfer (Eq.2.2.7) and the average fidelity F (Eq. 2.2.8), as functions of the time, for chain lengths $N = 31$ and $N = 200$, respectively. As happens with Heisenberg interactions, the maximum fidelity decreases with the increase of N.

The time when the maximum transfer at site N occurs, t_M^h, as we have recently already mentioned, is also dependent on the length of the channel, being $t_M^h \sim \frac{N}{2J}$ (2.2.3). The transfer time becomes a relevant parameter to take
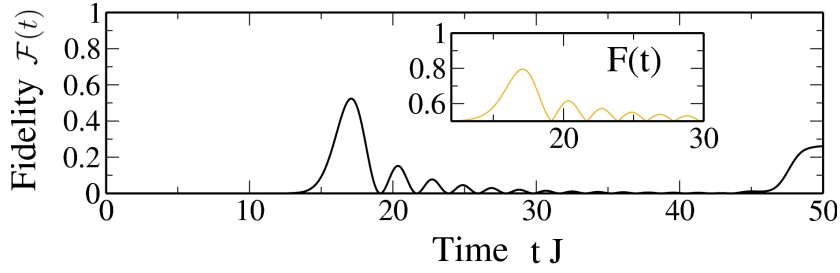
Figure 2.2.4: Fidelity $\mathcal{F}$ of the state transfer along a chain of $N = 31$ spins with unmodulated XY interactions. The inset shows the averaged fidelity F (Eq. 2.2.8).
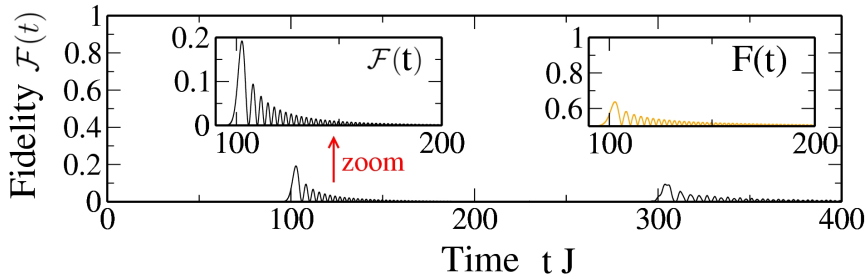

Figure 2.2.5: Fidelity $\mathcal{F}$ of the state transfer along a chain of $N = 200$ spins with unmodulated XY interactions. The left inset is a zoom of the main figure, and the right inset shows the averaged fidelity F (Eq. 2.2.8).

into account to characterize and assess the system's performance as a communication channel. The transfer time and the time window when the fidelity is relatively high must be evaluated in terms of the time-scale of the physical system and the possible occurrence of *decoherence* during the implementation of the communication protocol.

2.2.4 State transfer through modulated chains

2.2.4.1 Completely engineered couplings for perfect state transfer

By engineering the entire set of spin-spin couplings J_i in a nearest-neighbor chain, it is possible to notably increment the fidelity of the transmission. So much so that under some specific coupling designs it is possible to achieve perfect state transfer at some time, and not only that, there are infinitely

many ways of tailoring the system to allow perfect state transfer [1, 29, 60, 61, 79, 50, 19].

The first proposal of coupling distribution for perfect state transfer made by Christandl *et. al.* [29] considered an XY Hamiltonian

$$H_{XY} = -\frac{1}{2} \sum_{i=1}^{N-1} J_i (\sigma_i^x \sigma_{i+1}^x + \sigma_i^y \sigma_{i+1}^y), \quad \text{with} \quad J_i = J\sqrt{i(N-i)}. \qquad (2.2.11)$$

This system achieves perfect state transfer ($F = 1$) at time $t_{PST} = \frac{\pi N}{4 J_{max}}$, as can be seen in Fig. (2.2.6). There is a simple interpretation of the dynamical evolution generated by the Hamiltonian 2.2.11 in terms of the rotation of a spin-$\frac{N}{2}$ that has an external magnetic field applied to it [1].

We discuss about the necessary conditions for perfect state transfer in Chap. **4** where we also analyze the robustness against static perturbations for different couplings that allow perfect state transfer [120, 121].
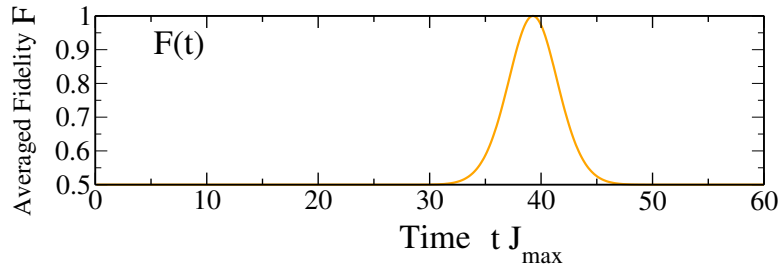

Figure 2.2.6: Averaged fidelity of the state transfer in $N = 50$ spin chain for the perfect state transfer system with XY interaction (2.2.11)

2.3 Vulnerability of quantum systems

As it was already mentioned, the manipulation of information in a quantum device is an extremely difficult task; not only for the tremendous differences in the different scales involved, it is also because of the vulnerability of quantum systems to uncontrolled external perturbations. Such disturbances are mainly due to the interaction with the device's environment. This unavoidable interaction produces the *decoherence* [118] of the quantum states, *ie.*, the loss or degradation of quantum information and quantum correlations.

The intrinsic vulnerability of quantum systems has lead to the exhaustive search of systems that allow information transfer without any dynamical control, since that reduces the coupling to the environment.

The systems not requiring any dynamic control that have been proposed until now for the transfer of information, in general, show that a high fidelity in the transmission comes together with a high cost in terms of the necessary effort to tailoring and to manipulate the system. Engineering processes demand a high accuracy and control of the quantum systems. Any failure in the manufacturing process can introduce static errors that can dramatically damage the information.

3 Transmission in boundary control channels without perturbations

3.1 Introduction

Quantum information processing has been extensively studied during the past years [64]. Nowadays, one of the main challenges of physical implementations is the manipulation of the quantum information with sufficient accuracy to prevent errors. We have already discussed the importance of transferring quantum information between different elements of a quantum computer [36]. Also, we have already discussed that spin chain systems have been proposed as quantum channels for the transmission of quantum states, where the spins act as the quantum bits [15, 102, 82, 96, 45, 106, 87, 47]. As usually the transfer of information through this kind of channels is far from efficient, many systems of these kind have been explored in order to improve their performance for the state transmission.

Most of these previous works focused on describing how well or not these systems perform the transfer, but little analysis of the intrinsic physical properties that allow to improve the transfer was done. Understanding which physical properties are responsible and essential to achieve a reliable transfer lead to generalized criteria about what kind of systems are suitable for state transfer.

The knowledge that unmodulated spin channels transfer information adequately only for really short chains has started an intensive search for modifications in the channel that increase the quality of the information transfer along longer channels. A number of proposals to manipulate the channel that enhance the transfer have emerged, such as the application of controlled and local external fields [21, 22] or the engineering of all the spin-spin interactions strengths [29, 30, 1, 60]. However, in general, all of this novel proposal requires also big modifications or accurate control.

The points stated above lead to some questions: Are there ways to minimize these laborious requirements? How can we optimize the transfer process? To answer and solve these queries, a elemental tool is the knowledge of the

essential physical properties required for a successful state transfer, in order to design the system for enhancing the state transfer with minimal resources or/and control.

Spin channel systems of finite size, without periodic boundary conditions, do not possess the property of being translationally invariant. The system gains another interesting and useful characteristics, it can produce localized states [95]. This kind of state appears, for example, in some models of quantum computers in presence of static disorder [49]. Moreover, the presence of "impurities", *ie.* different spin-spin interaction strength, local magnetic field, etc, break the translational invariance in the system, producing localized states. Big local changes on one or few spin sites produce highly localized states that can be used to store quantum information [8] and are useful to drive the propagation of entanglement through a quantum spin chain [7, 87].

For weaker local changes, it is not so clear which effects are produced on the system, with respect to the manipulation of quantum information. For this reason, we want to explore which is the role of the localized states, produced by variable local change on the state transfer. But before the study of the dynamic properties and dynamic behaviour, we want to focus on the system properties produced by the local change, e.g. in particular on the eigenenergies and the eigenstates. We will focus on the localization and entanglement content of the eigenstates.

So, we consider a boundary spin coupling different from the homogeneous channel interactions and study numerically the chains static properties. We analyze the localization of the eigenstates using as a measure the inverse participation ratio, and their bipartite entanglement using the concurrence.

As we will show, we distinguish two kinds of localized states, a) exponentially localized eigenstates of energies that lie outside a band of eigenenergies, and b) localized eigenstates that lie inside of this band, whose number depends on the length of the chain and the strength of the impurity. We also show that this second kind plays a fundamental role in the transmission of quantum states through the chain.

In most of the protocols for quantum state transfer, the state to be transferred is localized at one end of the quantum chain and the transmission is successful when the time evolution of the system produces an equally localized state at the other end of the chain. So it seems natural to investigate the time evolution of a localization measure to gain some insight into the problem of quantum state transfer.

So, the analysis of the time evolution of the inverse participation ratio of the total state of the system, when the initial state consists in a single excitation located on the boundary spin, allows the identification of different regimes for state transfer. In particular, we identify an "optimal" one, called so because in this regime, the transfer is achieved with a high quality around the fastest time possible.

The chapter is organized as follows, in Sec. 3.2 we present the XX Hamiltonian describing the quantum spin chain with a variable boundary coupling. In Sec. 3.2.1 we analyze in some detail the spectrum of the one spin excitations and their eigenstates. In Sec. 3.2.2 we present the results obtained for the inverse participation ratio for each one spin excitation eigenstate while the bipartite entanglement of the eigenstates is analyzed in Sec. 3.2.3. Finally, in Sec. 3.2.4, we discuss the relationship between localization and transmission of quantum states and we define a regime for optimal dynamics.

3.2 Boundary control channel

Let us consider a linear chain of N-qubits with XX interaction. The coupling strengths are homogeneous except at the boundary site, where the coupling is different.
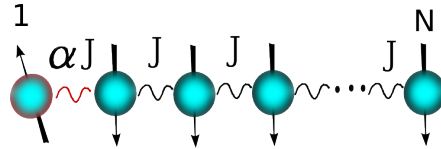

Figure 3.2.1: Spin chain system with one boundary control coupling αJ.

The system is described by the Hamiltonian

$$H(\alpha) = -\frac{1}{2}\alpha J(\sigma_1^x \sigma_2^x + \sigma_1^y \sigma_2^y) - \frac{1}{2}\sum_{i>1} J(\sigma_i^x \sigma_{i+1}^x + \sigma_i^y \sigma_{i+1}^y), \qquad (3.2.1)$$

where σ^μ are the Pauli matrices, J is the exchange coupling strength and αJ is the boundary control exchange strength, $\alpha = 1$ corresponds to the homogeneous case described in 2.2.3.2.

Since the Hamiltonian $H(\alpha)$, as well as H_{XY}, commutes with $S_z = \Sigma_i \sigma_i^z$, the number of excited spins is conserved (see Sec. 2.2.3.2 for more details).

Because we are interested in the transmission of a state with one excited spin from one end of the chain to the other, we focus on the eigenvectors of the one excitation subspace where the complete dynamics take place. To describe the eigenstates, we choose a basis given by the computational states of this subspace $|\mathbf{i}\rangle = |0...01_i0...0\rangle$, where $i = 1, \ldots, N$ so the basis set size equals the number of spins of the chain.

In the computational basis, the Hamiltonian H is represented by a $N \times N$ matrix

$$H = - \begin{pmatrix} 0 & \alpha J & 0 & \ldots & 0 \\ \alpha J & 0 & J & \ldots & 0 \\ 0 & J & 0 & \ldots & 0 \\ \vdots & \vdots & \vdots & \ddots & J \\ 0 & 0 & 0 & J & 0 \end{pmatrix}. \tag{3.2.2}$$

3.2.1 Energy spectrum and eigenstates

In this section we briefly recall some known results about the spectrum and the eigenstates of the Hamiltonian emphasizing those features that are of interest in the following Sections.

Eigenenergies

The one excitation spectrum consists of N eigenenergies, the N eigenvalues of H of Eq. (3.2.2), denoted by $\{E_1 \leq E_2 \leq ... \leq E_N\}$. Choosing the total number of spins even the resulting spectrum is symmetrical with respect to zero ($E = 0$ is not an eigenvalue), for any value of α. Then $\left\{E_1, ..., E_{\frac{N}{2}}\right\}$ are negative values whereas $\{E_{\frac{N}{2}+1}, ..., E_N\}$ are positive. In the homogeneous case ($\alpha = \alpha_J \equiv 1$), the energy spectrum lies between the values $\pm 2|J|$, this interval is usually called the *band* of eigenvalues. The length of the chain only changes the number of eigenvalues between those extreme values, the spectrum becomes continuous when $N \to \infty$.

The inhomogeneous case shows a different behaviour. For large enough α the minimal and the maximal eigenenergy become isolated from the band. There is a critical value α_c which separates the region of the spectrum where the energies make a band ($0 < \alpha < \alpha_c$) from the region where the energies make a band with two isolated energies ($\alpha > \alpha_c$). . The critical point α_c can be obtained analytically for large values of N, being $\alpha_c = \sqrt{2}$ [100]. We analyze
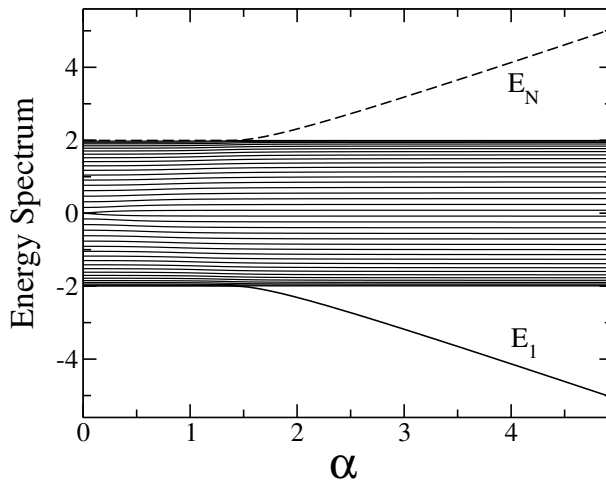
Figure 3.2.2: The one excitation spectrum vs. α for a spin chain with 40 spins. For α large enough the spectrum shows two isolated eigenenergies and one band $|E| \leq 2|J|$. The two isolated curves correspond to the minimal eigenenergy E_1 (continuous line) and the maximal eigenenergy E_N (dashed line). At the critical value α_c the isolated energies go into the band causing a slight distortion in the behaviour of energies inside the band. In this figure we use $|J| = 1$

this point later on, in the paragraph that contains Eq. (3.2.7). Just for the sake of completeness, the spectrum of finite size chains shows the transition between these two regimes more smoothly; and the approximate critical value is smaller than the one corresponding to $N \to \infty$, $\alpha_c \lesssim \sqrt{2}$, as shown Fig. 3.2.3.

For $\alpha \gg \alpha_c$ the minimal and maximal energies move apart from the band proportionally to $-\alpha$ and $+\alpha$ respectively. This behaviour is depicted in Fig. 3.2.2.

Figure 3.2.2 shows that most of the eigenenergies seem to be fairly independent of α, except for the minimal and maximal energies. But a more detailed study of the derivative of the eigenenergies with respect to α (see Fig. 3.2.4 and Sec. 3.2.3), shows two regions where the changes in the spectrum are more noticeable:

(i) for $\alpha \sim 0$ two eigenenergies become degenerate because the system changes from a chain with N coupled spins to a chain with $N - 1$ coupled spins
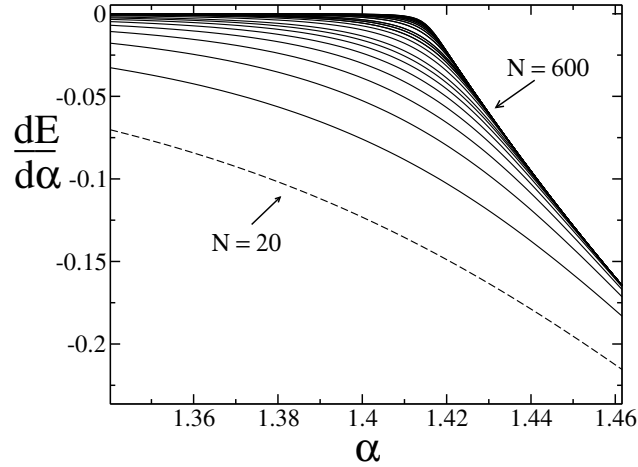
Figure 3.2.3: $\frac{dE_1}{d\alpha}$ vs. α for different lengths of the spin chain, from bottom to top, $N = 20, 30, ..., 100, 120, ..., 200, 250, .., 600$.

and an uncoupled spin (Fig. 3.2.4(b));

(ii) for $\alpha \lesssim \alpha_c$ there is a number of avoided crossings between successive eigenenergies, because of the "collision" between the minimal (or maximal) eigenenergy and the band (Fig. 3.2.4(a)).

Eigenstates

The eigenstates in the one excitation subspace $|\Psi_E(\alpha)\rangle$, whose eigenvalue equation is

$$H(\alpha)|\Psi_E(\alpha)\rangle = E|\Psi_E(\alpha)\rangle, \tag{3.2.3}$$

can be written as a superposition of the one excitation states

$$|\Psi_{E_j}(\alpha)\rangle = \sum_{n=1}^{N} \Psi_n^{(j)} |n\rangle, \tag{3.2.4}$$

where due to the symmetries of the Hamiltonian

$$\Psi_n^{(j)} = (-1)^n \Psi_n^{(N-j+1)}. \tag{3.2.5}$$

The coefficients $\Psi_n^{(j)}$ contain information about localization and entanglement properties of the eigenstates and, can be written as [95]

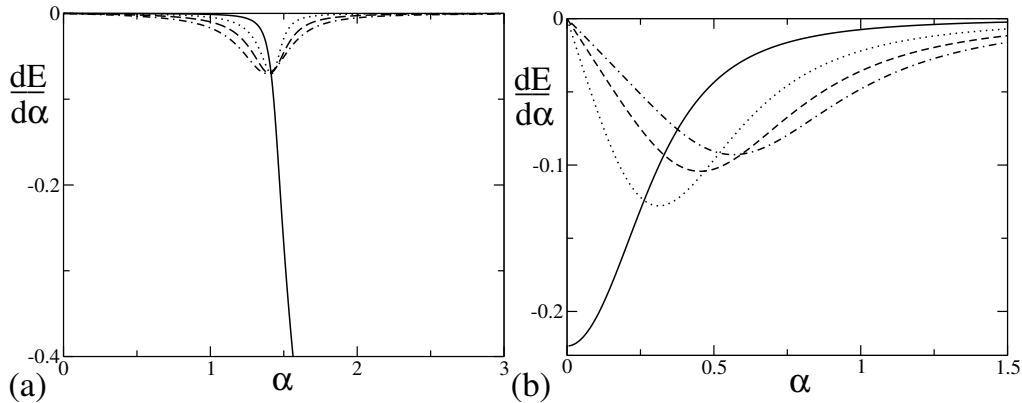$$\Psi_n^{(j)} = d e^{i\theta n} + d' e^{-i\theta n}. \tag{3.2.6}$$

Figure 3.2.4: (a) Behavior of $\frac{dE_i}{d\alpha}$ for the first four eigenvalues in the region near α_c. The continuous line corresponds to the derivative of E_1, the dotted to E_2, the dashed to E_3, and the dot-dashed to E_4. The derivative of E_1 approaches zero when the eigenvalue enters into the band. The small "valleys" in the derivatives of E_1, E_2 and E_3 show that these eigenvalues are non-increasing functions of α. When the derivative of the eigenvalues is nearly zero the distance between successive eigenvalues remains constant, but when the derivative is different from zero two successive eigenvalues tend to be closer to each other, presenting an avoided crossing. (b) $\frac{dE_i}{d\alpha}$ vs. α, for $i = \frac{N}{2}$ (continuous line) , $\frac{N}{2} - 1$ (dotted), $\frac{N}{2} - 2$ (dashed), and $\frac{N}{2} - 3$ (dashed-dotted). The spin chain has $N = 40$.

In a homogeneous chain, the eigenstates are wave-like superpositions of the one excitation states where the coefficients of the superpositions are given by Eq. (3.2.6) with θ real. In the other case, $\alpha \neq 1$, the eigenstates within the band are very similar to the states of the homogeneous case (Fig. 3.2.5 shows $\Psi_n^{(\frac{N}{2})}$ for $\alpha = 0.1$), but they differ in their coefficient on the boundary control site. For $\alpha > \alpha_c$ the minimal eigenenergy state $|\Psi_{E_1}\rangle$ is quite different (similarly for $|\Psi_{E_N}\rangle$), their coefficients $\Psi_n^{(1)}$ decay exponentially (Fig. 3.2.5 shows $\Psi_n^{(1)}$ for $\alpha = 1.6$).

The existence of a localized state when $\alpha \geq \sqrt{2}$ can be demonstrated an- alytically: Using the ansatz $\Psi_1 = u_1$ and $\Psi_n = (-1)^{n+1} e^{-n\kappa}$, for $n \geq 2$, to construct a state $|\Psi\rangle$, and replacing this state in Eq. 3.2.3, after some algebra we obtain that

$$e^{2\kappa} = \alpha^2 - 1, \tag{3.2.7}$$

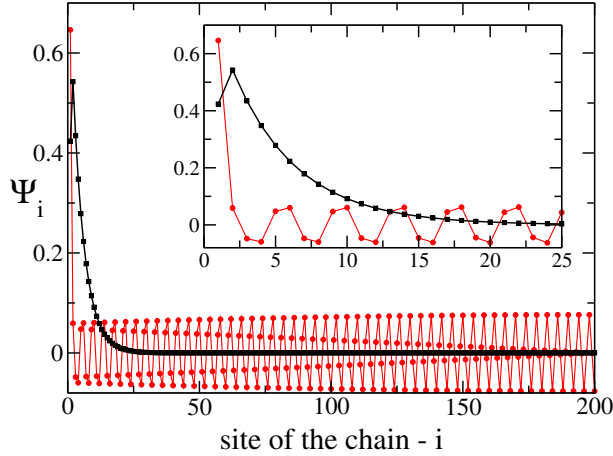so, to have a localized state, the condition $e^{2\kappa} \geq 1$ implies that $\alpha \geq \sqrt{2}$. This

Figure 3.2.5: The coefficients Ψ_i for two different eigenstates, $|\Psi_{E_1}(\alpha)\rangle$ with
$\alpha = 1.6$ (black squares) and $|\Psi_{E_{\frac{N}{2}}}(\alpha)\rangle$ with $\alpha = 0.1$ (red circles).
The lines are a guide to the eye. The states and the values of α
were chosen to obtain equal values for their inverse participation
ratios. The inset shows a zoom of the region near $i = 1$.

has been discussed previously, see, for example, the work of Stolze and Vogel
[100]. There, the authors exploit the mapping between the XX model with
one excitation and a non-interacting fermion model with one particle.

Density matrix

The density matrix for each eigenstate is given by

$$\hat{\rho}_E(\alpha) = |\Psi_E(\alpha)\rangle\langle\Psi_E(\alpha)|, \qquad (3.2.8)$$

which is a $N \times N$ matrix in the one excitation subspace.

3.2.2 Localization of the eigenstates

As stated above, the eigenenergies and eigenstates change according to the
strength of the boundary control coupling considered in the system. To quan-
tify and study their changes, we calculate the eigenstate localization as a
function of the boundary control coupling strength. For that purpose we use

the inverse participation ratio (IPR) [51],

$$L_{IPR}(|\Psi\rangle) = \frac{\sum\limits_{i=1}^{N} \Psi_i^2}{\sum\limits_{i=1}^{N} \Psi_i^4}, \tag{3.2.9}$$

where Ψ_i are the coefficients of the superposition (3.2.4) of the state. When the state is maximally localized (*ie.* Ψ_i is nonzero for only one particular value of i) $L_{IPR}(|\Psi\rangle)$ has its minimum value, 1; when the state is uniformly distributed (*ie.* $\Psi_i = 1/\sqrt{N}$ for all i) the IPR attains its maximum value, N. We call a state $|\Psi\rangle$ *extended* if $L_{IPR}(|\Psi\rangle) \sim \mathcal{O}(N)$, *ie.* the IPR is of the same order of magnitude as the length of the chain.

From (3.2.5), two states whose eigenenergies are symmetric with respect to zero, say $|\Psi_{E_j}\rangle$ and $|\Psi_{E_{N-j+1}}\rangle$ where $j \leq \frac{N}{2}$, have the same IPR, *ie.* $L_{IPR}(|\Psi_{E_j}\rangle) = L_{IPR}(|\Psi_{E_{N+1-j}}\rangle)$. As a consequence, each curve in Fig. 3.2.6 is double and we consider the IPR only for the states $\left\{ |\Psi_{E_1}\rangle, ..., |\Psi_{E_{\frac{N}{2}}}\rangle \right\}$.

Figure 3.2.6 shows the inverse participation ratio L_{IPR} of several eigenstates $\{|\Psi_{E_1}\rangle, ..., |\Psi_{E_N}\rangle\}$ as a function of the boundary control coupling α for a chain with $N = 200$ spins. We can identify three regions where the behaviour of the L_{IPR} is qualitatively different. These regions are separated by α_J and α_c. At α_J, all eigenstates are equally localized and, we find

$$L_{IPR}(\alpha_J) = \frac{2(N+1)}{3}. \tag{3.2.10}$$

(I) The first region $0 < \alpha < \alpha_J$ shows several localized eigenstates corresponding to energies close to zero, i.e. the center of the band. Calling $\alpha_{E_j}^m$ the value of α such that $L_{IPR}(E_j, \alpha) = L_{IPR}(|\Psi_{E_j}(\alpha)\rangle)$ attains its minimum, the numerical results show that $L_{IPR}(\alpha_{E_{\frac{N}{2}}}^m) < L_{IPR}(\alpha_{E_{\frac{N}{2}-1}}^m) < ...$ where $\alpha_{E_{\frac{N}{2}}}^m < \alpha_{E_{\frac{N}{2}-1}}^m < ...$, *ie.* an eigenstate is more localized as it is closer to $E = 0$. Besides, the number of localized states increases with N.

(II) In the second region $\alpha_J < \alpha < \alpha_c$, the eigenstates with energies close to the border of the band become more extended acquiring a IPR maximum close to α_c. These peaks become sharper when N grows, as can be observed if we compare Figs. 3.2.6 and 3.2.7. At α_c, these eigenstates are again equally localized, but for values of α larger than α_c, but very close to this value, the eigenstates become more localized. The size of
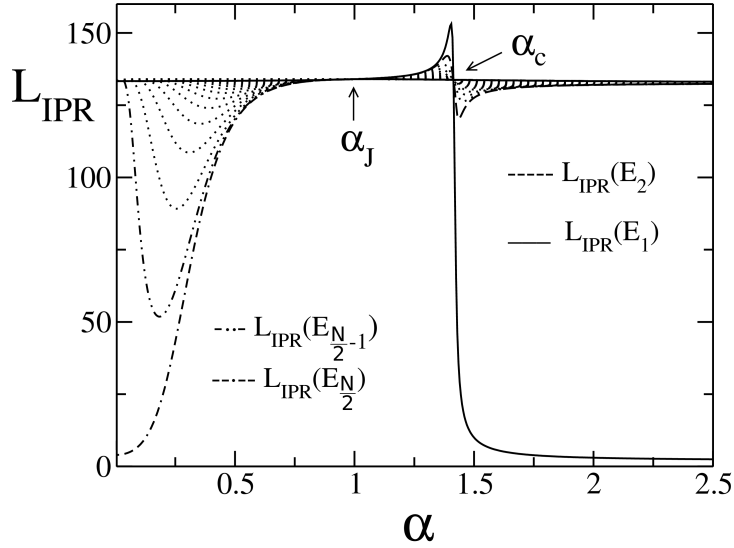
Figure 3.2.6: Localization measure ($L_{IPR} = \sum_i \Psi_i^2 / \sum_i \Psi_i^4$) of different one-excitation eigenstates vs. α, for a chain with $N = 200$ spins. The values of α_J and α_c are shown. For $\alpha \gg \alpha_c$, the curves of the IPR for the all eigenstates, except those corresponding to the minimal and maximal eigenenergies, collapse into a single curve. For $\alpha > \alpha_c$ the curves with $L_{IPR} \sim 1$ correspond to the minimal and maximal eigenenergy states. The steep behaviour of these curves when $\alpha \to \alpha_c^+$ shows the change from well localized to extended states. The localized states, with low IPR, that appear for $\alpha < \alpha_c$ correspond to states with eigenenergies near the center of the band. Near $\alpha = 0$ there are several localized states. Each curve is double as explained in the text.

the interval around α_c in which this critical behaviour can be observed depends on the length of the chain. These localization changes seem to be related to the avoided crossings in the spectrum previously described.

(III) In the last region $\alpha > \alpha_c$ there are only two eigenstates highly localized that correspond to the minimal and maximal eigenenergies, E_1 and E_N. The other states are extended through $N - 1$ sites of the chain.

We want to stress that the IPR gives a coarse description of the eigenstates, for example the states in Fig. 3.2.5, despite of their very different behaviour, are equally localized if the measure of localization is the IPR, effectively $L_{IPR}(\Psi_{E_1}) = L_{IPR}(\Psi_{E_{\frac{N}{2}}}) \simeq 5.6$ for both states. This indicates that the IPR
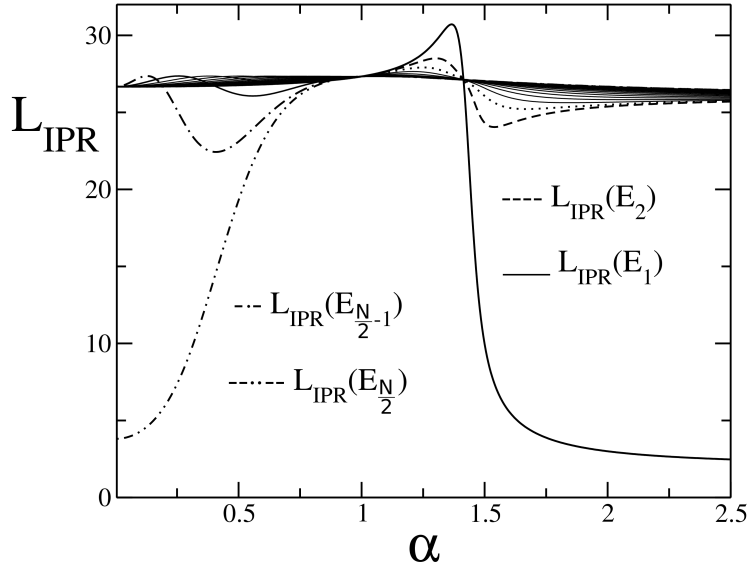
Figure 3.2.7: The IPR of different one excitation eigenstates vs. α, for a spin chain with $N = 40$. The changes around α_c are not as pronounced as in the chain with $N = 200$ spins, compare with Fig. 3.2.6.

can not distinguish the exponentially localized state from the state with a wave-like superposition extended over the chain if the latter has its coefficient Ψ_1 large enough.

This shows that the IPR is a good tool to quantify changes in the system due to the introduction of a boundary control spin, however it does not give information about where the eigenstate is localized. Moreover, it does not distinguish between quite different states as those described in Fig. 3.2.5. Studying the coefficients of the eigenstates, we can observe where they are localized. In the present case they are mainly localized on the boundary control site (see Fig. 3.2.5). However, since we are interested in the transmission of initially localized quantum states, and that a successful transmission results in another localized state, the IPR could provide an easy way to identify when the transmission has taken place.

Since the IPR does not distinguish between the exponentially localized states with energies that lie outside the band, and the localized states with energies inside the band it is necessary to study both kinds of states using a local quantity. In the next section we study the entanglement between the boundary control site and its first neighbor, this will allow us to classify the different

eigenstates accordingly with its entanglement content.

3.2.3 Entanglement of the eigenstates

3.2.3.1 Entanglement in terms of eigenenergies and eigenvalues

We measure the entanglement between two qubits using the *Concurrence* $C(\rho)$ [110] (see Eq. (2.1.12) in Sec. 2.1.1). The *reduced density matrix* for the spin pair (i,k), $\rho_E^{(i,k)}(\alpha)$, corresponding to the eigenstate $|\Psi_E(\alpha)\rangle$ is given by

$$\rho_E^{(i,k)}(\alpha) = Tr\, |\Psi_E(\alpha)\rangle \langle \Psi_E(\alpha)| = Tr\hat{\rho}_E(\alpha), \qquad (3.2.11)$$

where the trace is taken over the remaining $N - 2$ spins leading to a 4×4 matrix.

The structure of the reduced density matrix follows from the symmetry properties of the Hamiltonian. Thus, in our case the concurrence $C(\rho_{E_j}^{(i,k)})$ depends on i and k, *ie.* the indices of the sites where the spin pair lies. Note that in the translationally invariant case $C(\rho_{E_j}^{(i,k)})$ depends only on $|i - k|$. In what follows $C_{i,k} = C_{i,k}(\rho_{E_j}) = C(\rho_{E_j}^{(i,k)})$.

Using the definition $\langle \hat{A} \rangle = Tr(\hat{\rho}\hat{A})$, we can express all the matrix elements of the density matrix $\rho^{(i,j)}$ in terms of different spin-spin correlation functions. In particular, for nearest neighbors spins and the eigenstate $|\Psi_{E_j}\rangle$, we get

$$\rho_{E_j}^{(i,i+1)} = \begin{pmatrix} a_j & 0 & 0 & 0 \\ 0 & b_j & \langle \sigma_i^+ \sigma_{i+1}^- \rangle_{E_j} & 0 \\ 0 & \langle \sigma_i^+ \sigma_{i+1}^- \rangle_{E_j}^* & d_j & 0 \\ 0 & 0 & 0 & 0 \end{pmatrix}, \qquad (3.2.12)$$

where

$$a_j = \frac{1}{4}\langle(\sigma^z + I)_i(\sigma^z + I)_{i+1}\rangle_{E_j}, \qquad (3.2.13)$$

$$b_j = \frac{1}{4}\langle(\sigma^z + I)_i(I - \sigma^z)_{i+1}\rangle_{E_j}, \qquad (3.2.14)$$

$$d_j = \frac{1}{4}\langle(I - \sigma^z)_i(\sigma^z + I)_{i+1}\rangle_{E_j}, \qquad (3.2.15)$$

I is the 2×2 identity matrix, $\sigma_i^{\pm} = (\sigma_i^x \pm i\sigma_i^y)/2$, and

$$\langle \ldots \rangle_{E_j} = \left\langle \Psi_{E_j} \middle| \ldots \middle| \Psi_{E_j} \right\rangle. \tag{3.2.16}$$

Thus, the concurrence results to be

$$C_{i,i+1}(\rho_{E_j}) = \max\{0, 2 \mid \langle \sigma_i^+ \sigma_{i+1}^- \rangle_{E_j} \mid, 2\sqrt{|b_j d_j|}\}. \tag{3.2.17}$$

For the set of eigenstates that we are considering, the expression for the concurrence can be further simplified. After some algebra we get

$$b_j = (\Psi_{i+1}^{(j)})^2, \quad d_j = (\Psi_i^{(j)})^2, \tag{3.2.18}$$

and that

$$\langle \sigma_i^+ \sigma_{i+1}^- \rangle_{E_j} = \Psi_{i+1}^{(j)} \Psi_i^{(j)}. \tag{3.2.19}$$

So, we get that

$$C_{i,i+1}(\rho_{E_j}) = 2\left| \Psi_{i+1}^{(j)} \Psi_i^{(j)} \right|. \tag{3.2.20}$$

Using the Hellmann-Feynman theorem[1], and the symmetry properties of the Hamiltonian, we find that

$$\frac{\partial E_j}{\partial \alpha} = 2J \left\langle \Psi_{E_j} \middle| \sigma_1^+ \sigma_2^- \middle| \Psi_{E_j} \right\rangle. \tag{3.2.21}$$

From the expression for the reduced density matrix $\rho^{(i,i+1)}$ given in Eq. (3.2.12), we see that when $\langle \sigma_i^+ \sigma_{i+1}^- \rangle = 0$ the reduced density matrix is diagonal and the bipartite entanglement is zero. Moreover, from (3.2.21), when $\frac{\partial E_j}{\partial \alpha} = 0$ we have that $C_{12}(\rho_{E_j}) = 0$.

So, we find that the concurrence between the first two spins in the eigenstate $|\Psi_{E_j}\rangle$ is given by a simple relation of the energy derivative with the boundary control coupling strength αJ

$$C_{12} = \left| \frac{1}{J} \frac{\partial E_j}{\partial \alpha} \right|. \tag{3.2.22}$$

We are interested in the relationship between localization and entanglement for the whole one spin excitation spectrum. In particular, we want to show that the bipartite entanglement of a given eigenstate, which is a local quantity, between the boundary control site and its first neighbor detects the type of localization that the eigenstate possesses.

---

[1] The Hellmann-Feynman theorem: $\frac{\partial E_\lambda}{\partial \lambda} = \langle \psi(\lambda) | \frac{\partial H_\lambda}{\partial \lambda} | \psi(\lambda) \rangle.$

Entanglement between boundary sites

C$_{1,2}(\rho_{E_1})$ & C$_{1,2}(\rho_{E_N})$

First, we proceed to analyze the concurrence of the minimal eigenenergy state, $C_{1,2}(\rho_{E_1})$ as a function of α, the behaviour of this quantity is shown in Fig. 3.2.8 for a chain of $N = 200$ spins. At first sight, we see clearly that $C_{1,2}(\rho_{E_1})$ is different from zero where $L_{IPR}(|\Psi_{E_1}\rangle)$ (see Fig. 3.2.6) is noticeable, and that $C_{1,2}(\rho_{E_1}) \to 0$ when the eigenvalue enters into the band and, consequently, the eigenstate becomes extended.

So, when the minimal eigenenergy state is extended for $\alpha < \alpha_c$, the two first spins are disentangled and $C_{1,2}(\rho_{E_1}) = 0$ consistently with $\frac{\partial E_1}{\partial \alpha} = 0$ from (3.2.22). At the critical point α_c, the state starts to become localized increasing its degree of localization when $\alpha \gg \alpha_c$; in the same way, the pair of spins starts to became entangled with each other and almost disentangled from the rest of the chain, i.e. $C_{1,2}(\rho_{E_1}) \sim 1$.

Actually, the data shown in Fig. 3.2.8 corresponds too to $C_{1,2}(\rho_{E_N}(\alpha))$, this can be seen by the following argument.

As in the case of the IPR, the concurrence C_{12} for eigenstates with symmetrical eigenenergies with respect to zero (E_j and E_{N-j+1}) is the same. From Eqs. (3.2.5) and (3.2.22), it is straightforward to demonstrate the latter statement where

$$C_{12}(\rho_{E_j}) = C_{12}(\rho_{E_{N-j+1}}), \quad j = 1, \dots, M, \qquad (3.2.23)$$

since

$$\frac{\partial E_j}{\partial \alpha} = -\frac{\partial E_{N-j+1}}{\partial \alpha}. \qquad (3.2.24)$$

C$_{1,2}(\rho_{E_j})$

Following with the analysis of the entanglement between the first two spins in the chain for the minimal energy eigenstate, we calculate the concurrence of the states with energies inside the bands. Fig. 3.2.9 shows $C_{12}(\rho_{E_j})$ as a function of α for $j = 2, \dots, M$. Note that the same scenario is observed for $C_{12}(\rho_{E_j})$ with $j = N - 1, \dots, M + 1$.

From Fig. 3.2.9, and calling α_i^m the abscissa where $C_{12}(\rho_{E_i}(\alpha))$ has its maximum, we observe that $\alpha_{\frac{N}{2}}^m < \dots < \alpha_2^m$ and $C_{12}(\rho_{E_{\frac{N}{2}}}(\alpha_{\frac{N}{2}}^m)) > \dots > C_{12}(\rho_{E_2}(\alpha_2^m))$. This observation suggests that the ordering of the maximum
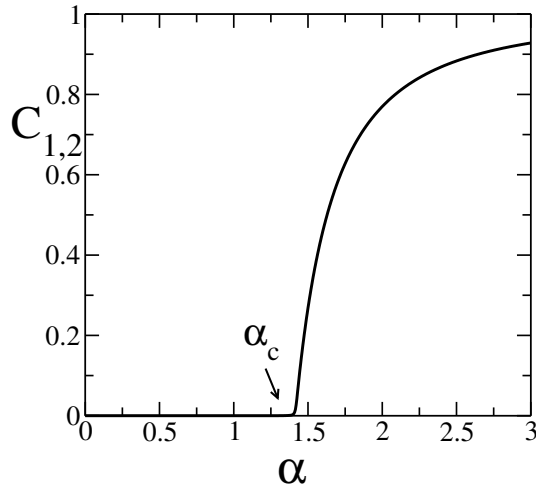
Figure 3.2.8:   Entanglement between the first spin (the boundary control site) and its nearest neighbor for the eigenstate of the minimal eigenenergy E_1. It is measured by the concurrence $C_{1,2}(\rho_{E_1})$ as a function of α in a chain of $N = 200$ spins. When the state is localized, $\alpha > \alpha_c$, spins 1 and 2 are also entangled. Before the critical point($\alpha \leq \alpha_c$) when the state is extended, $C_{1,2}(\rho_{E_1}) = 0$ consistently with $\frac{\partial E_1}{\partial \alpha} = 0$ for $\alpha \leq \alpha_c$.

of the concurrence C_{12} for the different eigenstates follows closely the ordering dictated by the amount of localization of these eigenstates, *ie.* only the most localized states around the boundary control site have a noticeable entanglement. We will use this observation as a guide to formulate a transmission protocol in the next Sec. 3.2.4.

As we have shown, the concurrence and the derivative of the energy are related in a simple way, see (3.2.22). On the other hand it is well known that the eigenvalues $E_i(\alpha)$ inside the band are rather insensitive to changes in α, indeed $\frac{\partial E_i(\alpha)}{\partial \alpha} \simeq 0$ almost everywhere, *except* near an avoided crossing with another eigenvalue. In this sense, the behaviour shown by the concurrence in Fig. 3.2.9 reflects the presence of successive avoided crossings between $E_1(\alpha)$ and $E_2(\alpha)$, between $E_2(\alpha)$ and $E_3(\alpha)$, and so on. The abscissa of the peak in the concurrence of a given eigenstate roughly corresponds to the point where the eigenvalue becomes almost degenerate.

As a matter of fact, the scenario depicted in Fig. 3.2.9 is not only a manifestation of the avoided crossings in the spectrum, indeed it can be considered as a precursor of the resonance state that appears in the system when $N \rightarrow \infty$.
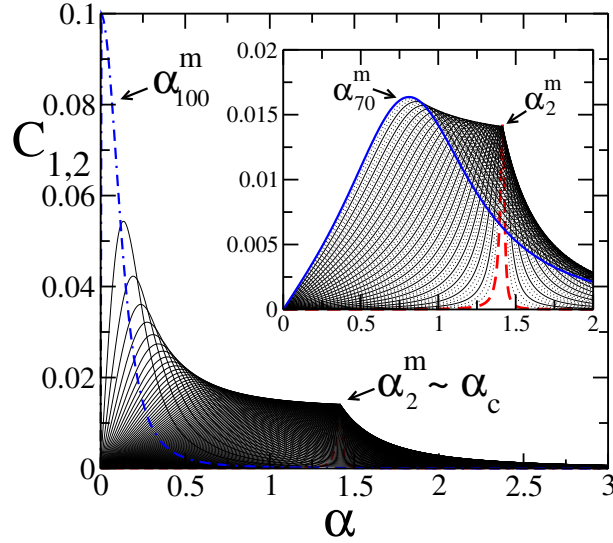
Figure 3.2.9: Concurrence $C_{12}(\rho_{E_j}(\alpha))$ as a function of the boundary control strength α, for $j = 2, 3, \ldots, 100$. The results belong to a chain of $N = 200$ spins. Each curve $C_{12}(\rho_{E_j}(\alpha))$ has a single peak. The peaks are ordered by eigenenergy, the rightmost peak corresponds to $C_{12}(\rho_{E_2}(\alpha))$ (red dashed line), the peak to its left corresponds to $C_{12}(\rho_{E_3}(\alpha))$, and so on. The leftmost peak corresponds to the curve with the highest eigenenergy shown in the figure, E_{100} (blue dashed-dotted line), belong to the energy of the center of the band. The inset shows the concurrence $C_{12}(\rho_{E_j}(\alpha))$ for $j = 2, \ldots, 70$

Recently, Ferrón *et al.* [42] have shown how the behaviour of an entanglement measure can be used to detect a resonance state. In a chain a resonance state appears in the limit $N \to \infty$, however the peaks in the concurrence obtained for N large, but finite, can be used to obtain approximately the energy of the resonance state [42, 88].

For completeness, we show $C_{12}(\rho_{E_i}(\alpha))$ for a shorter chain of $N = 40$ spin in Figs. 3.2.10(a)-3.2.10(c). The qualitative analysis made above for $N = 200$ is also valid here.

Because bipartite entanglement is a local quantity while IPR is global, we are interested to know how is the behavior of the bipartite entanglement of other pairs of spins and what features of C_{12} remain or not when looking at some pair of spins $(i, i+1)$. From Eq. (3.2.20), $C_{i,i+1}(\rho_{E_j}) = 2\left|\Psi_{i+1}^{(j)}\Psi_i^{(j)}\right|$,

we observe that the concurrence is directly proportional to the site-coefficient of the eigenstate. Due to the spatial localization of the eigenstates on the boundary control site (see Fig. 3.2.5). The coefficients $\left|\Psi_i^{(j)}\right|$ relatively far from the boundary control site are almost null,

$$\left|\Psi_i^{(j)}\right| \sim 0, \text{ for } i \gg 1.$$

Therefore, we can conclude that pairs of spins located far from the boundary control site are weakly entangled. For this reason, we restrict our attention to C_{23}, *i.e.* the first pair on the chain that does not include the boundary control site (see the above panels in Fig.3.2.10).

$C_{1,2}(\rho_{E_j})$ and $C_{2,3}(\rho_{E_j})$

Comparing the behaviour of $C_{1,2}(\rho_{E_j}(\alpha))$ and $C_{2,3}(\rho_{E_j}(\alpha))$ we can recognize similarities and differences:

Figures 3.2.10(a) and 3.2.10(d) show the concurrence for the eigenstate with the lowest energy, E_1. Both pairs of spins are disentangled when $0 < \alpha \lesssim \alpha_c$. For $\alpha \gtrsim \alpha_c$, the eigenstate is exponentially localized on the border sites and because of that, the entanglement between these sites increases (like display in Fig. 3.2.5 but taking into account that there it is for $N = 200$). But for stronger boundary control coupling strength, $\alpha > \alpha_c$, the eigenstate is even more localized in the border causing maximal entangled $C_{1,2}(\rho_{E_1})$, and a decrease of $C_{2,3}(\rho_{E_1})$. Therefore, for these coupling strengths, $C_{1,2}(\rho_{E_1}) > C_{2,3}(\rho_{E_1})$.

Figures 3.2.10(b), 3.2.10(c), 3.2.10(d), and 3.2.10(e) show the concurrence for the eigenstates with energies E_j ($j = 2, ..., \frac{N}{2}$). Both $C_{1,2}(\rho_{E_j}(\alpha))$ and $C_{2,3}(\rho_{E_j}(\alpha))$ attain their maximum values in the region $0 < \alpha \lesssim \alpha_c$. Calling α_j^m the abscissa of the concurrence maximum related to the state ρ_{E_j}, we observe the following order

$$\alpha_2^m > ... > \alpha_{\frac{N}{2}}^m \text{ for } C_{1,2};$$

and something more complicated

$$\alpha_2^m > ... > \alpha_{13}^m, \ \alpha_{14}^m = ... = \alpha_{17}^m = 0 \text{ and } \alpha_{18}^m > \alpha_{19}^m > \alpha_{20}^m > 0 \text{ for } C_{2,3}.$$

While the maximum values of $C_{1,2}(\rho_{E_j}(\alpha_j^m))$ increase with j, $C_{2,3}(\rho_{E_j}(\alpha_j^m))$ decreases with j until $j = 17$.
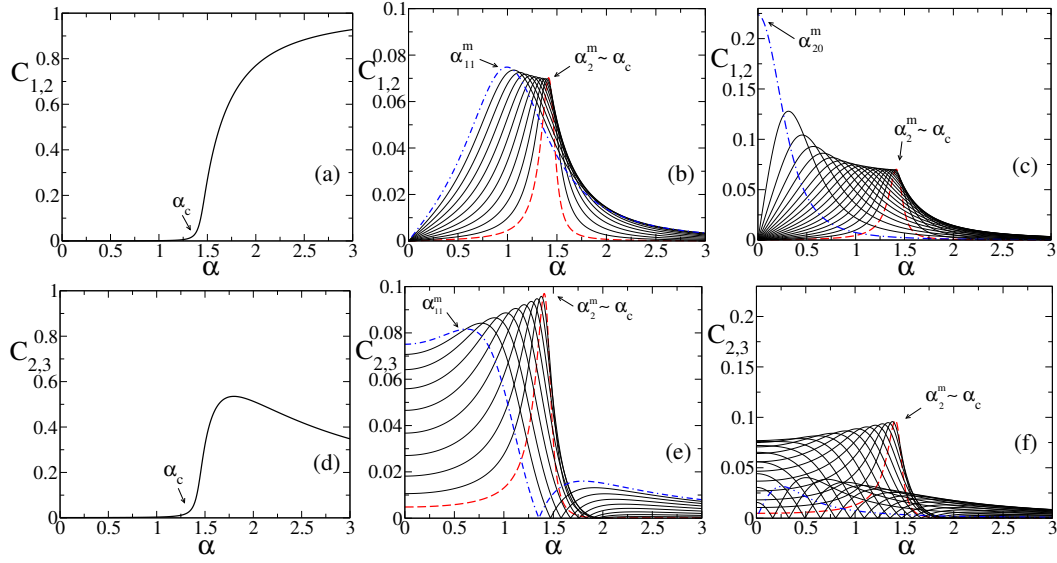
Figure 3.2.10: Bipartite entanglement of the eigenstates between nearest spin-sites measured by the concurrence in a chain of $N = 40$ spins. The upper panel (Figs. 3.2.10(a)-3.2.10(c)) shows the entanglement $C_{1,2}(\rho_{E_j}(\alpha))$, *ie.* between the first spin (the boundary control site) and its nearest neighbor, for each eigenstate related with its reduced density matrix ρ_{E_j}: **(a)** $C_{1,2}(\rho_{E_1}(\alpha))$, **(b)** $C_{1,2}(\rho_{E_j}(\alpha))$ for $j = 2, ..., 11$. Each curve has a single peak ordered by eigenenergy, the rightmost peak corresponds to $C_{12}(\rho_{E_2}(\alpha))$ (red dashed line), the peak to its left corresponds to $C_{12}(\rho_{E_3}(\alpha))$, and so on. The leftmost peak corresponds to the curve with the highest eigenenergy shown in the figure, E_{11} (blue dashed-dotted line). **(c)** $C_{1,2}(\rho_{E_j}(\alpha))$ for $j = 2, ..., 20$. Here the curve with the highest eigenenergy is E_{20} (blue dashed-dotted line); while the panel above (Figs. 3.2.10(d)-3.2.10(f)) shows the entanglement $C_{2,3}(\rho_{E_j}(\alpha))$: **(d)** $C_{2,3}(\rho_{E_1}(\alpha))$, **(e)** $C_{2,3}(\rho_{E_j}(\alpha))$ for $j = 2, ..., 11$, (f) $C_{2,3}(\rho_{E_j}(\alpha))$ for $j = 2, ..., 20$. We compare in detail $C_{1,2}$ and $C_{2,3}$ in the text.

Last, we stress two differences. The first one is, since that, at $\alpha = 0$ the boundary control site ($i = 1$) is uncoupled to the chain, it is also disentangled with the neighbor spin ($i = 2$), *i.e.* $C_{1,2}(\alpha = 0) = 0$. On the other hand, $C_{2,3}(\alpha = 0) > 0$ for any eigenstate with the only exception of the one with energy from the middle of the band, E_{20}. The second one is that, while $C_{1,2}(\rho_{E_j})$ attains only a single maximum, $C_{2,3}(\rho_{E_j})$ $j = 2, ..., 19$ have two single

maxima as a function of α, and between them, both spins are disentangled for some value of α. Only $C_{2,3}(\rho_{E_{20}})$ starts disentangled at $\alpha = 0$ and then attain only a single maximum.

3.2.4 Dynamical localization of the total state

We want to understand now, how these, previously discussed, localization properties of the eigenstates, are manifested in the dynamical evolution of the total state of the system; and how they affect the transmission of states. For that, we consider as initial state of the system one single excitation situated on the first site of the spin chain, *ie.* $|\psi(t = 0)\rangle = |\mathbf{1}\rangle$. This state evolves in time, $|\psi(t)\rangle$, under the action of the Hamiltonian of the system (2.1.7).

We calculate again the inverse participation ratio (3.2.9) but, this time, the L_{IPR} of the total state of the system $L_{IPR}(|\psi(t)\rangle)$. In Fig. 3.2.11, we show it for a spin chain of $N = 200$ and for different values of α. We can distinguish, at least, four well defined dynamical behaviours, each one associated to the number of localized states in the system observed in Fig. 3.2.6.

- Fig. 3.2.11(a) is for $\alpha = 0.1$ where the system has only two double <u>highly localized</u> eigenstates at the center of the band[2], one of them being almost maximally localized;

- Fig. 3.2.11(b) is for $\alpha = 0.4$ where there are <u>several localized</u> eigenstates, but not so strongly localized;

- Fig. 3.2.11(c) is for α_J, the homogeneous chain, where all of the eigenstates are <u>equally localized</u> (3.2.10);

- Fig. 3.2.11(d)-(e) are for $\alpha \sim \alpha_c$ near the transition zone and, finally,

- Fig. 3.2.11(f) is for $\alpha = 3$ where the system has <u>exponentially localized</u> eigenstates.

Initially, the state is totally localized, since $L_{IPR}(|\mathbf{1}\rangle) = 1$. With the time, and because of the interactions between the spins, the state begins to delocalize. The excitation of the first spin begins to spread on to the other spins [34]. How and how much is this dispersion, depends on the value of α; the more dispersion, the more delocalized is the state. What we also observe in Figs. 3.2.11(b)-3.2.11(e) is that, at some time, the state is relocalized, not totally, but at least partially. From the behaviour of L_{IPR}, we can not dis-

---

[2]For odd N, because of the symmetry, there is a single highly localized eigenstate.
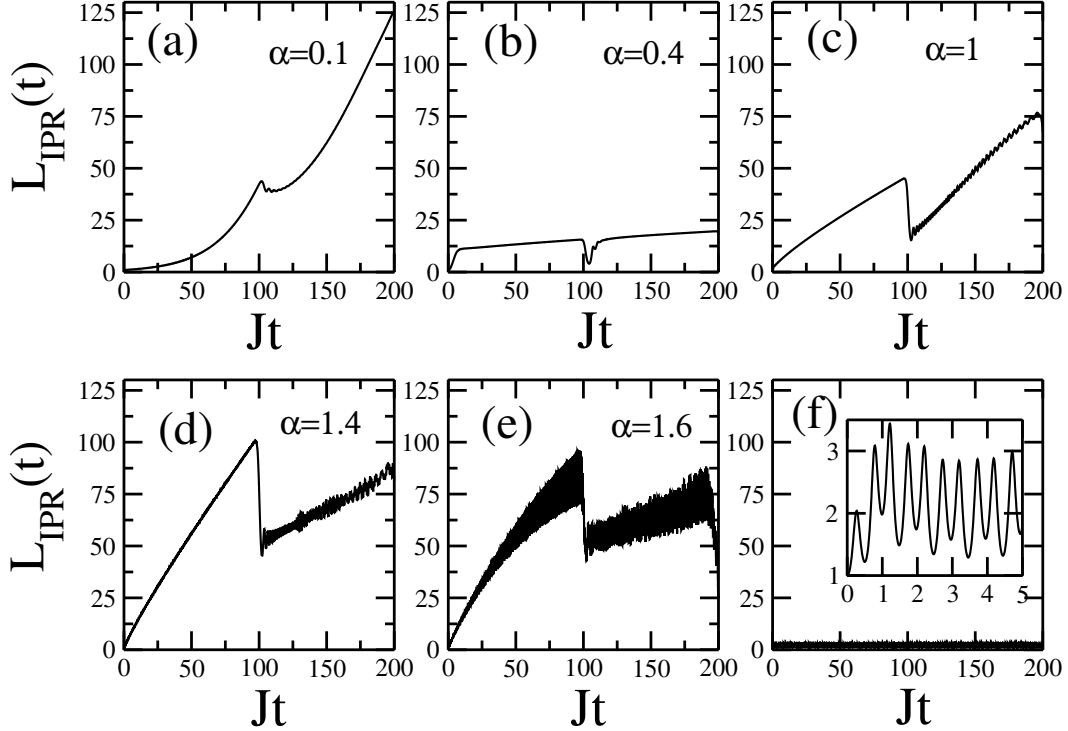
Figure 3.2.11: Dynamical behaviour of L_{IPR} vs. Jt, for different values of α. (a) $\alpha = 0.1$, (b) $\alpha = 0.4$, (c) $\alpha = 1$, (d) $\alpha = 1.4$, (e) $\alpha = 1.5$, and (f) $\alpha = 3$. In all the cases $|1\rangle$ is the initial condition. The inset in (f) shows the small oscillations that characterize the behaviour of L_{IPR} for $\alpha = 3$, in this case the state of the system is localized even for very long times. In (f) the initial excitation goes back and forth between the boundary control site and the rest of the chain with a frequency given, basically, by the energy difference between the two lowest eigenenergies. The steep change near $t_M^h \sim 100 = \frac{N}{2J}$, that can be observed in all the panels except in (f), signals the "arrival" of the excitation at the end of the chain. Note that the refocusing, *ie.* that the value of L_{IPR} drops, is different in each regime, but in (b) the refocusing leads to $L_{IPR} \sim O(1)$. The results are for a chain with $N = 200$.

Looking at the homogeneous chain (Fig. 3.2.11(c)), we observe how the

state begins to linearly delocalize, this trend continues in a semi-infinite chain because there is nothing to stop it; but, when the chain has a finite size, the excitation is spreading but now, this spread has a limit: the end of the chain. The presence of this border causes a partial relocalization of the initial state, but now, at the other end of the chain. What is more, this makes sense, since the time where this relocalization happens is precisely the mesoscopic time of this system $t_M^h = \frac{N}{2J}$.

Once we are convinced that this relocalization indicated by L_{IPR} means that we can recover on the last spin, at least partially, the initial state of the first spin just from the point of view of the transmission of quantum states, what we should be looking for is a value of α that minimizes L_{IPR} at the corresponding mesoscopic time, $L_{IPR}(t_M^\alpha) \sim 1$. In that sense, from Fig. 3.2.11, we observe a favorable regime for state transmission in 3.2.11(b) where, as we have already mentioned, the system has several localized eigenstates. This regime seems to be the least dispersive and the best in the transmission at comparatively short times, namely $\sim t_M^h$. Therefore, we want to explore more this interesting and promising regime. But before that, it is worth mentioning why the behaviour of L_{IPR} looks so different on Figs. 3.2.11(a) and 3.2.11(f).

For large values of α, such as in 3.2.11(f), the system has exponentially localized eigenstates, that produce that the initial state remains spatially localized (on the first spin site) even for very long times. This dynamical regime has been proposed to store quantum states [7] and, more generally, this kind of states with isolated eigenvalues has been proposed as a possible scenario to implement practically a stable qubit [73].

For α quite small, such as in 3.2.11(a), the relocalization of the state happens, but only at long time. Figure 3.3.2(a) shows that nearly total relocalization takes place at times around $t_M \sim \frac{3N}{2J}$ when $N = 200$. Even more, there is a relationship between the value of α and the time where the relocalization happens. For smaller α, the time increases notably while the refocusing is improved (data do not shown). It can be shown that this regime with $\alpha \sim 0$, where the system has only two (or one for odd N) highly localized eigenstates, is also suitable and interesting for state transmission. The only disadvantage of this regime is that the transmission is achieved only at very long time. We will come back to this point later.

3.3 Two boundary control coupling channel

We use the regime identified in Fig. 3.2.11(b) to implement the simplest transmission protocol, as proposed by Bose [15, 16] that we have already described in Sec. 2.2.3.1, and the transmission of an entangled state. But, as our results suggest and from the knowledge that mirror symmetry in the exchange couplings ($J_i = J_{N-i}$) is a favorable condition to improve the state transfer [1, 60, 115, 61, 62], we consider a second boundary control coupling at the end of the chain where the transmission should be detected.
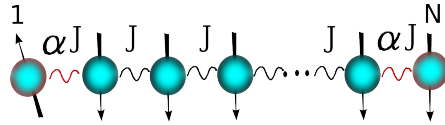
Figure 3.3.1: Spin chain system with two boundary control couplings.

So, the Hamiltonian that describe this system is

$$H^\alpha = -\frac{1}{2}\sum_{i=1}^{N-1} J_i(\sigma_i^x \sigma_{i+1}^x + \sigma_i^y \sigma_{i+1}^y), \quad \text{with} \quad \begin{cases} J_1 = J_{N-1} = \alpha J \\ J_i = J \;\; i = 2, ..., N-2 \end{cases}$$

$$(3.3.1)$$

3.3.1 Dynamical localization of the total state

Considering a boundary control coupling at the end of the chain introduces a set of localized states around this site. The overall properties of the spectrum do not change, however the presence of localized states at the end of the chain would facilitate the transmission of states (or entanglement) from one end of the chain to the other.

To observe it, as an example, Fig. 3.3.2 and Fig. 3.3.3 show how the behaviour of $L_{IPR}(t)$ changes when a symmetrical boundary control coupling is considered at the ends of a chain with $N = 200$. When $\alpha = 0.1$, the refocusing of the state happens noticeably faster when two boundary control couplings are considered than with only one. Instead, when $\alpha = 0.35$, the improvement is noticed in the stronger refocusing of the state.

We explored the behaviour of $L_{IPR}(t)$ for larger values of α, but there are no significant changes for $\alpha \gtrsim 1$ (not shown). The information provided by Fig. 3.3.3 sheds light on our presumption that for boundary control couplings
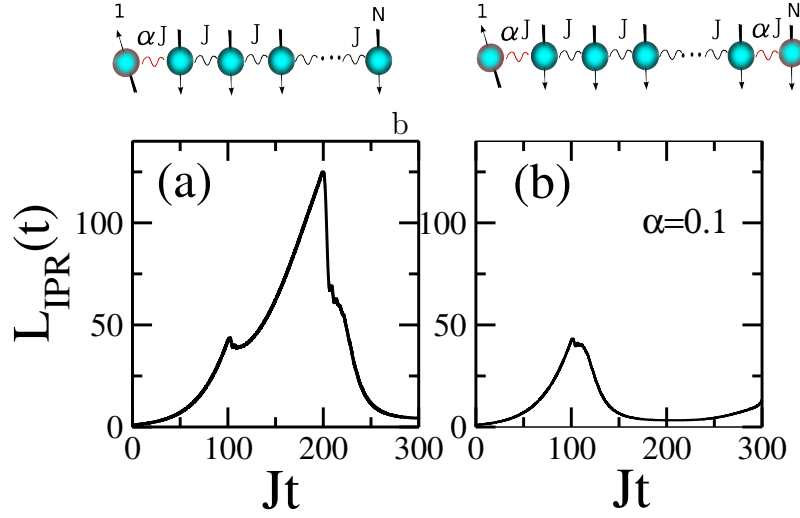
Figure 3.3.2: Dynamical behaviour of $L_{IPR}(t)$ in a chain of $N = 200$ spins with (a) one boundary control coupling $J_1 = \alpha J$, and (b) two symmetrical boundary control couplings $J_1 = J_{N-1} = \alpha J$. In the figure, the boundary control coupling strength is αJ with $\alpha = 0.1$.
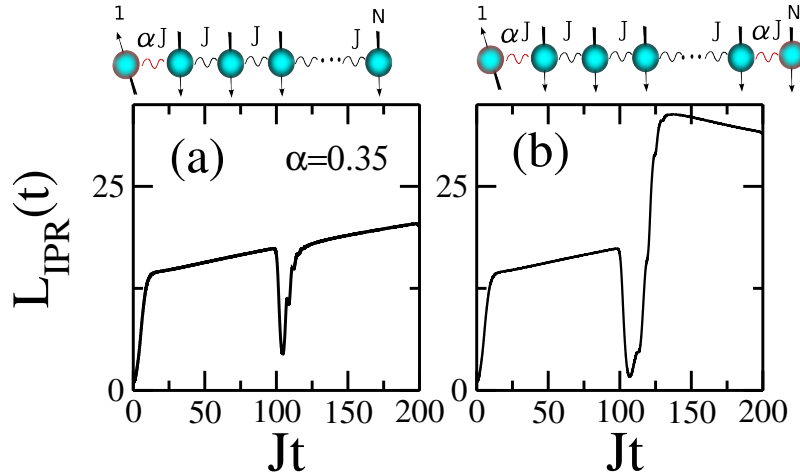

Figure 3.3.3: Dynamical behaviour of $L_{IPR}(t)$ in a chain of $N = 200$ spins with (a) one boundary control coupling located on the first site of the chain ($i = 1$) and (b) two symmetrical boundary control couplings $J_1 = J_{N-1} = \alpha J$. In the figure, the boundary control coupling strength is αJ with $\alpha = 0.35$ and the refocusing time is $t \sim \frac{N}{2J}$.

with strength $0.3 \lesssim \alpha < 1$ there is an *optimal regime for state transfer.*

3.3.2 Transmission of states and entanglement

In the simplest protocol of transmission (as described in [15] and Sec. 2.2.3.1) the initial state, $|1\rangle$ evolves following the Hamiltonian dynamics, and the quality of the transmission is measured by the fidelity (2.2.7)

$$\mathcal{F}_{1,N} = \langle 1|\rho_N(t)|1\rangle, \tag{3.3.2}$$

where $\rho_N(t)$ is the state at the end of the chain where the transmission is received, and t is the "arrival" time.

For the transmission of an entangled state the protocol is slightly different, again we follow the protocol described in [15]. Using an auxiliary qubit A, and the first spin of the chain, one of the Bell states (2.1.10)

$$|\psi^+\rangle = \frac{1}{\sqrt{2}}(|1_A 0_1\rangle + |0_A 1_1\rangle) \tag{3.3.3}$$

is prepared. After the preparation of the initial state the system evolves accordingly with its Hamiltonian and the concurrence between A and the spin at the receiving end of the chain, $C_{A,N}(t)$, is evaluated.
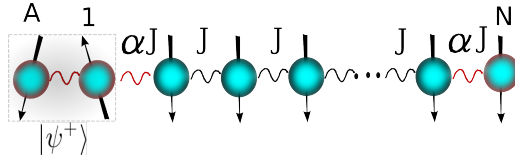
Figure 3.3.4: Spin chain with an entangled state $|\psi^+\rangle$ prepared on the auxiliary qubit A and the first spin in the chain.

In Fig. 3.3.5 we show the fidelity for the simplest transmission protocol and the concurrence between the auxiliary qubit and the last spin of the chain, both as functions of the time. We consider a chain of $N = 200$ spins and boundary control coupling strength of $\alpha = 0.4$. The maximum value of the fidelity and the concurrence are remarkably high. Just to compare, we obtain $C_{max} \simeq 0.9$ for $\alpha = 0.4$, while for the homogeneous XY chain (*ie.* $\alpha = 1$) we obtain $C_{max} \simeq 0.44$, and for an unmodulated Heisenberg chain (with 200 spins) $C_{max}^{un} \simeq 0.23$ [15, 16]. It is worth to remark that this large value of the

fidelity is not necessarily the largest possible obtainable tuning adequately the value of α.

As a matter of fact, that a chain with two symmetrical boundary control couplings outperforms a homogeneous one as a transmission device has been already reported in [109]. In that work, Wójcik *et al.* analyzed the transmission of quantum states focusing in the regime $\alpha \to 0$ where as we have already mentioned, nearly perfect transfer is achieved but at really long times. In Sec. 3.3.3.1, we briefly describe these results. Here, we extend their results showing that the transfer of quantum states is feasible for shorter transfer times with a very good fidelity ($\mathcal{F} \gtrsim 0.8$) while keeping the linear scaling between the transfer time and the length of the chain. To achieve this transfer scenario we exploit the information provided by the IPR: for large enough values of α there is a time of order $\frac{N}{2J}$ such that $L_{IPR} \sim 1$.
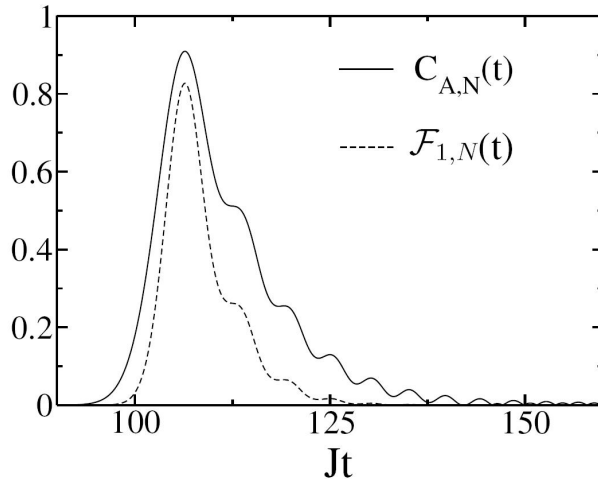
Figure 3.3.5: The concurrence, $C_{A,N}$ (solid black line) and the fidelity $\mathcal{F}_{1,N}$ (dashed black line) vs. Jt for a XY interaction chain of $N = 200$ spins and two symmetrical boundary control couplings αJ, with a coupling strength $\alpha = 0.4$.

The identification of regimes where the transmission of quantum states can be achieved with large fidelity and for (relatively) short times is of great importance. The different dynamical regimes of the fidelity in a chain with two boundary control couplings is rather difficult to analyze except when $\alpha \to 0$, see [109]. Figure 3.3.7 and 3.3.6 show the complex landscape of the fidelity of transmission versus the strength of the boundary control couplings and time.

Some of these dynamical features of state transfer are best understood using the IPR. In particular, for α fixed, the first maximum of the fidelity as a function of the time coincides with a minimum of L_{IPR}. This observation, once systematized, provides the dynamical regime where the transmission can be achieved with large fidelity and *always* for times $\sim \frac{N}{2J}$.
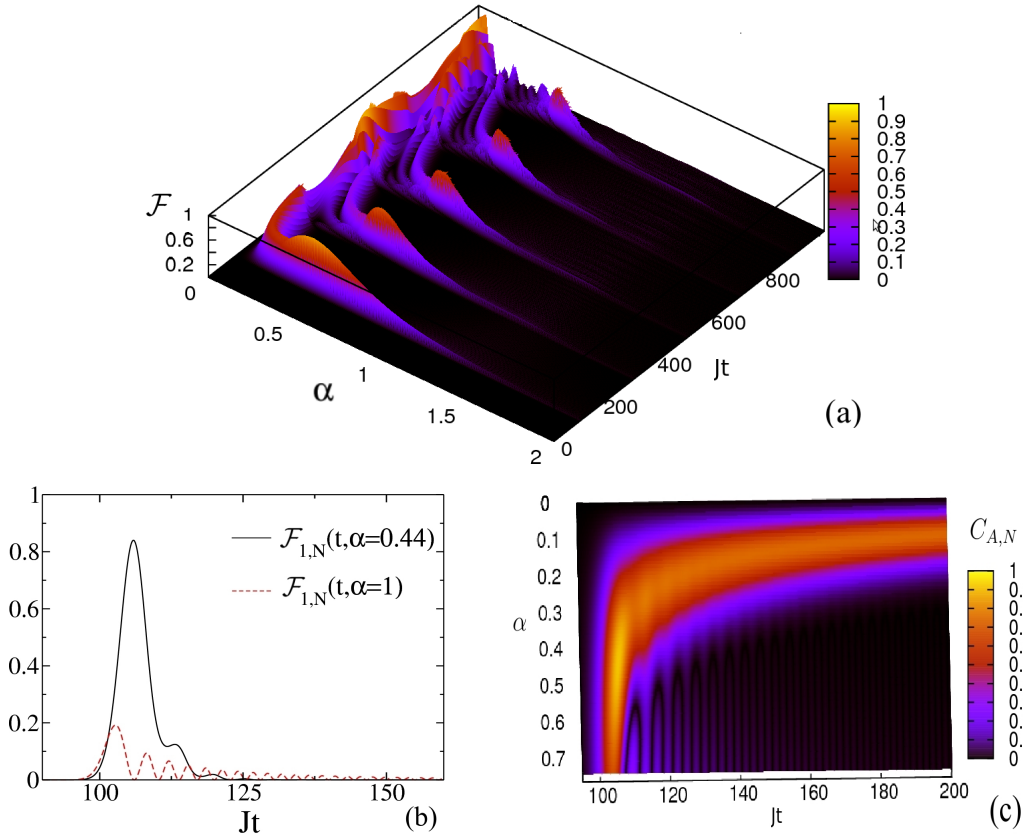
3.3.3 Optimal regime for state transfer

Figure 3.3.6: (a) The fidelity of transmission $\mathcal{F}$ as a function of the strength of the boundary control couplings α and time t for a chain with $N = 200$ spins. The dynamical behavior can be compared with the previous results already shown and discussed for $N = 200$. In (b) we compare the performance of the unmodulated XX spin chain ($\alpha = 1$) with the same system with two optimal boundary control couplings ($\alpha_{opt} = 0.44$). In (c) the concurrence $C_{A,N}(\alpha, Jt)$.
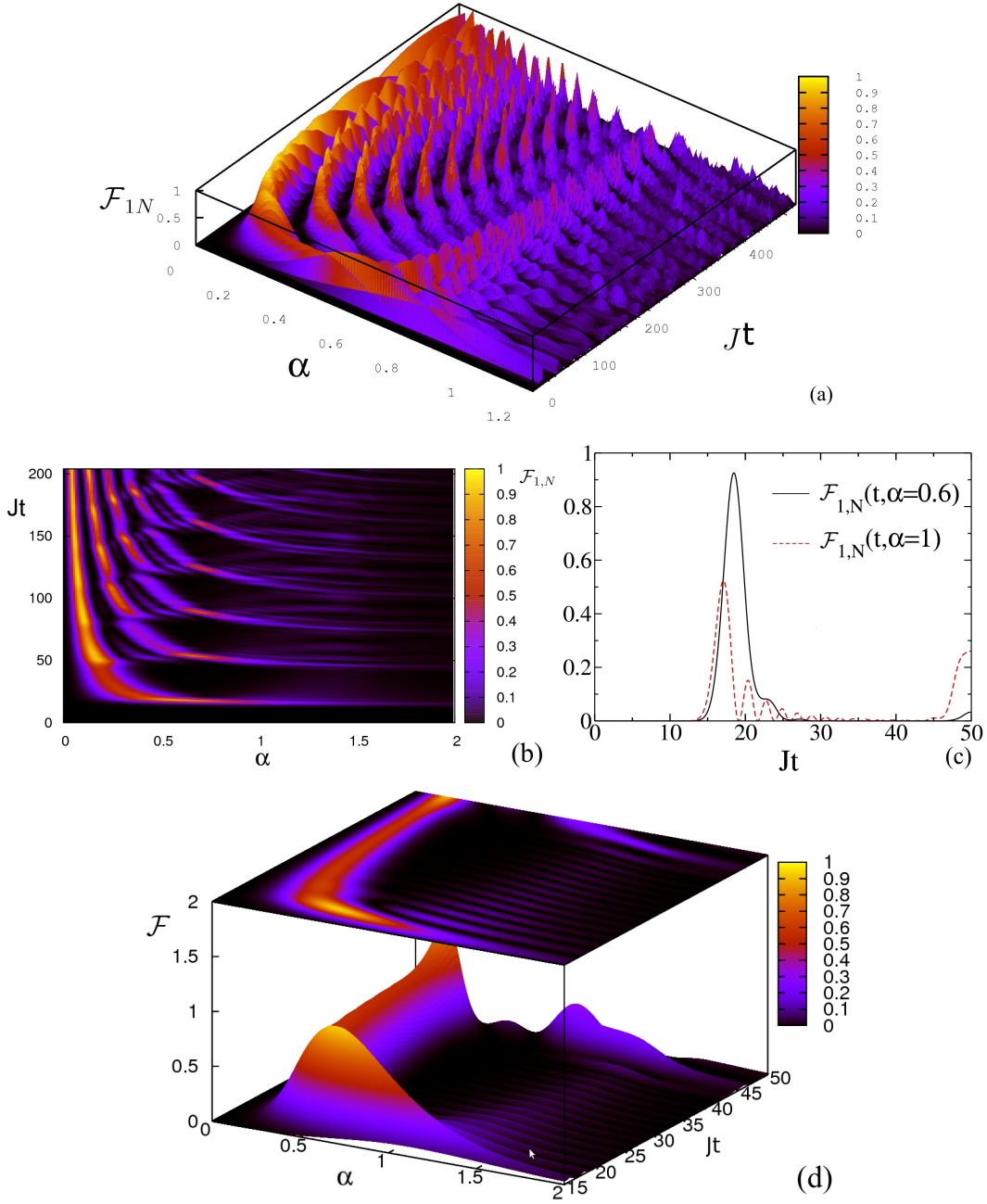
Figure 3.3.7: (a),(b) and (d) The fidelity of transmission $\mathcal{F}$ as a function of the strength of the boundary control couplings α and time t. We emphasize in the large transmission fidelity attained at an early time. For a chain of $N = 31$ spins, $\mathcal{F} \simeq 0.92$ for $\alpha \simeq 0.6$ at time $t \simeq 18.5 \sim \frac{N}{2J}$. In (c) we compare the performance of the unmodulated XX spin chain ($\alpha = 1$) with the same system with two optimal boundary control couplings ($\alpha_{opt} \simeq 0.6$).

Our results about the time behaviour of the IPR show that for $t_{IPR} \sim \mathcal{O}(\frac{N}{2J})$ there is always a local minimum (see Figs. 3.2.11 (b) and 3.3.3). We have already identified this minimum as a sign that the state has been transferred. The smaller the value of the minimum, the better is the quality of the transfer. Noticing that in this region the time t_{IPR} is rather independent of α, we should optimize the value of α in order to minimize the value of the minimum of the IPR at times $\sim t_{IPR}$ in order to allow us to find the best fidelity achievable for time $t^{\alpha_{opt}} \sim t_{IPR}$. We call $\alpha_{opt}(N)$ the value such that the fidelity $\mathcal{F}(t^{\alpha_{opt}})$ attains its maximum for a given N and for

$$t^{\alpha_{opt}} \sim \frac{N}{2J}. \qquad (3.3.4)$$

As Figs. 3.3.5, 3.3.6 and 3.3.7 show, when the transfer of a given state takes place the fidelity shows a well defined maximum at time $t^{\alpha_{opt}} \sim t_{IPR} \sim \mathcal{O}(\frac{N}{2J})$. The height of the maximum, $\mathcal{F}_{max}$ is a smooth function of α for $\alpha > 0.3$, and the same is valid for the transfer time $t^{\alpha_{opt}}$.
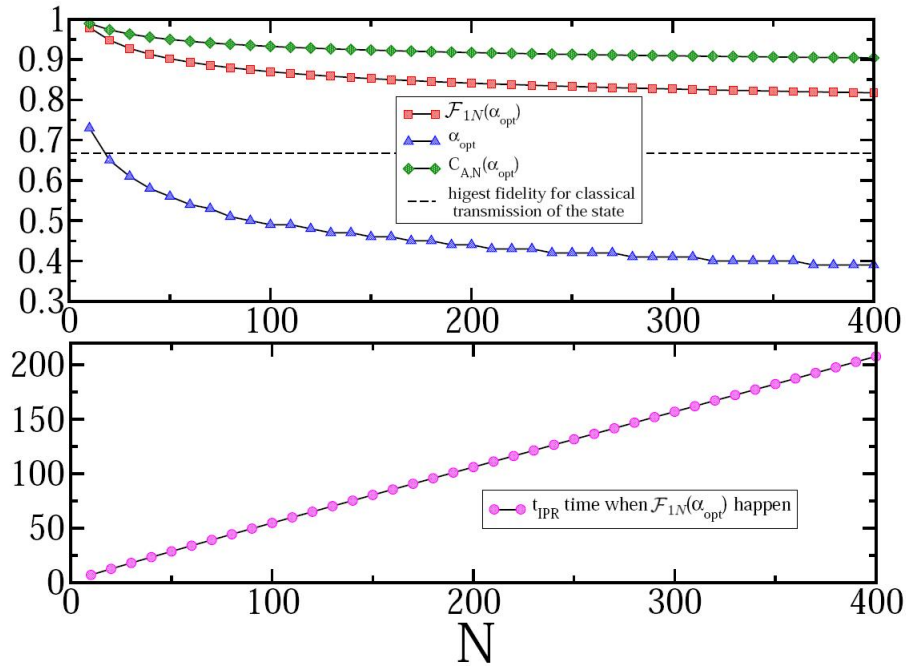
Figure 3.3.8: The data shown in the upper panel corresponds to the maximum fidelity of transmission achievable for times $t^{\alpha_{opt}} \sim t_{IPR} \sim \mathcal{O}(\frac{N}{2J})$ for different chain lengths N (squares), $\alpha_{opt}(N)$ (triangles) and the concurrence $C_{A,N}$(diamonds). The protocol of transmission is described in the text and in Sec. 2.2.3.1.

Figure 3.3.8 summarizes our findings about the fidelity of transmission following the recipe outlined in the two paragraphs above. The upper panel shows the maximum transmission fidelity achievable for a chain of length N and the corresponding optimum value of α. Fitting these numerical data, we obtain that $\alpha_{opt} \simeq 1.06 N^{-\frac{1}{6}}$. As can be appreciated, $\mathcal{F} \gtrsim 0.8$ even for $N = 400$. The maximum value of the fidelity is also well above the one predicted for an unmodulated chain, and above $\frac{2}{3}$, that is the highest fidelity for classical transmission of a quantum state as shows Fig. 2.2.3. The lower panel shows the transmission time $t^{\alpha_{opt}}$ vs. N. The linear scaling of $t^{\alpha_{opt}}$ with N is rather clear and the fit gives us

$$t^{\alpha_{opt}} \simeq 1.05 \frac{N}{2J}. \qquad (3.3.5)$$
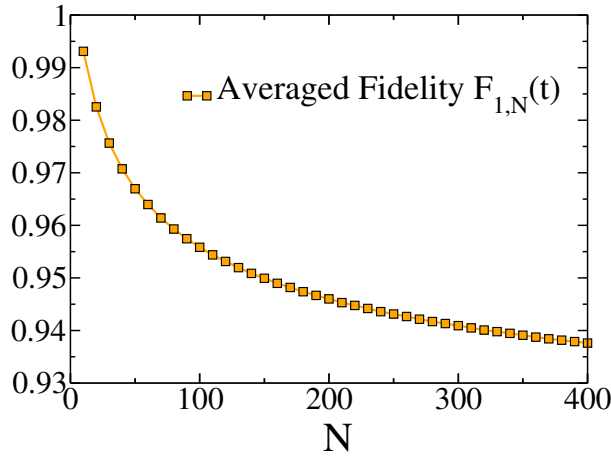
Figure 3.3.9: The maximum averaged fidelity F of Eq. (2.2.8) of the state transmission along a chain of N spins with homogeneous XX interactions but with two *optimal boundary control couplings* $\alpha_{opt} J$. The corresponding values for the transfer time $t^{\alpha_{opt}}(N)$ and $\alpha_{opt}(N)$ are shown in Fig. 3.3.8.

3.3.3.1 Weak boundary coupling regime for state transfer

Finally we want to remark that another focus of our work was the very weak boundary coupling regime, $\alpha \sim 0$, but we do not show our results because in the course of our investigation we found that it had already been studied in detail by Wojcik *et al.* [109]. However, we want to shortly summarize here their results about this interesting and useful regime.

When $\alpha J \ll \frac{1}{\sqrt{N}}$, an almost perfect state transfer is achieved, with $F \approx 1 - \mathcal{O}(\alpha^2 J_{max}^2 N)$ considering $|1\rangle$ as the initial state. The performance of the state transfer has a strong dependence on the parity of N. For even (odd) N the dynamic of the system is dominated by two (three) eigenstates that belong to the energies in the middle of the energy spectrum[3]. The energy differences between these dominant levels determine the transfer time, which is obtained as $t_{M,even}^{\alpha_0} = t_{even}^{\alpha_0} \sim \frac{\pi}{2\alpha^2 J_{max}}$ and $t_{M,odd}^{\alpha_0} = t_{odd}^{\alpha_0} \sim \frac{\pi\sqrt{N}}{2\alpha J_{max}}$.

We will return later to consider these systems in Chap. 5 when we study some other aspects of this nice regime for state transfer.

3.4 Discussion

We have studied the effects produced on the homogeneous system when a boundary control coupling is considered. We first analyzed system properties such as energies and eigenstates. We show that the bipartite entanglement of the eigenstates, between the boundary spin and its first neighbor, is proportional to the derivative of the energy with respect to the boundary coupling. Because of this, an analysis of the entanglement, trough the concurrence, as a function of the strength of the boundary coupling, put on evidence the presence of avoided crossings in the energy spectrum.

We also analyzed the localization of the eigenstates, using the inverse participation ratio, distinguishing in this way different regimes in terms of the localization degree and the share of eigenstates that are simultaneously localized. In particular, we distinguish that, while a large boundary-coupling produces exponential localization in some eigenstates, weak boundary-coupling produces localization on the boundary-site. These regimes, with different kinds of localized eigenstates, show also strong differences in the transmission of states.

With the analysis of the inverse participation ratio as a function of the time, we analyzed the dynamical localization of the total state. Exponentially localized eigenstates produce that the initial state remains spatially localized for very long times and can be used to store quantum states. In contradistinction, the regime with boundary-site localized eigenstates is suitable for quantum state transmission, since the transfer is notably improved in comparison with the homogeneous system. We considered two symmetrical boundary control

---

[3]An analysis with the IPR of the eigenstates shows two (three) eigenstates highly localized for even (odd) N.

couplings and implemented a protocol of transmission, studying the fidelity of transmission and the transmission of entanglement. We found an optimal regime for state transmission where the system transfer the state or the entanglement with high fidelity in a comparatively very short time. We found the optimal values of the boundary couplings for any chain length $\alpha_{opt} = 1.06N^{-\frac{1}{6}}$, and the corresponding transfer times, which scale linearly with N, are given approximately by $t^{\alpha_{opt}} = 1.05\frac{N}{2J} \sim t_M^h$.

We want to state here that, in parallel to our work, L. Banchi and *et. al.* arrived at similar results for the optimal regime but from a different approach. In their work [9], they consider the system (3.3.1) as non-interacting fermionic particles, they look for the conditions to have an approximately linear dispersion relation making the system less dispersive in its dynamics, achieving, in this way, a fast transmission with a good quality of transfer. The *optimal regime* is a very interesting finding that has recently lead to more works [10, 11, 121].

4 Transmission in completely engineered channels for perfect state transfer. Robustness of the transmission under perturbations.

We have already discussed about how relevant it is to find quantum systems that allow for state transfer without any dynamical manipulations during the transfer procedure, or with only minimal additional requirements. The motivation for this search is the need to avoid the introduction of errors or perturbations in the system. We recall that the advantage of these systems is that by not intervening in its dynamic evolution, the system remains almost decoupled from the environment, thus avoiding the decoherence of the state, *ie.* a consequent loss of information.

In the previous chapter, we studied and showed how local control of the boundary spin couplings in an initialized spin chain can cause a large enhancement of the transmission fidelity from one end of the chain to the opposite end [109, 119], without any dynamical intervention apart from the preparation and measurement of the state. It has been shown, also recently, that a similar scenario happens in an unpolarized chain [9, 113]. There are a number of very interesting possibilities if the handling of all the couplings in the chain is allowed. Even perfect state transfer can be achieved, by a proper engineering of the entire set of spin-spin couplings in the chain [1, 29, 60, 61].

Some chains able to transfer quantum states have been implemented experimentally, for example, using small numbers of spins in liquid state NMR [71, 78, 116, 117, 5] and slightly larger numbers of them in solid-state NMR [26, 94]. Spin defects in diamond seem to show a promising direction for near future implementations [76, 27, 112]. Important experimental challenges are posed by the lack of individual addressibility of the spins and, more importantly, by their vulnerability to decoherence [118]. Imperfections in the implementation of spin-chain systems also cause decoherence and were predicted to produce localization of the quantum information [28, 63, 25, 2] which was recently demonstrated experimentally [3].

Consequently, a successful characterization of the perfect state transfer protocols should consider the presence of errors in order to identify those that

would perform the most ideally possible, but in situations close to the experimental setups. Two perfect state transfer protocols that require engineered spin-couplings [29, 60] have been analyzed for this reason, considering static perturbations [28, 93, 61]. Other important points to consider, if we are concerned with a more realistic approach to the problem, are the timing errors on the readout time when the perfect state transfer is achieved [61] and the speed of transfer of the different protocols [114]. But, considering that the number of possible systems that could be used for perfect state transfer [60, 61] is infinite, a performance comparison between them should be aimed at finding a system which is as robust against perturbations as possible. For that purpose it is important to find out which intrinsic properties of a system make it robust against perturbations.

In this chapter, we tackle these questions analyzing different energy distributions that allow for perfect state transfer and comparing their robustness against static perturbations. We characterize the robustness of the systems by calculating their transmission fidelity. In order to find the relevant properties of the systems that make them robust, we analyze how the eigenstates and eigenenergies are perturbed. We find that the localization properties of the eigenstates of a spin chain are intimately connected to its robustness.

The chapter is organized as follows, in Sec. 4.1 we present the XX model describing the quantum spin chain and the necessary conditions for perfect state transfer. In Sec. 4.2 we analyze different energy eigenvalue configurations of the system and the corresponding spin-coupling distributions. In Sec. 4.3.1 we analyze the fidelity of the transfer of the different configurations, and the influence of perturbations on the transmission is discussed in Sec. 4.3.2. Subsequently, in Sec. 4.4, we analyse how the individual perturbed eigenstates and eigenvalues contribute to the dynamics of quantum information transport. Finally, in Sec. 4.5 we present our conclusions.

4.1 Perfect state transfer channels

We consider the state transfer in a chain of N spins-$\frac{1}{2}$ with a modulated XX interaction between nearest neighbors. Taking into account an external magnetic field, the Hamiltonian is

$$H = \frac{1}{2} \sum_i J_i (\sigma_i^x \sigma_{i+1}^x + \sigma_i^y \sigma_{i+1}^y) - \frac{1}{2} \sum_i b_i \sigma_i^z, \qquad (4.1.1)$$

where again σ_i^μ are the Pauli matrices of the ith spin, b_i is the local external field and J_i is the exchange coupling strength.

The Hamiltonian H conserves the number of excited spins (see Sec. 2.2.3.2 for more details); and since we want to study the transmission of a state in the subspace of one excited spin, we write the Hamiltonian in this basis, so H is represented by a $N \times N$ matrix

$$H = \begin{pmatrix} -b_1 & J_1 & 0 & \ldots & 0 \\ J_1 & -b_2 & J_2 & \ldots & 0 \\ 0 & J_2 & -b_3 & \ldots & 0 \\ \vdots & \vdots & \vdots & \ddots & J_{N-1} \\ 0 & 0 & 0 & J_{N-1} & -b_N \end{pmatrix}. \tag{4.1.2}$$

Condition for perfect state transfer

For a spin chain possessing mirror symmetry with respect to the center of the chain, *i.e.*, $J_i^2 = J_{N-i}^2$ and $b_i = b_{N+1-i}$, the necessary and sufficient condition for perfect state transfer is

$$E_{k+1} - E_k = (2m_k + 1)\pi/t_{\text{PST}}, \tag{4.1.3}$$

where the set of eigenenergies $\{E_k\}$ is ordered, $E_k < E_{k+1}$. The condition (4.1.3) must be fulfilled for all pairs of successive energies, where the m_k may be arbitrary integers. The shortest time t_{PST} for which (4.1.3) is fulfilled is the first time at which perfect state transfer is achieved [60, 62]. Since (4.1.3) implies strictly periodic time evolution, perfect state transfer occurs again and again, at all odd multiples of t_{PST}.

4.2 Energy and spin-coupling distributions

Every set of integers m_k in (4.1.3) leads to a unique energy spectrum enabling perfect state transfer and hence, as we shall explain below, to a unique set of coupling constants J_i. Therefore, there are infinitely many spin chains allowing perfect state transfer. But, are all of them equally efficient for transferring information? How is their perfect state transfer capability affected by perturbations through inaccuracies in the coupling constants or from coupling to

external degrees of freedom? What properties are necessary to stabilize the system against such perturbations?

We tackle these questions by studying the transmission robustness of different perfect state transfer channels in the presence of static perturbations. We characterize these spin-channel systems by their energy eigenvalue distributions. A given spectrum that satisfies the condition (4.1.3) defines a unique Hamiltonian with positive symmetric couplings J_i, which can be obtained by solving an inverse eigenvalue problem [53]. For simplicity we choose $E_k = -E_{N+1-k}$, $\forall k$, which imposes $b_i = 0$, $\forall i$ [62].

In order to study a range of different eigenvalue distributions systematically, we start from the case of an equidistant energy spectrum, $m_k = $ const. in (4.1.3), which was discussed in Ref. [29]. To obtain more perfect state transfer chains we change the equidistant spectrum by distributing the energy values more densely either in the center or towards the boundaries of the energy spectrum. The class of energy spectra which we discuss can be parametrized as follows:

$$E_k(k_\beta, \ell) = -A_{(k_\beta, \ell)}\text{sgn}(k - k_0)[(k_\beta - |k - k_0|)^\ell - k_\beta^\ell]. \qquad (4.2.1)$$

We assume that N is odd, $k = 1, ..., N$ numbers the energy eigenvalues in ascending order, as before, and $k_0 = \frac{N-1}{2}$ marks the center of the spectrum. The shape of the spectrum is controlled by an exponent ℓ and a reference index k_β which can assume two values; $k_\beta = k_b = k_0$ or $k_\beta = k_c = 0$. The overall width of the spectrum is controlled by $A_{(k_\beta, \ell)}$.

The equidistant energy spectrum (constant density of eigenvalues) is given by $E_k(k_c, 1)$. The density of eigenvalues in the center of the spectrum increases for both $E_k(k_c, n)$ and $E_k(k_b, \frac{1}{n})$ with integer $n \geq 2$. A larger density of eigenvalues close to the boundaries of the spectrum is obtained for $E_k(k_b, n)$ and $E_k(k_c, \frac{1}{n})$. The shapes of the two spectra defined by these two possibilities for a given n are different, as are those of $E_k(k_c, n)$ and $E_k(k_b, \frac{1}{n})$, respectively. For non-integer exponent ℓ the energies of Eq. (4.2.1) normally do not fulfill the commensurability condition (4.1.3) and have to be slightly readjusted to make perfect state transfer possible.

Figure 4.2.1(a) shows the energy eigenvalues for the equidistant spectrum, $E_k(k_c, 1)$, along with the four possibilities just discussed, for $n = 2$. The corresponding exchange couplings J_i (normalized by the maximum coupling strength J_{max}) are shown in Fig. 4.2.1(b). The coupling distribution determines the transmission velocity as we shall discuss in Sec. 4.3. To facilitate the

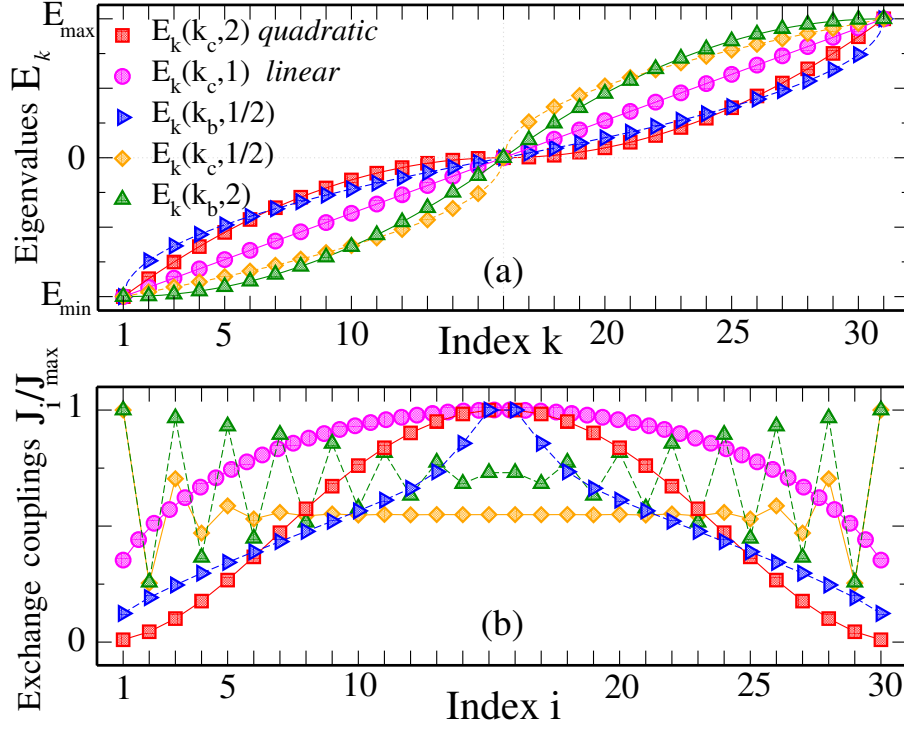reading of the graph, Fig. 4.2.2 shows the same data, each panel corresponds to a single energy distribution.

Figure 4.2.1: (a) Energy eigenvalue distributions $E_k(k_\beta, \ell)$. The symbols represent the energy values and the lines give the exact functional dependence of Eq. (4.2.1). (b) Exchange couplings determined by solving the inverse eigenvalue problem for each of the spectra given in panel (a). To facilitate the reading of the graph, Fig. 4.2.2 shows all of these curves separately.

4.3 Perfect state transfer stability of energy distributions

4.3.1 Unperturbed transfer

To compare the perfect state transfer performance of the spin-channels with the different energy eigenvalue distributions of Fig. 4.2.1, we calculated their
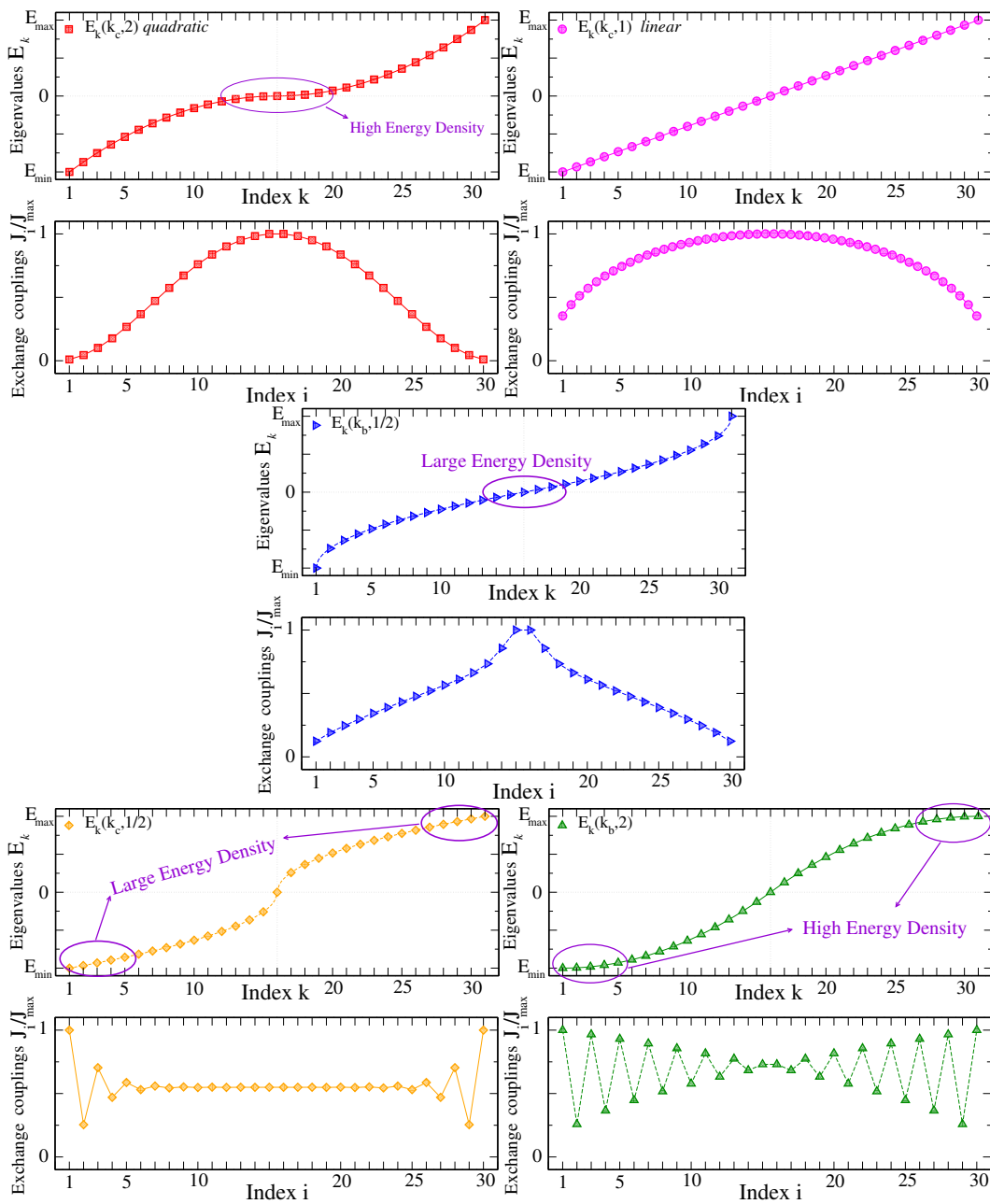
Figure 4.2.2: Energy eigenvalue distributions $E_k(k_\beta, \ell)$ and their corresponding exchange couplings J_i. For more detail and comparisons see Fig. 4.2.1.

averaged fidelity of Eq. (2.2.8)

$$F(t) = \frac{|f_N(t)| \cos \gamma}{3} + \frac{|f_N(t)|^2}{6} + \frac{1}{2}.$$

Figure 4.3.1 shows the fidelity of state transfer from one end of the chain to the other, as a function of time. The time scale is given in units of the first perfect state transfer time t_{PST}.

Time scales and transfer speed

At this point it is important to note that the dynamics of the system has at least two other relevant time scales besides the time t_{PST}, which we shall use as the time unit. The first such time scale is t_M defined in Eq. (2.2.2). As we have already mentioned, for homogeneous chains t_M is fixed by the maximum group velocity of the spin waves given by $v_g = \frac{dE}{dk}$ (where k now temporarily denotes the wave number). Unfortunately this concept breaks down for the systems of interest here, since translational invariance is broken by the non-uniform couplings J_i and the wave number is no longer defined. Our numerical results show that t_{PST} can be larger than t_M, see for example, Fig. 4.3.1(c) and 4.3.1(d). At t_M the excitations created at $t = 0$ at site $i = 1$ interfere constructively but not perfectly at site $i = N$. Perfect interference occurs only later, at $t = t_{PST}$, after the excitations have traveled back and forth between the ends of the chain many more times. Fig. 4.3.1(a) and 4.3.1(b) show that the *linear* $E_k(k_c, 1)$ and *quadratic* $E_k(k_c, 2)$ distributions achieve perfect transfer without a secondary maximum of the fidelity at some earlier time. For those two systems t_{PST} is thus equal to the t_M of the spin chain.

To make a quantitative analysis of the speed of the transfer, we consider as a reference the known value t_M^h of Eq. (2.2.3). The transfer obtained at that instant is not perfect, but by switching couplings on and off to perform consecutive swap operations, perfect transfer may be achieved at $t_M^{swap} \sim \frac{\pi N}{2J}$ [86, 75]. In terms of the maximum coupling J_{max}, the perfect state transfer time for the linear distribution is

$$t_{PST}^{lin} = \frac{\pi N}{4 J_{max}}, \tag{4.3.1}$$

which is two times faster than the consecutive swaps assuming $J = J_{max}$, $t_{PST}^{lin} = \frac{1}{2} t_M^{swap}$, but slower than the free evolution, $t_{PST}^{lin} = \frac{\pi}{2} t_M^h$, in a homogeneous chain. The other distributions are about 15 times slower than the linear case as listed in the caption of 4.3.1.

The second important time scale is given by the duration of the perfect state transfer maximum of the fidelity, Δt, i.e. the time during which the fidelity is very close to unity. Δt can be interpreted as the time of residence of the perfectly transmitted state on the last site of the chain; it determines the timing precision required for perfect state read-out. While the *quadratic* distribution is much slower than the linear one in terms of transfer time, its advantage is a much longer time window. We will return to this point later in Sec. 4.4.
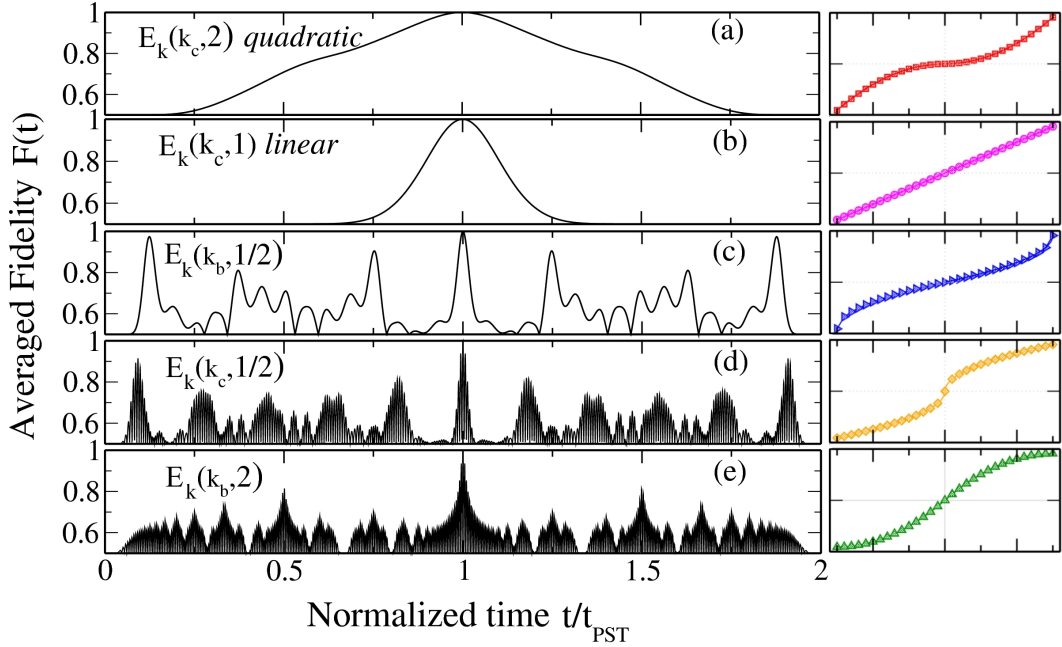
Figure 4.3.1: Averaged fidelity of the state transfer in a $N = 31$ spin chain for the different energy distributions shown in Fig. 4.2.1 as a function of time. The *linear* $E_k(k_c, 1)$ and *quadratic* $E_k(k_c, 2)$ distributions achieve the perfect transmission with the first echo, while the other cases achieve it after several echoes. In panels (d) and (e), the black regions are due to fast oscillations because of the coupling strength oscillations shown in Fig. 4.2.1(b). The transfer times are given by $t_{PST}^{lin} = \frac{\pi N}{4 J_{max}}$ and $t_{PST} \sim \gamma t_{PST}^{lin}$ with $\gamma = 15.4, 17, 15, 14.5$ for a *quadratic*, $E_k(k_b, \frac{1}{2})$, $E_k(k_c, \frac{1}{2})$ and $E_k(k_b, 2)$ distribution respectively.

4.3.2 Perturbed transfer

So far, we have discussed the performances of different spin-channels without any external perturbation. However, since the perfect engineering of all spin couplings is highly improbable, the study of the performance of different spin-coupling distributions under perturbations by flawed spin couplings becomes relevant.

4.3.2.1 Static random spin-coupling imperfections

To study the robustness of the spin chains against perturbations we introduce static random spin-coupling imperfections quantified by δ_i

$$J_i \longrightarrow J_i(1 + \delta_i), \qquad (4.3.2)$$

where each δ_i is an independent uniformly distributed random variable in the interval $[-\varepsilon_J, \varepsilon_J]$. ε_J is a positive real number that characterizes the maximum perturbation strength relative to J_i. The kind of disorder depends on the particular experimental method used to engineer the spin chains. Implementations using superconductor flux qubits seem to match, to some extent, this model for the perturbation [54].

4.3.2.2 Perfect state transfer under static perturbations

Perturbed time evolution

We calculate numerically the fidelity time evolution

$$\overline{F}(t) = \langle F(t) \rangle_{N_{\mathrm{av}}} \qquad (4.3.3)$$

averaged over N_{av} different realizations of the random imperfection values δ_i. Figure 4.3.2 shows the averaged fidelity evolution for the different energy eigenvalue distributions for a common ε_J value. Only two cases are strongly distinguished by their robustness against the perturbation: the *linear* distribution, which was previously studied by De Chiara *et. al.* [28], and the *quadratic* distribution. As the near-perfect echoes in Fig. 4.3.2(a) and 4.3.2(b) show, disorder at the level of $\varepsilon_J = 10^{-2}$ does not significantly affect perfect state transfer in both cases. In contrast, panels (c) and, especially, (d) and (e) of the same figure, show a rather rapid decay of the fidelity (black line) down to

useless levels. The colored lines in panels (c), (d) and (e) show the fidelities of the unperturbed systems for comparison.
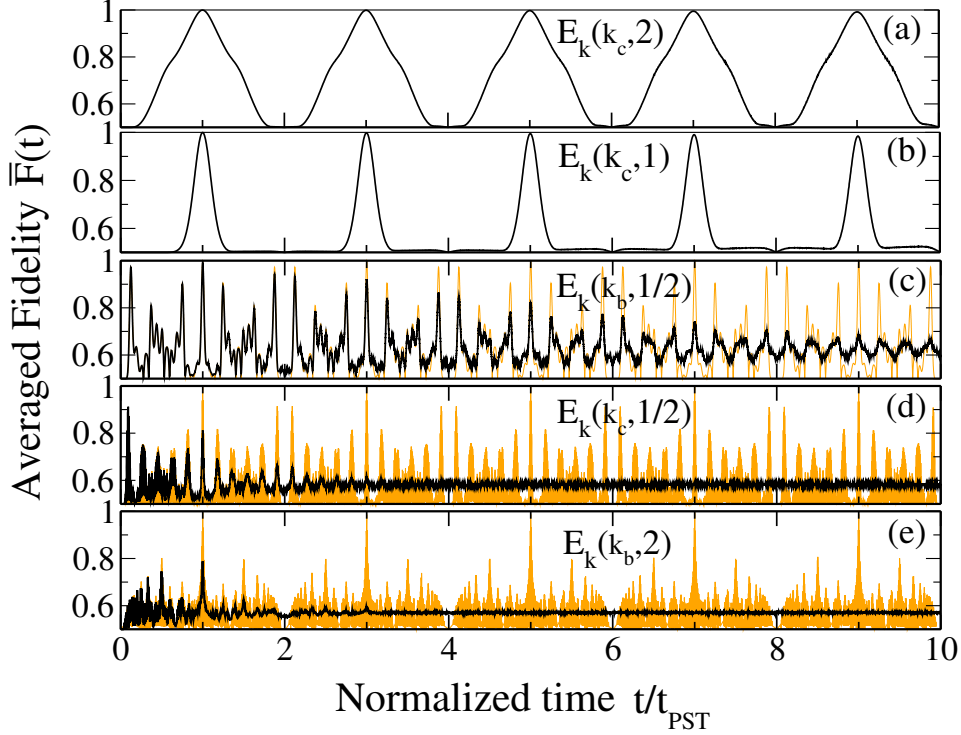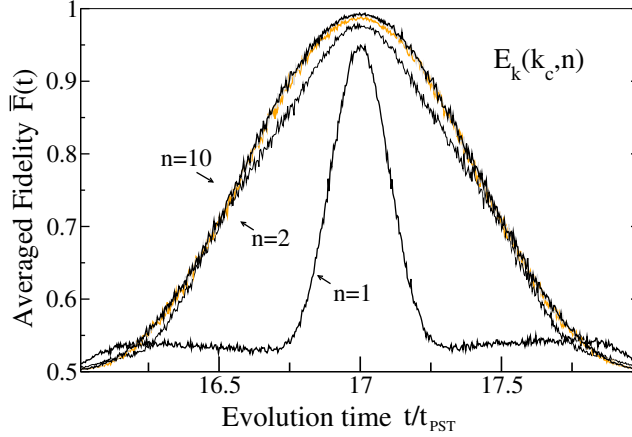

Figure 4.3.2:   Averaged fidelity of the state transfer in a $N = 31$ spin chain with random perturbations of strength $\varepsilon_J = 10^{-2}$ averaged over $N_{av} = 10^2$ realizations for the different energy distributions from Fig. 4.2.1 as a function of time. The colored lines in (c), (d) and (d) show $F(t)$ for the systems without perturbation ($\varepsilon_J = 0$).

To compare the performance of the transmission of the *linear* $E_k(k_c, 1)$ and the *quadratic* $E_k(k_c, 2)$ distributions, we observe in more detail the arrival of their 9th echo in Fig. 4.3.3. The *quadratic* distribution is notably more robust than the *linear* distribution, since the fidelity of the former distribution is larger, and also its time window to measure the state, Δt, is larger. Since both distributions belong to the same kind of eigenvalue distributions $E_k(k_c, n)$, it is natural to ask for the performance of a system with a higher exponent n, *ie.* $E_k(k_c, n > 2)$. To answer this question, we added in Fig. 4.3.3 the 9th echoes for $n = 3$ (colored line) and for $n = 10$, respectively. These data show that both the maximum fidelity and the length Δt of the time window for the state

read-out increase with n for energy eigenvalue distributions of type $E_k(k_c, n)$. However, the increase from $n = 3$ to $n = 10$ is insignificant compared to the increase from $n = 2$ to $n = 3$.

Figure 4.3.3: Averaged fidelity of the state transfer in a $N = 31$ spin chain with random perturbations of strength $\varepsilon_J = 10^{-2}$ averaged over $N_{av} = 10^2$ realizations for eigenvalue distributions $E_k(k_c, n)$. Shown is the range of times around the 9th echo of the perfect state transfer in the unperturbed chain, for $n = 1, 2, 10$ (black lines), and $n = 3$ (faint colored line very close to the $n = 10$ results).

The increase of Δt with growing n can be explained by the changes of the exchange couplings J_i shown in Fig. 4.2.1(b). When n changes from 1 to 2 the J_i decrease close to the boundaries and increase in the center of the chain. This trend continues even more strongly for larger values of n as show Fig. 4.3.4. The small spin couplings close to the boundaries of the chain prevent the spreading of the information once it is localized at one of the chain ends, thus leading to larger values of Δt.

Keeping this in mind, *i.e.* that, energy eigenvalue distributions $E_k(k_c, n)$ with larger n are generally more robust, we focus the following analysis on $n = 1$ and $n = 2$, when we refer to this kind of distributions. We do this, because the robustness properties of $E_k(k_c, n > 2)$ are quite similar to the quadratic distribution, $E_k(k_c, n = 2)$.
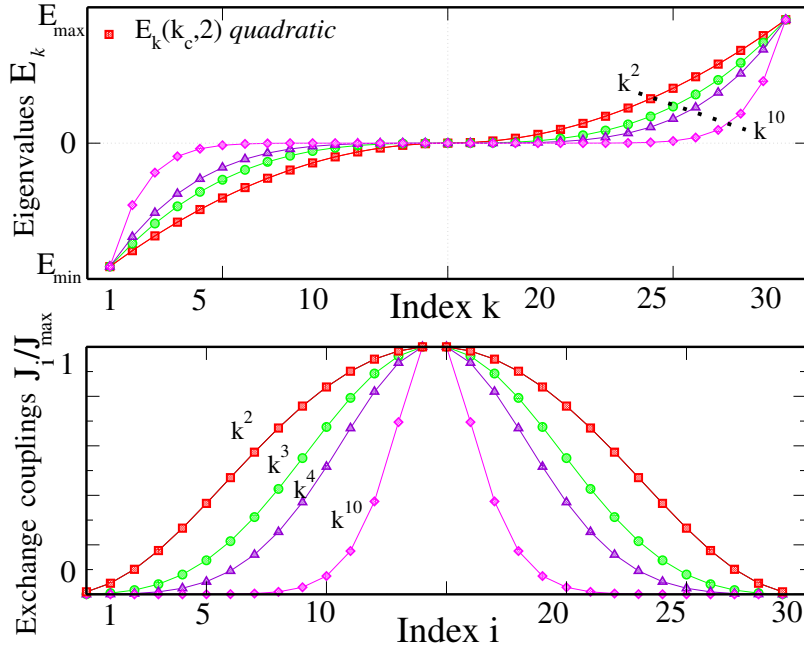
Figure 4.3.4: (Top panel) Energy eigenvalue distributions $E_k(k_\beta, n)$ for $n = 2, 3, 4, 10$ in a $N = 31$ spin chain. The symbols represent the energy values and the lines give the exact functional dependence of Eq. (4.2.1). (Bottom Panel) Exchange couplings determined by solving the inverse eigenvalue problem for each of the spectra $E_k(k_\beta, n)$.

Robustness of perfect state transfer under static perturbations

To determine the robustness of the different distributions, we calculate the averaged fidelity $\overline{F}(t_{\mathrm{PST}}, \varepsilon_J)$ as a function of the perturbation strength ε_J for the first perfect state transfer time t_{PST} determined from the unperturbed case. Figure 4.3.5 shows results for different energy distributions and for a wide range of perturbation strengths. The *linear* and *quadratic* distributions turn out to be the most robust ones for all perturbation strengths of interest, yielding quite similar results for weak perturbations ($\varepsilon_J \lesssim 0.2$) where the fidelity is larger than $F = 0.9$. For larger perturbation strengths, the *quadratic* distribution is most robust, but probably not robust enough for quantum information processing although it could be relevant for other practical purposes where the experimental errors lie in this region.
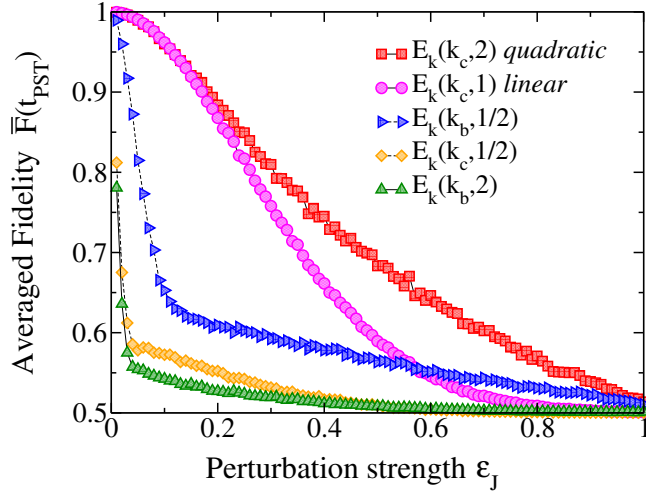
Figure 4.3.5: Averaged fidelity at time t_{PST} as a function of the perturbation strength ε_J for the different energy distributions from Fig. 4.2.1 with $N = 31$ and $N_{av} = 10^2$.

Decoherence time

Recently, it has been shown that the relative decay of the mesoscopic echoes between a perturbed evolution and the corresponding unperturbed evolution could be used to determine and characterize the decoherence time of the spin-chain channel [4]. Similarly, to determine the decoherence time for each perturbation strength, we study the state transfer fidelity for different perfect state transfer echoes as a function of their respective perfect state transfer echo times $t_{\mathrm{PST}}^i = (2i - 1)t_{\mathrm{PST}}$, *i.e.*, the times where the *i-th* perfect state transfer echo arrives at site N for an unperturbed evolution.

Figure 4.3.6 shows the fidelity $\overline{F}(t_{\mathrm{PST}}^i, \varepsilon_J)$ as a function of t_{PST}^i, for different perturbation strengths ε_J. The left panel shows the fidelity for the *quadratic* distribution while the right panel illustrates the *linear* distribution. The decoherence time, *i.e.*, the decay time as a function of t_{PST}^i is longer for the *quadratic* distribution than for the linear one, which could be relevant for implementation purposes because it gives more opportunities to eventually perform a measurement. Additionally the fidelity of the quadratic distribution converges to an asymptotic value higher than that of the *linear* distribution due to the localization effects caused by the small couplings in the borders, as discussed above. As we showed in the previous Chap. 3, weak coupling between terminal qubits and the intervening spin chain were recently used as

key elements in our proposal [119] and others [109, 9, 113, 81] for quantum information transfer by spin chains. A quantitative analysis of the decoherence time merits a more careful study because of the different limiting values of the fidelity for different spin-coupling distributions.

Figure 4.3.6 clearly shows the importance of achieving perfect state transfer with the first spin-wave, *i.e.*, $t_{PST} \sim t_M$, because the perturbation affects strongly the successive waves. For example, the $E_k(k_b, \frac{1}{2})$ distribution although having similar energy and coupling distributions compared with the most robust cases, shows a strongly reduced transfer fidelity because it achieves perfect state transfer at a time eight times longer than t_M.
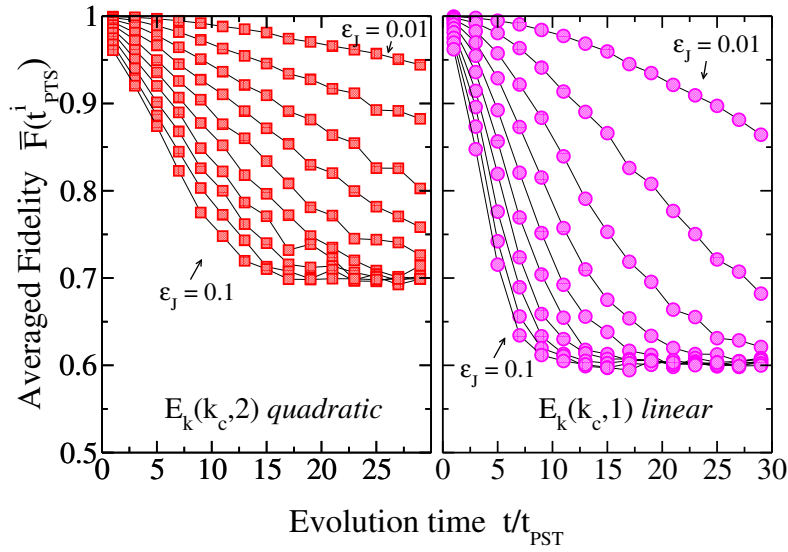
Figure 4.3.6: Averaged fidelity at odd multiples of t_{PST} (symbols) for the linear and quadratic energy eigenvalue distributions, $E_k(k_c, n)$ ($n = 1, 2$). Chain length is $N = 31$, averages were performed over $N_{av} = 10^2$ realizations. Perturbation strengths are $\varepsilon = 0.01, 0.02, ..., 0.1$.

4.4 Robustness and Localization

We have shown that certain systems are more robust against perturbations than others. In order to optimize the engineered spin coupling distributions it is decisive to understand which properties of the system are relevant for the robustness of the perfect state transfer. To this end we determine how each

energy eigenstate contributes to the dynamics for each of the spin-channels.

Energy eigenstate distribution and localization in the spin-sites

We expand the states $|i\rangle$ (a single excitation at site i) in the eigenstate basis $|i\rangle = \sum_k a_{k,i}|\Psi_k\rangle$, where k numbers the energy eigenstates in ascending order, as usual. Figure 4.4.1 shows the weights

$$P_{k,i} = |a_{k,i}|^2, \qquad (4.4.1)$$

for the different energy spectra from Fig. 4.2.1. The mirror symmetries with respect to both the center of the chain and the center of the energy spectrum are due to the spatial mirror symmetry of the couplings, and the symmetric tridiagonal nature (with zero diagonal) of the Hamiltonian matrix, respectively. Under perturbations of the couplings the spatial symmetry of the patterns of Fig. 4.4.1 is destroyed, while the spectral symmetry is not (as we discuss below and show in Fig 4.4.2).

As can be observed in Fig. 4.4.1, the degree of localization of the energy eigenstates varies strongly between the different eigenvalue distributions. The most robust distributions seem to generate the most strongly localized energy eigenstates; in panels (a), (b) and (c) of Fig. 4.4.1 each energy eigenstate basically seems to be localized on two lattice sites. The quadratic distribution [panel (a)] seems to have the most strongly localized eigenstates; in particular the eigenstates that belong to the center of the band are highly localized on the boundaries of the chain. This is particularly clear from the upper panels in Fig. 4.4.1, showing the contributions $P_{k,1}$ of the energy eigenstates $|k\rangle$ to the initial state $|i = 1\rangle$ with a single excitation localized at the boundary of the chain. In comparison, the other energy distributions show a larger spread in the contributions of the energy eigenstates to each site eigenstate $|i\rangle$. Nevertheless, we observe similarities of the distribution of $P_{k,i}$ between the *linear, quadratic* and $E_k(k_b, \frac{1}{2})$ distributions.

As we discussed and showed in the previous chapter 3, the presence of localized states at the boundaries of the spin chain can improve the transmission of quantum states [119, 113, 55, 68]. These localized states arise when the coupling of the boundary sites is weaker than the coupling between inner sites or if external fields are applied at the boundary sites. Next, we study how the different energy levels are affected by perturbations for the different energy distributions.
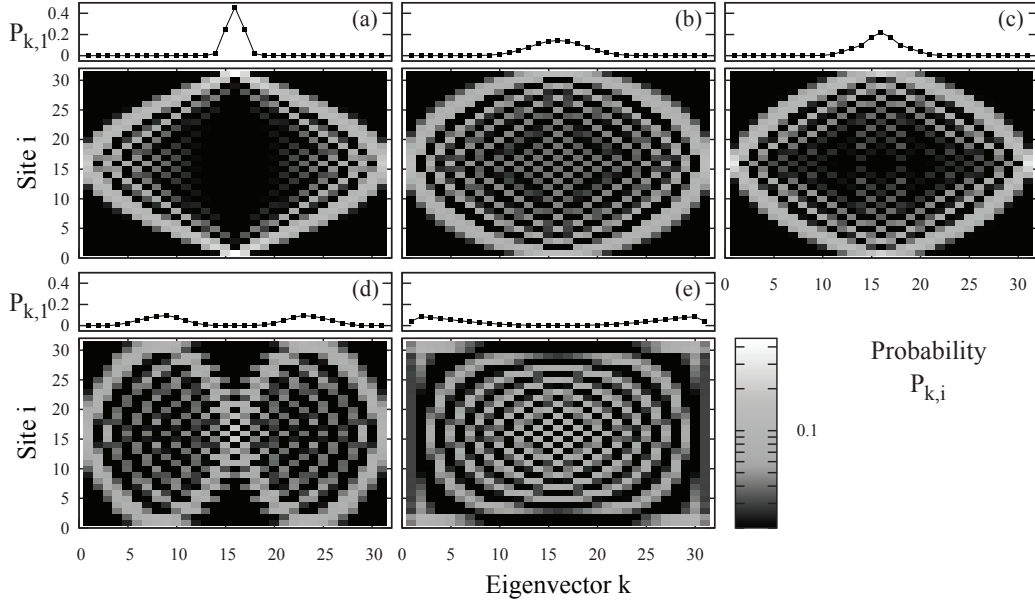
Figure 4.4.1: Eigenvector probability $P_{k,i}$ of the site (computational) states $|i\rangle$. $P_{k,i} = a_{k,i}^2$, where $|i\rangle = \sum_k a_{k,i}|\Psi_k\rangle$. The top part of each panel shows the probabilities $P_{k,1}$ of the initial state $|\Psi_0\rangle = |1\rangle$, and thus shows which energy eigenstates contribute to the state transfer. The panel labels refer to the different energy distributions given in Fig. 4.2.1, where (a) $E_k(k_c, 2)$ *quadratic*, (b) $E_k(k_c, 1)$ *linear* (c) $E_k(k_b, \frac{1}{2})$, (d) $E_k(k_c, \frac{1}{2})$, and (e) $E_k(k_b, 2)$.

Perturbed energy levels

We generated distributions of energy eigenvalues E_k for the different kinds of unperturbed energy spectra and for different perturbation strengths ε_J. For small ε_J we observe a symmetric distribution of the perturbed eigenvalues E_k around their respective unperturbed values. The width of that distribution scales with the perturbation strength. For larger values of ε_J the distributions of the perturbed E_k become asymmetric with respect to the unperturbed energy level; the low-lying levels tend to be pulled down, while the high-lying levels are pushed up by the same amount. (The energy spectrum of the perturbed Hamiltonian matrix is still symmetric). The value of ε_J where the asymmetry sets in depends on the type of unperturbed energy spectrum and is largest for the quadratic case. We show some examples of the deviation of the perturbed eigenvalues E_{k,ε_J} due to the perturbation with strength ε_J from

the unperturbed values $E_{k,0}$ in Fig. 4.4.2.
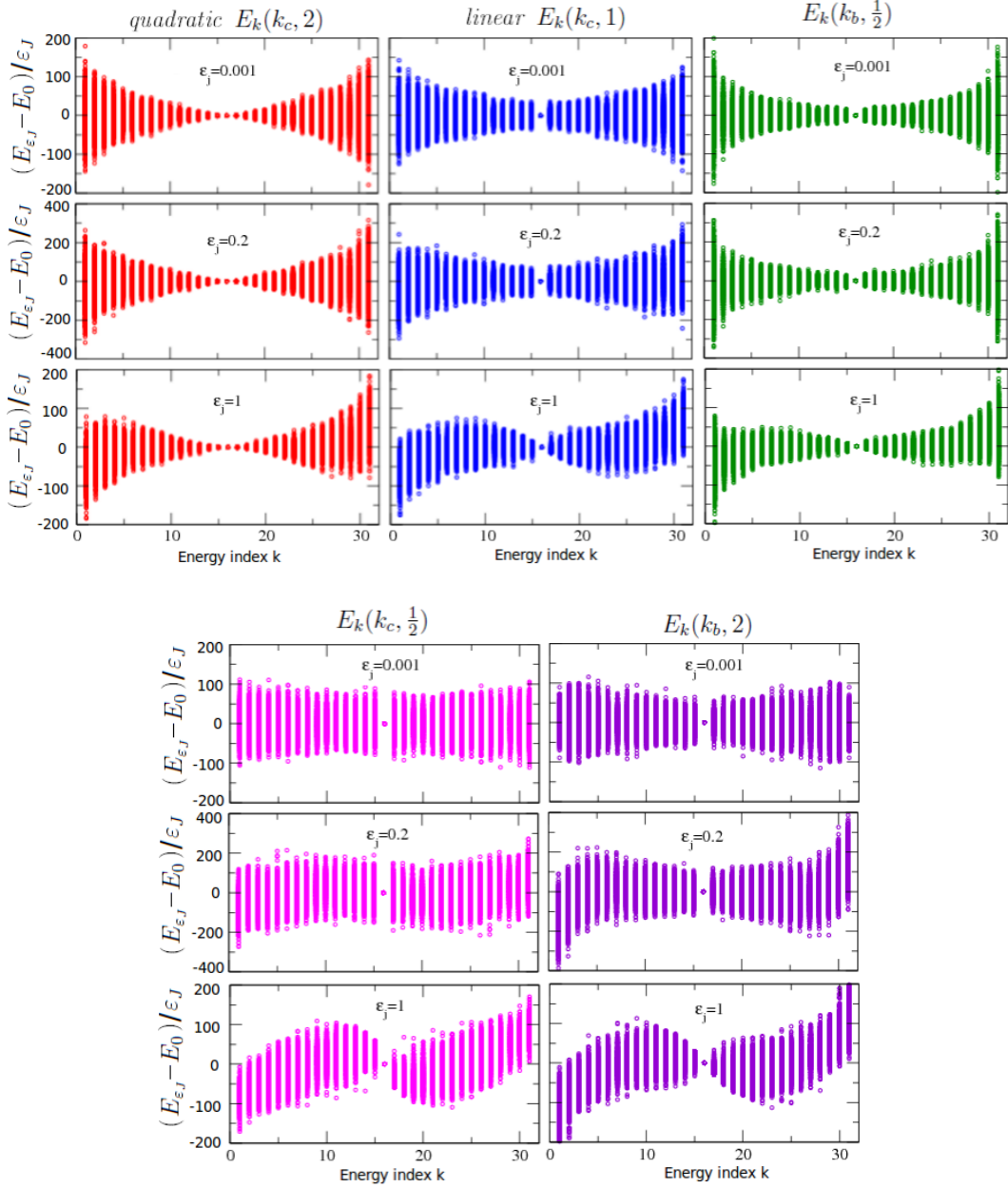
Figure 4.4.2: Deviations of the perturbed eigenvalues E_{k,ε_J} due to the perturbation with strength ε_J from the unperturbed values $E_{k,0}$ for the different energy distributions of Fig. 4.2.1. The data shown are for $\varepsilon_J = 0.001, 0.2, 1$ and $N_{av} = 10^3$ realizations.

To see more quantitatively what is going on in detail, we show in Fig. 4.4.3 the *standard deviations*[1] of the energy levels for the different kinds of unperturbed spectra. Each data point represents an average over $N_{av} = 10^3$ realizations of the random perturbations.
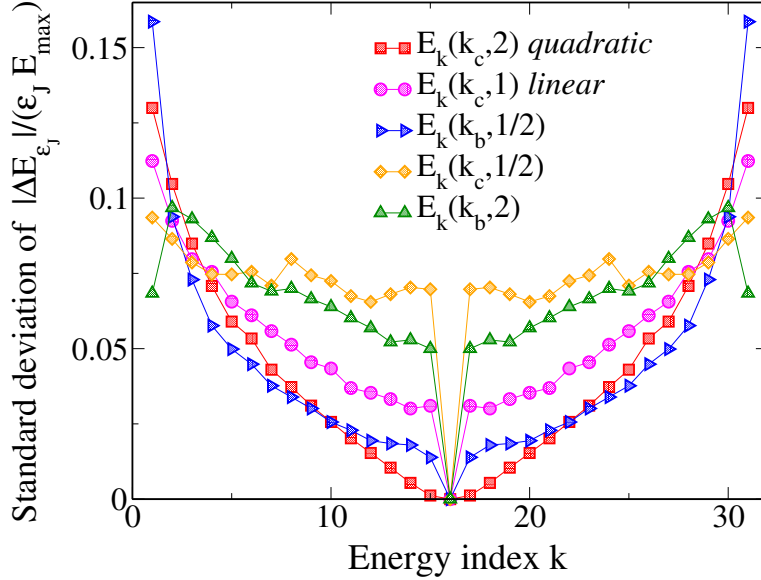
Figure 4.4.3: Standard deviation of the energy levels $|\Delta E_{\varepsilon_J}| = |E_{\varepsilon_J} - E_0|$ due to the perturbation with strength ε_J for the different energy distributions of Fig. 4.2.1. For weak perturbations (small ε_J) the standard deviation turns out to be proportional to $\varepsilon_J E_{max}$, which we use as a unit here. The data shown are for $\varepsilon_J < 0.1$; $N_{av} = 10^3$ realizations were used for the calculations.

The symmetry of the data with respect to the center $E = 0$ of the energy spectrum, and the fact that the zero energy eigenvalue is not affected by the randomness at all, are due to the nature (symmetric, tridiagonal, zero diagonal elements) of the Hamiltonian matrix.

The key observation explaining the differences in state transfer robustness is made by combining the information provided by Fig. 4.4.3 and the upper panels of Fig. 4.4.1. Those panels show that for the quadratic energy spectrum

---

[1]The standard deviation is a measure of the dispersion in a statistic and probabilistic framework. It shows how much the data vary from their mean value: $s = \sqrt{\frac{1}{N-1}\sum\limits_{i=1}^{N}(x_i - \overline{x})^2}$.

$E_k(k_c, 2)$ the initial state $|i = 1\rangle$ of the state transfer process is formed by the superposition of a small number of energy eigenstates in the center of the energy spectrum. In all the other types of energy spectrum, the initial state shows wider distributions in the energy quantum number k. At the same time, the sensitivity to perturbations (which is what is shown in Fig. 4.4.3) shows a comparatively wide minimum, with value zero in the center of the spectrum, whereas all other types of spectrum show roughly constant nonzero values in the central region of the spectrum, with a single exceptional zero right in the center. The observed particular robustness of the *quadratic* energy spectrum can thus be ascribed to the fact that the initial state consists of a particularly small number of energy eigenstates coming from a part of the energy spectrum which is particularly insensitive to perturbations in the spin coupling constants. For the less robust distributions, the variance is roughly independent of the energy in the center of the energy band, while for the quadratic energy spectrum the variance decreases continuously towards the band center. For that distribution (and for the two other distributions shown
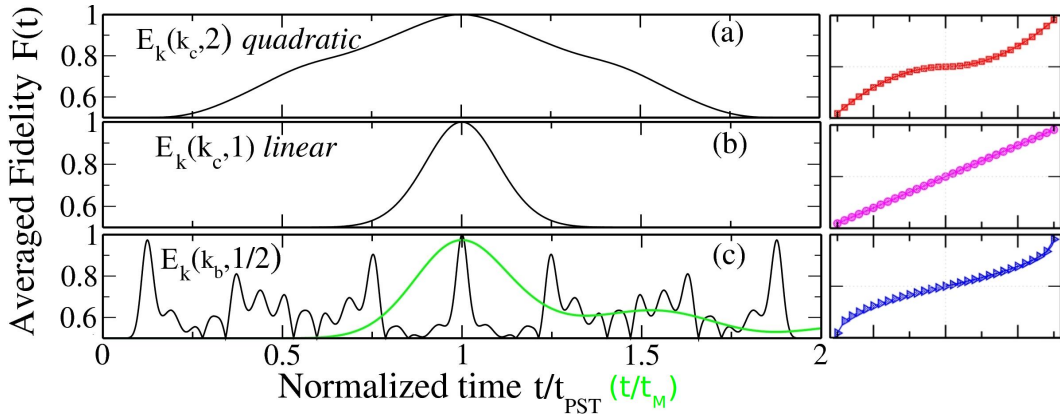
Figure 4.4.4: Averaged fidelity of the state transfer in a $N = 31$ spin chain for the *linear*, *quadratic* and $E_k(k_b, \frac{1}{2})$ energy distributions as a function of time. The *linear* and *quadratic* distributions, achieve perfect state transfer with the first echo; while the $E_k(k_b, \frac{1}{2})$ distribution achieve it after several echoes, $t_{PST} \sim 8t_M$. The green curve shows $\bar{F}$ on the time scale $\frac{t}{t_M}$. On this time scale the similarities, in terms of the $P_{k,i}$ and E_k, between these different energy distributions became more apparent.

in the upper panels of Fig. 4.4.1) all energy eigenstates are quite strongly localized. A glance at Fig. 4.2.1(b) shows that the corresponding coupling

patterns have the smallest couplings close to the ends of the chain, in the region where those energy eigenstates are localized, which are the most important for the state transfer.

Since we discuss a constant *relative* strength ε of the disorder, the *absolute* changes of the couplings tend to be smaller near the ends of the chain, causing only small changes in the energy eigenvalues. This explains the particular robustness of the quadratic distribution. We remark that while the $E_k(k_b, \frac{1}{2})$ distribution has similarities to the linear or quadratic distribution, it is less robust because it achieves the perfect state transfer only after several mesoscopic times, $t_{PST} \sim 8t_M$; and as we have already discussed and shown in Fig. 4.3.6, perturbations affect more and more strongly the successive waves. In Fig. 4.4.4 the performance of the fidelity for the $E_k(k_b, \frac{1}{2})$ distribution at time $\frac{t}{t_M}$ (green color curve) is compared with the performance of the quadratic and linear distributions.

Perfect state transfer under timing errors

Another important aspect characterizing the robustness of the transmission is the length of the time window where high fidelity is obtained for the transmitted state. In this context, we are not only considering errors in the engineered spin couplings, but also the timing error of the measurement [61]. To that end we analyze the term $|f_N(t)|^2 = |\langle \mathbf{N}|e^{-iHt/\hbar}|\mathbf{1}\rangle|^2$ from (2.2.8) at time $t_{PST} + \delta t$. Taking into account the spatial symmetry, $|f_N(t_{PST} + \delta t)|^2$ is given by

$$
\begin{aligned}
|f_N|^2 &= |\sum_{k,s}(-1)^{k+s}P_{s,1}P_{k,1}e^{-i(E_k-E_s)(t_{PST}+\delta t)}| \\
&\approx |\sum_{k,s}P_{s,1}P_{k,1}(1-\delta t(E_k-E_s)+ \\
&\quad i^2\frac{\delta t^2}{2!}(E_k-E_s)^2-...)| \\
&\approx 1 - \frac{\delta t^2}{2!}\sum_{k,s}P_{s,1}P_{k,1}(E_k-E_s)^2, \quad\quad (4.4.2)
\end{aligned}
$$

where $P_{k,1} = |\langle \Psi_k|1\rangle|^2$. Even without the Bloch-sphere average (2.2.8) which would be necessary for a comparison with Fig. 4.3.1, the result above shows why the quadratic distribution displays the longest window of time. The probabilities $P_{k,1}$ (see Fig. 4.4.1) are sharply peaked in the center of the energy

band and essentially zero otherwise. Furthermore, due to the quadratic nature of the energy spectrum, the relevant energy differences $E_k - E_s$ are particularly small (see Fig. 4.2.1(a)) making the fidelity deviate from unity only at rather large δt values.

4.5 Conclusion

We have studied the robustness of spin chain systems designed for perfect state transfer under static perturbations. We explored different perfect state transfer systems by choosing different energy spectra distributions that satisfy the perfect state transfer conditions. From the energy spectrum of a given chain, the spin-spin coupling constant pattern can be obtained by solving an inverse eigenvalue problem. The robustness of each system was studied by calculating its transmission fidelity under static perturbations of the couplings. We found that robustness is characterized by two main features. One is the reduction of the transfer fidelity induced by the perturbed couplings and the other is the duration of the time window during which the transmitted state may be read out with high fidelity. The most robust systems are those with linear and quadratic energy eigenvalue distributions. These systems achieve perfect state transfer at the time of the first fidelity maximum. That time may be called the spin-wave echo time, and the less robust systems reach perfect state transfer only after several spin-wave echoes. By analyzing how the energy eigenstates and eigenvalues are affected by the perturbations, we found that the most robust distributions have strongly spatially localized eigenstates. Thus, because the initial state is localized in one end of the chain, only few eigenstates participate in the transfer. Because of the localization properties of the eigenstates the perturbations in the spin couplings close to the chain boundaries are the only significant source of errors. Since these couplings are rather weak for the most robust systems, a given relative perturbation strength only causes a small absolute perturbation in the couplings and thus in the energy eigenvalues, leading to the observed robustness. The weak couplings close to the ends of the chain also lead to a longer residence time of the transmitted state at its target site at the chain boundary, causing a longer time window for read-out.

5 Spin chains for robust state transfer: Modified boundary couplings vs. completely engineered chains

We have seen that, considering quantum spin systems capable of transferring information with high fidelity without requiring any dynamic control in order to avoid the loss of information by the interaction with the environment, is not sufficient to ensure a reliable and realistic channel for information transfer. Imperfections, as static disorder, can drastically affect the reliability of the quantum communication channels. Thus, although there are infinitely many ways to engineer the spin-spin coupling for perfect state transfer without any dynamical control, this amazing transfer fidelity comes at a high price in terms of the accuracy required to design each interaction to avoid the loss of information [28, 62, 120, 93]. Therefore, in order to assess the reliability of quantum systems as realistic channels for information transfer, it is essential to study the influence of imperfections. Indeed, in the previous chapter, we explored the robustness of some perfect state transfer channels against static perturbations, finding that the quality of transfer is often strongly impaired by perturbations [120]. Therefore some questions emerge: Is it really necessary to optimize every single interaction in a chain? Can we find simpler systems showing good transfer properties under perturbations?

In this chapter we focus on the behavior of essentially homogeneous chains where only the first and last couplings can be adjusted. We show that under perturbations these chains can achieve an optimized state transfer comparable to or even better than that of fully engineered perfect state transfer systems. Two interesting regimes for transmission can be observed when the boundary couplings are varied; for unperturbed chains these regimes have been recently studied (see Chap. 3 and Refs. [109, 41, 119, 9, 113, 10, 11]):

(i) an optimized (length-dependent) value of the boundary couplings which renders quantum state transfer approximately dispersionless, and

(ii) the limit of very weak boundary couplings.

For both regimes we study the robustness against perturbations, showing

that transfer efficiency comparable to or better than that of the most robust perfect state transfer systems can be reached without the demanding engineering of a large number of couplings.

The chapter is organized as follows, in Sec. 5.1 we present the XX model describing the quantum spin chain channels for state transfer. In Sec. 5.2 we formulate the static disorder model to consider for the spin-spin coupling interaction. These first two sections have material very similar to that already presented but, nevertheless, we show it again in the light of what we have learnt from the two previous chapters. Besides, we use these sections to introduce notation that allows us to name each one of the many different systems that will be under consideration, including two different models of coupling disorder.

In the following two sections we analyze the fidelity of the transfer of the optimized state transfer and perfect state transfer systems under static perturbations of the transmission channel. While in Sec. 5.3.1 we compare the performance of the optimized state transfer in the optimal coupling regime vs. the perfect state transfer with linear energy distribution; in Sec. 5.3.2 we compare the performance of the optimized state transfer in the weak coupling regime vs. the perfect state transfer with quadratic energy distribution. Finally, in Sec. 5.4 we present our conclusions.

5.1 Spin chains as state transfer channels

We consider a spin-$\frac{1}{2}$ chain with XX interactions between nearest neighbors, described by the Hamiltonian

$$H = \frac{1}{2} \sum_{i=1}^{N-1} J_i \left(\sigma_i^x \sigma_{i+1}^x + \sigma_i^y \sigma_{i+1}^y \right), \qquad (5.1.1)$$

where once again σ_i^μ are the Pauli matrices, N is the chain length, and J_i is the exchange interaction coupling. We assume the mirror symmetry $J_i = J_{N-i}$, which is essential for perfect state transfer (see Subsec. "Condition for perfect state transfer" in Sec. 4.1).

Again, the goal is to transmit a quantum state $|\psi_0\rangle$ initially stored on the first spin ($i = 1$) to the last spin of the chain ($i = N$). $|\psi_0\rangle$ is an arbitrary normalized superposition of the spin down ($|0\rangle$) and spin up ($|1\rangle$) states of the first spin, with the remaining spins of the chain initialized in a spin down state. Note that more general initial states can be treated without much additional

effort, since the Hamiltonian (5.1.1) is equivalent to one of non-interacting fermions. The Hamiltonian (5.1.1) conserves the number of up spins (see Sec. 2.2.3.2 for more details); therefore, the dynamic evolution of the initial state is restricted to the subspace of one excited spin. Once more, to evaluate how well an unknown initial state is transmitted, we use the transmission fidelity, averaged over all possible $|\psi_0\rangle$ from the Bloch sphere (Eq. (2.2.8))

$$F(t) = \frac{|f_N(t)|\cos\gamma}{3} + \frac{|f_N(t)|^2}{6} + \frac{1}{2}$$

By the symmetries of the system, this fidelity can be expressed in terms of the single-excitation energies E_k and the eigenvectors $|\Psi_k\rangle$ of H, in the following way

$$|f_N(t)| = \left|\sum_{k,s}(-1)^{k+s}P_{k,1}P_{s,1}e^{-i(E_k-E_s)t}\right| \tag{5.1.2}$$

where, recall Eq. (4.4.1), $P_{k,1} = a_{k,1}^2$ are the eigenvector probabilities on the first site of the chain, since $|\mathbf{i}\rangle = \sum a_{k,i}|\Psi_k\rangle$.

As we have seen previously, perfect state transfer channels are distinguished by commensurate energies E_k, that is, all transition frequencies share a common divisor to make $f_N = 1$ in Eq. (5.1.2) at a suitable perfect state transfer time t_{PST} [29, 60]. This condition is obtained by suitably modulating the spin-spin couplings J_i [61, 60, 120].

A long unmodulated homogeneous spin channel, $J_i = J \ \forall i$, cannot transfer a state perfectly, since due to the dispersive quantum dynamics the transfer fidelity decreases with the number of spins in the channel, as we have already discussed and shown in Sec. 2.2.3.1 and 2.2.3.2. At t_M the excitations created at $t = 0$ at site $i = 1$ interfere constructively but not perfectly at site $i = N$. In fact, rigorous perfect state transfer in a homogeneous chain is possible only for $N \leq 3$ [29, 30]. However, as we show in Chap. 3, the transfer can be noticeably improved just by modulating the couplings of the spins at the ends of the channel.

We consider again the two surface spins $i = 1$ and N interacting with the inner spins with $J_1 = J_{N-1} = \alpha J$ while the remaining spins form a homogeneous chain with $J_i = J$ (see Sec. 3.3 and Eq. (3.3.1)). We call now this Hamiltonian H^α, where $\alpha \in (0,1]$ is a control parameter.

Two regimes for α can be used for optimized state transfer:

(i) the *optimal-coupling regime* ($\alpha = \alpha_{opt} \sim N^{-\frac{1}{6}}$) possessing an almost equidistant spectrum E_k in the middle of the energy band, resulting

in a quasi dispersionless fast transfer with high fidelity (see Sec. 3.3.3 and Refs. [119, 9, 113]); and

(ii) *the weak-coupling regime* ($\alpha \ll 1$). In that regime the transmitted state appears and then reappears roughly periodically at the receiving end of the chain. *Almost perfect transfer* is achieved with the first arrival due to the fact that only very few eigenstates from the center of the energy band are involved, which are highly localized at the boundaries of the chain (see Sec. 3.3.3.1 and Refs. [109, 119, 113]).

The characteristic features of the two regimes just mentioned, are those that we also observe to be essential for the robustness of perfect state transfer spin-chain channels against perturbations (see Chap. 4 and Ref. [120]). The most robust systems either showed

(1) an equidistant (linear) energy spectrum generating the analog of dispersionless wave packet transfer or,

(2) a large density of states in the center of the band with the corresponding eigenstates localized at the boundary sites of the chain, thus dominating the end-to-end transfer [120].

One class of perfect state transfer systems is characterized by a power-law spectrum

$$E_k = sgn(k)|k|^m, \text{ where, } k = -\frac{N-1}{2}, ..., \frac{N-1}{2} \qquad (5.1.3)$$

and the exponent m is a positive integer. We specifically address here the *linear* energy distribution, $m = 1$, and call the corresponding Hamiltonian H^{lin} [29], and the *quadratic* case, $m = 2$, with Hamiltonian H^{quad} [120].

The optimized state transfer system described by H^α, that requires control of only two boundary couplings, would certainly be simpler to implement than the perfect state transfer systems that need the engineering of all the couplings along the chain. In the following we compare the transmission performance of optimized state transfer and perfect state transfer systems under the influence of disordered couplings in the *channel* assuming perfect control of the boundary couplings because they are experimentally more accessible and controllable, and therefore we consider the imperfections there negligible. We make the same assumption for the engineered chains.

5.2 Static random disorder

Static disorder[1] in the couplings within the transfer channel is described by

$$J_i \rightarrow J_i + \Delta J_i, \ i = 2, ..., N - 2, \qquad (5.2.1)$$

with ΔJ_i being a random variable. We consider two possible coupling disorder models:

(a) *relative static disorder,* where each coupling is allowed to fluctuate by a certain fraction of its ideal size, $\Delta J_i = J_i \delta_i$ (this kind of disorder is considered by us in Sec. 4.3.2 and [120], and in Refs. [28, 86]); and

(b) *absolute static disorder,* where all couplings may fluctuate within a certain fixed range which we measure in terms of $J_{max} = \max J_i$: $\Delta J_i = J_{max} \delta_i$ (this kind of disorder was considered in Ref.[93]).

Each δ_i is an independent and uniformly distributed random variable in the interval $[-\varepsilon_J, \varepsilon_J]$. $\varepsilon_J > 0$ characterizes the strength of the disorder. The two coupling disorder models are equivalent for the optimized state transfer systems since all couplings are equal there. However, in the fully engineered perfect state transfer systems $J_{max} - J_{min}$ depends on the type of system and tends to increase with N, so absolute disorder is expected to be more damaging than the relative one in perfect state transfer systems. The kind of disorder depends on the particular experimental method used to engineer the spin chains.

5.3 Performance of the state transfer

In the following, we calculate numerically the fidelity time evolution $\overline{F}(t_M) = \langle F(t_M) \rangle_{N_{\mathrm{av}}}$ averaged over N_{av} different realizations of the random imperfection values δ_i.

---

[1]We refer to "static disorder, "perturbation" and "noise" as synonymous

5.3.1 Optimal coupling regime for state transfer vs. linear energy distribution for perfect state transfer

System properties

When $\alpha = \alpha_{opt}$ in H^α, the spectrum is linear in the middle of the energy band [Fig. 5.3.1(a) and 5.3.2(a)]. The probability $P_{k,1}$ of the kth energy eigenstate to participate in the state transfer is shown in Fig. 5.3.1(b) as a function of k, for $N = 200$, and in Fig. 5.3.2 for different chain lengths N. $P_{k,1}^{\alpha_{opt}}$ has a Lorentzian shape[2], and $P_{k,1}^{lin}$ is Gaussian[3], as shows Fig. 5.3.3. Our numerical fitting gives

- **Lorentzian**
$$P_{k,1}^{\alpha_{opt}} \simeq \frac{1}{\pi} \frac{\Gamma}{(k-k_0)^2 + \Gamma^2}, \qquad (5.3.1)$$

  with $k_0 = \frac{N+1}{2}$ and $\Gamma \simeq (\frac{10}{N})^{-0.63}$ considering $J = 1$, the maximum value is
$$P_{max}^{\alpha_{opt}} = \frac{1}{\pi}(\frac{10}{N})^{0.63}; \qquad (5.3.2)$$

- **Gaussian**
$$P_{k,1}^{lin} \simeq A e^{-\frac{(k-k_0)^2}{2\sigma^2}}, \qquad (5.3.3)$$

  with $A \simeq \frac{0.8}{\sqrt{N}}$ and $\sigma \simeq \frac{\sqrt{N}}{2}$, the maximum value is

$$P_{max}^{linear} = \frac{0.8}{\sqrt{N}}. \qquad (5.3.4)$$

Reminding that the dynamics of these systems is governed by the term

$$P_{k,1} P_{s,1} e^{-i(E_k - E_s)t}, \qquad (5.3.5)$$

as shown by Eq. 5.1.2; only the linear part of the spectrum, just where $P_{k,1} \neq 0$, plays a relevant role in the transfer fidelity. Also shown in Fig. 5.3.3 are the corresponding quantities for the linear perfect state transfer chain. The similarities between these two systems suggest a comparison of their transfer properties when perturbations are added, as is discussed below. The inset in

---

[2]Lorentzian probability distribution: $P_{k,1}^{\alpha_{opt}} \simeq \frac{1}{\pi} \frac{\Gamma}{(k-k_0)^2 + \Gamma^2}$, where parameter k_0 is the location of the peak of the distribution and Γ is the half-width at half-maximum.

[3]Gaussian probability distribution: $P_{k,1}^{lin} \simeq A e^{-\frac{(k-k_0)^2}{2\sigma^2}}$ where parameter k_0 is the mean (location) and σ^2 is the variance.
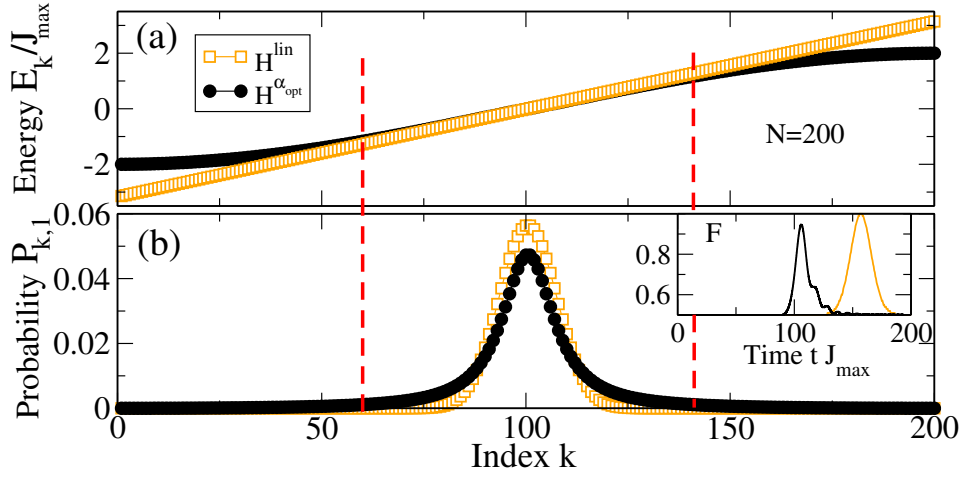
Figure 5.3.1: Properties of the $H^{\alpha_{opt}}$ system (black solid dots) and the H^{lin} system (orange open squares) for a chain length $N = 200$. (a) Eigenenergies E_k. (b) Probabilities $P_{k,1}$ of the initial state $|\psi_0\rangle = |\mathbf{1}\rangle$. The dashed vertical lines show the dominant energy eigenstates $|k\rangle$ that contribute to the state transfer. $P_{k,1}^{\alpha_{opt}}$ is Lorentzian and $P_{k,1}^{lin}$ Gaussian (see Fig. 5.3.3). Inset: Evolution of the averaged fidelity of the state transfer.

Fig. 5.3.1(b) shows the averaged transfer fidelity of the unperturbed linear perfect state transfer and α_{opt} systems, as functions of time. The maximum fidelity of the α_{opt} system[4] is clearly smaller than unity, and it decreases with each revival of the signal. However, the transfer time t_M of the α_{opt} system is shorter: $t_M^{lin} = t_{PST}^{lin} = \frac{\pi N}{4J_{max}}$ (4.3.1)[29, 120] and $t_M^{\alpha_{opt}} = t^{\alpha_{opt}} \sim \frac{N}{2J_{max}}$ (3.3.4)[119]; hence

$$t_{PST}^{lin} \sim \frac{\pi}{2} t^{\alpha_{opt}}. \tag{5.3.6}$$

---

[4]The maximum fidelity of the α_{opt} system as a function of N, the length of the spin channel, is displayed in Fig. 3.3.9.
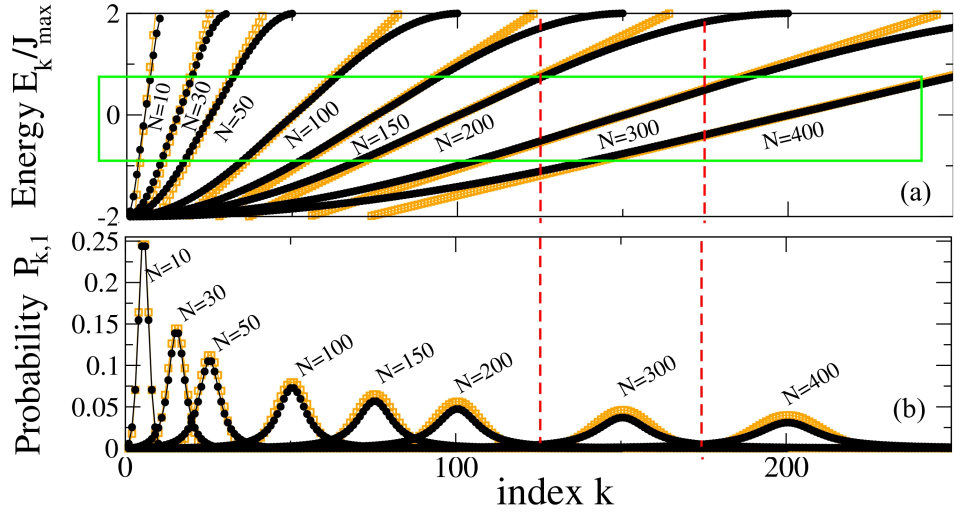
Figure 5.3.2: Properties of the $H^{\alpha_{opt}}$ system (black solid dots) and the H^{lin} system (orange open squares) for different chain lengths N. (a) Eigenenergies E_k. (b) Probabilities $P_{k,1}$ of the initial state $|\psi_0\rangle = |\mathbf{1}\rangle$.
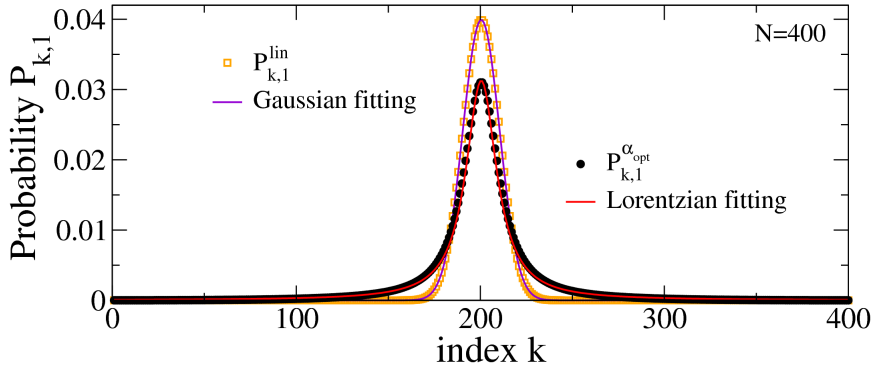
Figure 5.3.3: Curve fitting of the probabilities $P_{k,1}$ for the $H^{\alpha_{opt}}$ and H^{lin} systems in a chain length $N = 400$. $P_{k,1}^{\alpha_{opt}}$ is Lorentzian; and $P_{k,1}^{lin}$ is Gaussian. The fitting values are shown in the text.

Robustness of state transfer

The main results of the comparison between the linear perfect state transfer and α_{opt} systems are shown in Fig. 5.3.4. Figure 5.3.4(a) shows the fidelity at time t_M, the transfer time of the unperturbed case. The transfer fidelity is

averaged over the Bloch sphere, as well as over the disorder, for a chain with $N = 200$, as a function of the disorder strength ε_J.
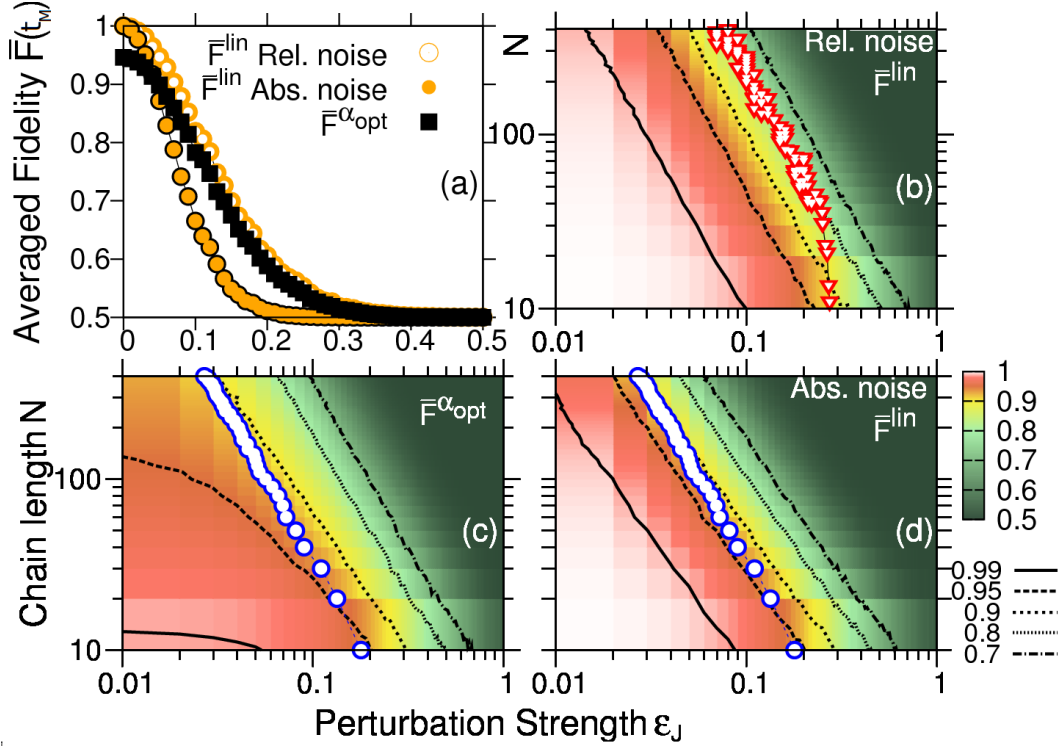
Figure 5.3.4: Averaged fidelity $\overline{F}$ at time t_M as a function of the perturbation strength ε_J and the chain length N, averaged over N_{av} realizations, for H^{lin} and $H^{\alpha_{opt}}$ systems. Relative and absolute static disorder are considered. **(a)** $\overline{F}^{lin}$ with relative disorder (open circles) and absolute disorder (orange circles) and $\overline{F}^{\alpha_{opt}}$ (black squares) for both kinds of disorder when N=200 and $N_{av} = 10^3$. **(b)** $\overline{F}^{lin}$ with relative disorder . The open triangles indicate when $\overline{F}^{lin} = \overline{F}^{\alpha_0}_{odd}$ shown in Fig. 5.3.7(c). To the left of the symbols $\overline{F}^{lin} > \overline{F}^{\alpha_0}_{odd}$ (the difference being small, however), while to the right $\overline{F}^{\alpha_0} > \overline{F}^{lin}$. For a better comprehension, Fig. 5.3.5(a) shows the fidelity difference $\overline{F}^{lin} - \overline{F}^{\alpha_0}_{odd}$. **(c)** $\overline{F}^{\alpha_{opt}}$ with both kinds of disorder and **(d)** $\overline{F}^{lin}$ with absolute disorder . The open circles indicate when $\overline{F}^{lin} = \overline{F}^{\alpha_{opt}}$. To the left of the symbols $\overline{F}^{lin} > \overline{F}^{\alpha_{opt}}$ and to the right $\overline{F}^{\alpha_{opt}} > \overline{F}^{lin}$. The fidelity difference $\overline{F}^{lin} - \overline{F}^{\alpha_{opt}}$ is shown in Fig. 5.3.5(b).

The linear perfect state transfer system with relative static disorder has a transfer fidelity higher than that of the boundary controlled system for all ε_J, but for $\varepsilon_J \gtrsim 0.1$ (where the fidelity is already rather low) the difference in fidelity between the two systems becomes insignificant. However, with absolute static disorder, there is a finite perturbation strength ($\varepsilon_J \approx 0.05$) where the α_{opt} system becomes better than the linear perfect state transfer system. Hence, if a fidelity very close to unity is desired, the complete engineering of the couplings and very good disorder protection are mandatory. However, if only a moderate fidelity is needed (or possible, due to high disorder level) a boundary-controlled system might do.
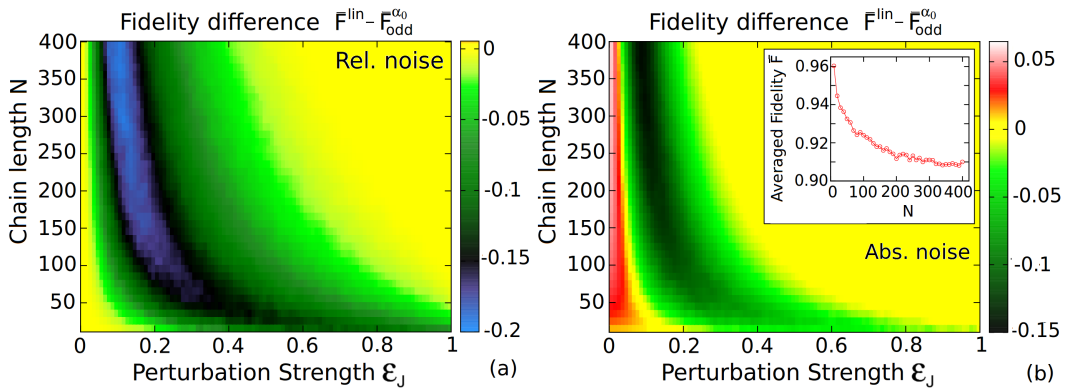
Figure 5.3.5: Averaged fidelity differences $\Delta\overline{F}$ at time t_M as a function of the perturbation strength ε_J and the chain length N, averaged over $N_{av} = 10^3$ realizations. **(a)** $\overline{F}^{lin} - \overline{F}^{\alpha_0}_{odd}$ with relative disorder. $\Delta\overline{F} = 0$ at the values (N, ε_J) is shown as open triangles in Fig. 5.3.4(b). **(b)** $\overline{F}^{lin} - \overline{F}^{\alpha_{opt}}$ with absolute disorder. $\Delta\overline{F} = 0$ at the values (N, ε_J) is shown as open circles in Fig. 5.3.4(c) and 5.3.4(d). Inset: Show the value of the fidelities at the crossing point $\Delta\overline{F} = 0$, as a function of N.

In order to see how the transfer properties depend on the chain length we show in Figs. 5.3.4(b)-5.3.4(d) the average fidelity for each systems discussed above as a contour and color plot in the (ε_J, N) plane. The contour lines are straight lines (representing power laws) in most cases, with deviations for the boundary-controlled system at weak disorder case. The open circles in Figs. 5.3.4(c) and 5.3.4(d) indicate where the fidelity of the boundary-controlled chain is equal to that of the linear perfect state transfer chain with absolute static disorder ; to the right of the open circles the boundary-controlled chain

has higher fidelity. This behaviour of both fidelities can be better appreciated in Fig. 5.3.5(b) where we show the difference between them.

The results above already indicate that there is no simple general answer to the question whether fully engineered or boundary-controlled spin chains provide better quantum state transfer properties in the presence of disorder. The static disorder model, strength and chain length all are important factors in answering that question. We arrive at similar conclusions in our next example.

5.3.2 Weak Coupling Regime for state transfer vs. quadratic energy distribution for perfect state transfer

System properties

When the boundary spins are weakly coupled to the channel, *i.e.*, $\alpha J_{max} = \alpha_0 J_{max} \ll \frac{1}{\sqrt{N}}$ in H^α, an almost perfect state transfer, $F \approx 1 - \mathcal{O}(\alpha^2 J_{max}^2 N)$, is achieved (for details, see Ref. [109] and Sec. 5.3.2). In this parameter region, the parity of N is relevant. This can be understood by studying the spectral properties of the "channel" of $N-2$ spins connecting the transmitting and receiving qubits. For odd (even) N the dynamic of the channel is dominated by two (three) states situated symmetrically about the center of the energy spectrum [109]. The energy differences between these dominant levels determine the transfer time which is obtained as

$$ t_{M,even}^{\alpha_0} \quad = \quad t_{even}^{\alpha_0} \sim \frac{\pi}{2\alpha^2 J_{max}} \tag{5.3.7} $$

and

$$ t_{M,odd}^{\alpha_0} \quad = \quad t_{odd}^{\alpha_0} \sim \frac{\pi\sqrt{N}}{2\alpha J_{max}} \tag{5.3.8} $$

[109]. Since the transfer time is N independent for even N and $\alpha_0 J_{max} < \frac{1}{\sqrt{N}}$, the transfer is faster for odd N.

As we showed in Chap. 4, the fully engineered (perfect state transfer) chain with odd N and a quadratic energy spectrum has very similar properties: few energy eigenstates dominate the state transfer, making it the most robust perfect state transfer system for relative disorder [120]. We therefore compare this last system to the boundary-controlled chain at weak coupling. We find

that the transfer time of the quadratic perfect state transfer chain is

$$t_M^{quad} = t^{quad} \sim \frac{\pi N^2}{8 J_{max}} \tag{5.3.9}$$

which is longer than $t_{odd}^{\alpha_0}$ for $\alpha \gtrsim \frac{4}{N^{3/2}}$ for reasonably large N.

To appreciate the transfer times and the performance of the fidelity as a function of time, we show the averaged fidelity, $\overline{F}(t)$ for the H^{quad} and H^{α_0} systems, and for even and odd chain length N, in Fig. 5.3.6.
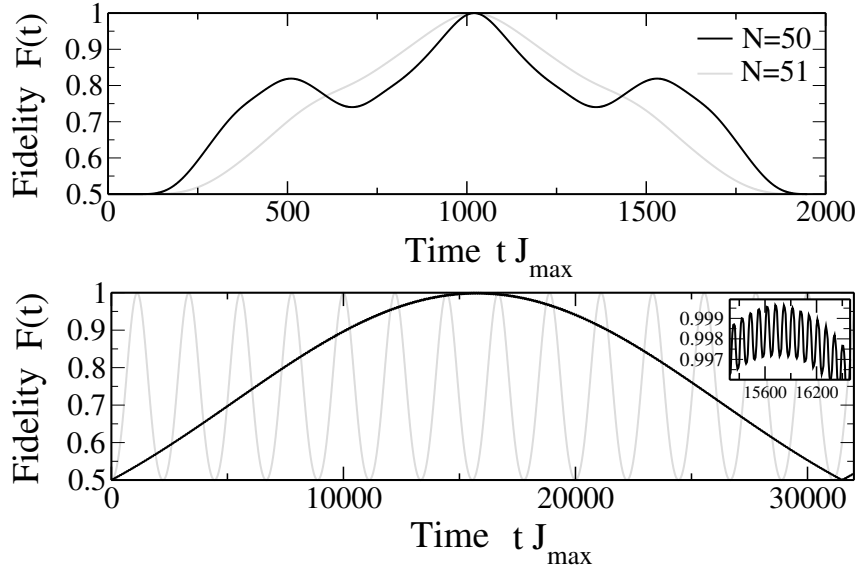
Figure 5.3.6: Averaged transmission fidelity $\overline{F}(t)$ in an even $N = 50$ chain length (gray color) and odd $N = 51$ (black line). Top panel: $\overline{F}^{quad}(t)$; Bottom panel: $\overline{F}^{\alpha_0}(t)$. The maximum fidelity is achieved at the spin-wave echo time t_M. That time is discussed in the text.

Robustness of state transfer

Figures 5.3.7(a) and (b) show the averaged fidelities for chains with $N = 200$ and $N = 201$, respectively, for the quadratic perfect state transfer system and the weak-coupling boundary-controlled system, at time t_M determined by the unperturbed cases, and for $\alpha = 0.01$. Again, as in the linear case, absolute disorder is much more detrimental for the transmission than relative disorder. This is connected to the fact that the maximum and minimum couplings in

the chain may differ by orders of magnitude, with the small couplings always close to the ends of the chain [120]. Consequently, a fluctuation of a given absolute size may completely spoil the state transport when it affects one of the small couplings close to the boundary. For the boundary-controlled system the two kinds of disorder are again equal by definition. Therefore, for absolute disorder the weak-coupling optimized state transfer system performs always better than the quadratic perfect state transfer system. For relative disorder the parity of N determines the appearance of behaviours markedly different for N odd or even. The fidelity of the boundary-controlled system is similar or higher (lower) than that of the perfect state transfer system when N is even (odd).

Figures 5.3.7(c) and 5.3.7(d) show the fidelity as a contour and color plot in the (ε_J, N) plane for $\alpha = 0.01$ and odd N. The contour lines are again power laws. The open symbols in Fig. 5.3.7(c) (squares) indicate where the fidelities for odd and even weak-coupling boundary-controlled systems are equal. To the left of the symbols the fidelity is higher for odd N. The difference between these fidelities is displayed in Fig. 5.3.8(a). The open symbols (diamonds) in Fig. 5.3.7(d) indicate where the fidelities for odd quadratic perfect state transfer systems (with relative disorder) and for even weak-coupling boundary-controlled systems are equal. To the left of the symbols the fidelity is higher for the quadratic perfect state transfer system, but for small perturbation strength differences between the two systems are quite small as can be appreciated in Fig. 5.3.8(b).

We want to remark that if an actual implementation were to be used, the faulty couplings of the chain could be tested following the recipe given in Ref. [108], which allows the coupling strength estimation of a XX spin chain with an external magnetic field applied to it. In this case the best possible time to remove the state from the chain can be obtained from the numerical integration of the Schrödinger equation, just looking for the smallest time when the fidelity is near 1. In case the indirect Hamiltonian tomography [24] turns out to be too expensive or cumbersome to perform, the best time to remove the state from the chain is the design time, *i.e.*, the time t_M when the fidelity of the "nonfaulty chain", the one that was intended to be implemented, achieves its best performance.
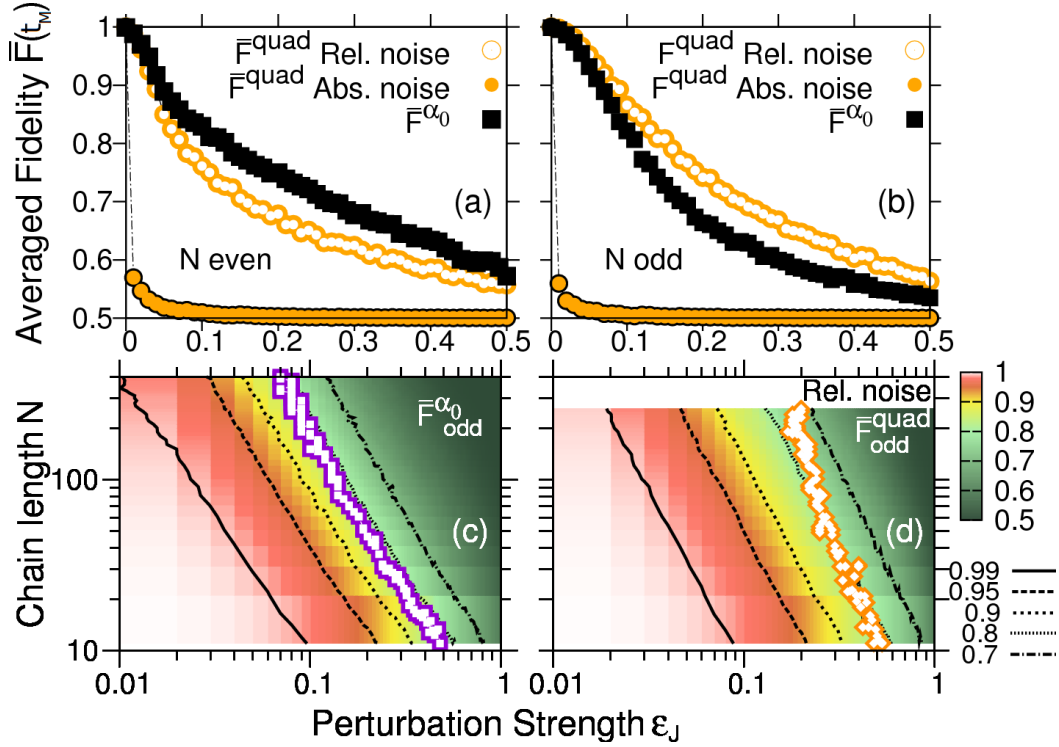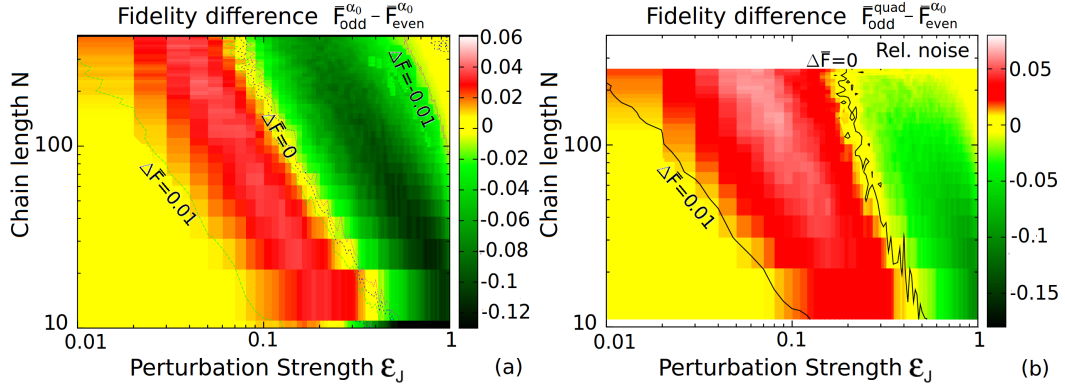
Figure 5.3.7: Averaged fidelity at time t_M as a function of the perturbation strength ε_J and of the chain length N, averaged over N_{av} realizations, for $H^{quad}(\alpha = 0.01)$ and H^{α_0} systems when relative and absolute disorder are considered. **(a)** $\overline{F}^{quad}$ with relative disorder (open circles) and absolute disorder (orange circles) and $\overline{F}^{\alpha_0}$ (black squares) for both kinds of disorder when $N = 200$ and $N_{av} = 10^3$. **(b)** Same as panel (a) for $N = 201$. **(c)** $\overline{F}^{\alpha_0}$ with both kinds of disorder for odd N. The open squares show when $\overline{F}^{\alpha_0}_{odd} = \overline{F}^{\alpha_0}_{even}$(not shown), where $\overline{F}^{\alpha_0}_{odd} > \overline{F}^{\alpha_0}_{even}$ to the left of the symbols. See in Fig. 5.3.8(a) the fidelity difference $\overline{F}^{\alpha_0}_{odd} - \overline{F}^{\alpha_0}_{even}$. **(d)** $\overline{F}^{quad}_{odd}$ with relative disorder. The open diamonds indicate when $\overline{F}^{\alpha_0}_{even} = \overline{F}^{quad}_{odd}$, where $\overline{F}^{quad}_{odd} > \overline{F}^{\alpha_0}_{even}$ to the left of the symbols. The difference $\overline{F}^{quad}_{odd} - \overline{F}^{\alpha_0}_{even}$ is displayed in Fig. 5.3.8(b).

On the other hand, a detailed analysis of the statistics of the fidelity as a function of time is lacking; so far most studies focus on its average over realizations of the noise. For a particular class of engineered chains [29], De Chiara *et al.* [28] have shown that the time signal of the fidelity becomes fractal. In this sense, it is difficult to assess how much information is lost

because of a bad timing for the readout of the state at the receiving end of the channel.

Figure 5.3.8: Averaged fidelity differences $\Delta\overline{F}$ at time t_M as a function of the perturbation strength ε_J and the chain length N, averaged over $N_{av} = 10^3$ realizations. **(a)** $\overline{F}_{odd}^{\alpha_0} - \overline{F}_{even}^{\alpha_0}$. The open squares in Fig. 5.3.7(c) show $\Delta\overline{F}(N, \varepsilon_J) = 0$. **(b)** $\overline{F}_{odd}^{quad} - \overline{F}_{even}^{\alpha_0}$ with relative disorder. The open diamonds in Fig. 5.3.7(d) display $\Delta\overline{F}(N, \varepsilon_J) = 0$.

5.4 Summary and conclusions

For **relative disorder**, Fig. 5.4.1 shows a comparison between all of the systems considered here, linear perfect state transfer and boundary-controlled with optimal α_{opt} as well as quadratic perfect state transfer and weak-coupling ($\alpha = 0.01$) boundary-controlled, for both even and odd lengths. For each system the figure shows the line in the (ε_J, N) plane where $\overline{F} = 0.9$. Open symbols denote perfect state transfer systems; closed symbols correspond to boundary-controlled systems. To the left of the symbols the transfer fidelity of each system is $\overline{F} > 0.9$. It is interesting to note that the lines for the three boundary-controlled systems lie next to each other (at least for long chains), while one of the perfect state transfer systems (quadratic, even) lies clearly below (performs less well) and the other two perfect state transfer systems lie slightly above. This situation changes, however, for different levels of fidelity. For example, the $H_{odd}^{\alpha_0}$ system outperforms H^{lin} in the region to the right of the crossover marked by the open triangles in Fig. 5.3.4(b). Note that to the left of that crossover the fidelities of the two systems differ only by up to 4%.

On the other hand, to the right of the crossover displayed in Fig. 5.3.7(d), $H_{even}^{\alpha_0}$ is the best choice.
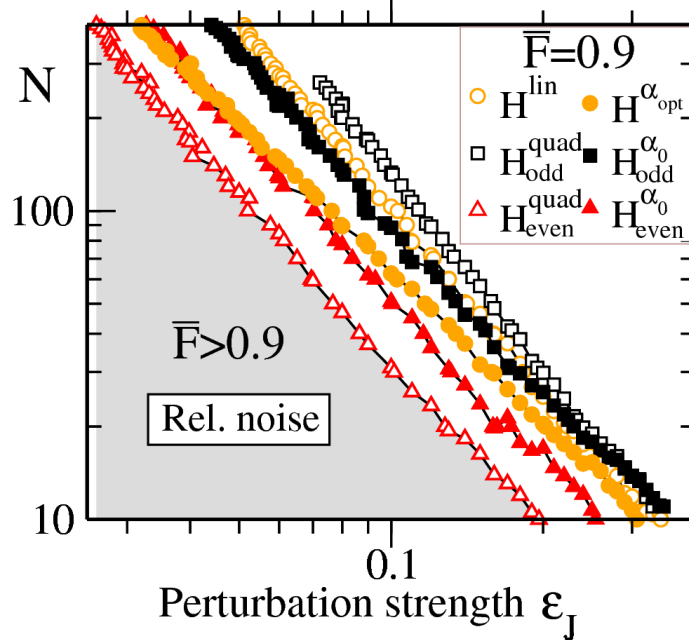
Figure 5.4.1: Contour lines of the averaged transfer fidelity $\overline{F} = 0.9$ for fully-engineered perfect state transfer systems (closed symbols) and boundary-controlled α−optimized state transfer systems. To the left of the symbols the transfer fidelity $\overline{F} > 0.9$ for every system.

For **absolute disorder**, there is almost always a boundary-controlled system with fidelity larger than that of the perfect state transfer systems. Only for very small perturbation strength can perfect state transfer systems be better than optimized state transfer systems, but the fidelities are similar.

Considering **only the perfect state transfer systems**, H_{odd}^{quad} performs better than H^{lin} for relative disorder with similar transfer fidelity for small perturbations. Conversely, H^{lin} is drastically the more robust choice for absolute disorder. Considering **only the optimized state transfer systems**, $H_{odd}^{\alpha_0}$ achieves the highest state transfer fidelities.

For all the channels with $\overline{F} \to 1$ in the vanishing perturbation strength limit we find a power law $N\varepsilon_J^\beta = const$ for the contours of constant fidelity, with β near 2, generalizing the fidelity scaling law found for the linear perfect state transfer system with relative disorder [28]. This quantifies the sensitivity of

the channels to perturbations as a function of the system size: Increasing the channel length, the transfer fidelity becomes more sensitive to the perturbations.

If the **transfer speed** is important, independent of the kind of disorder, the faster transfer is achieved by the non-engineered $H^{\alpha_{opt}}$ system, closely followed by the engineered H^{lin} system. The other systems are significantly slower.

To summarize, we show that in most situations the transmission performance of boundary-controlled spin chains renders the full engineering of the couplings of a spin chain unnecessary in order to obtain quantum state transmission with high fidelity under static perturbations.

6 Conclusion

In this thesis we studied the performance, reliability and robustness of quantum information transfer through spin channels. Our research work represent one step more in the task to assess the feasibility to develop and implement quantum computers, since the communication between their parts is one of the main blocks to build them and make them scalable and powerful.

Our contributions allow to understand both aspects: how static perturbations affect the transmission in quantum channels and which are the system properties that make it robust against pertubations. This new knowledge becomes essential to be able to face and overcome the problems that arise in the experimental implementations.

We found an *optimal boundary-controlled channel* for the transfer of states and entanglement, by studying the localization properties of the total state. We called it "optimal channel" because it only requires minimal control of both ends of the channel to achieve a fast, efficient and robust transfer under static perturbations.

We also studied the performance of fully engineered spin-channels that achieve perfectly the task of information transfer in the absence of perturbations. We analyzed their robustness against static perturbations and timing errors. We tried to quantify how disturbances affect the quality of the transfer. Some systems are more robust than others, so we distinguish which are the intrinsic characteristics, such as the spatial localization of the eigenstates, that make them robust.

We found similarities in the intrinsic characteristics of the most robust channels of all those that we studied. We compared their performances against different kinds of perturbations. We conclude that in many situations, the channels that require less engineering effort, those that we call boundary-controlled spin chains, are similar or even more efficient against perturbations than the channels fully engineered for perfect state transfer. Moreover, the optimal channels mentioned above, achieve the faster transfer.

The knowledge garnered through this thesis could be of fundamental importance for practical and experimental purposes, since simpler systems are more

practical and feasible to handle. Anyway, there is a lot more to understand, related not only to those issues raised in this thesis, but to quantum information processing implementations in general. Nowadays, we are still far away from a real implementation of the desirable quantum computer; but we are always getting a little bit closer.

List of Figures

Bibliography

[1] C. Albanese, M. Christandl, N. Datta, and A. Ekert. Mirror inversion of quantum states in linear registers. *Physical Review Letters*, 93:230502, Nov. 2004. URL `http://adsabs.harvard.edu/abs/2004PhRvL..93w0502A`.

[2] J. Allcock and N. Linden. Quantum communication beyond the localization length in disordered spin chains. *Physical Review Letters*, 102 (11):110501, Mar. 2009. doi: 10.1103/PhysRevLett.102.110501. URL `http://link.aps.org/doi/10.1103/PhysRevLett.102.110501`.

[3] G. A. Álvarez and D. Suter. NMR quantum simulation of localization effects induced by decoherence. *Physical Review Letters*, 104(23):230403, June 2010. doi: 10.1103/PhysRevLett.104.230403. URL `http://link.aps.org/doi/10.1103/PhysRevLett.104.230403`.

[4] G. A. Álvarez, E. P. Danieli, P. R. Levstein, and H. M. Pastawski. Decoherence as attenuation of mesoscopic echoes in a spin-chain channel. *Physical Review A*, 82(1):012310, July 2010. doi: 10.1103/PhysRevA.82.012310. URL `http://link.aps.org/doi/10.1103/PhysRevA.82.012310`.

[5] G. A. Álvarez, M. Mishkovsky, E. P. Danieli, P. R. Levstein, H. M. Pastawski, and L. Frydman. Perfect state transfers by selective quantum interferences within complex spin networks. *Physical Review A*, 81(6):060302, June 2010. doi: 10.1103/PhysRevA.81.060302. URL `http://link.aps.org/doi/10.1103/PhysRevA.81.060302`.

[6] L. Amico, R. Fazio, A. Osterloh, and V. Vedral. Entanglement in many-body systems. *Reviews of Modern Physics*, 80(2):517–576, May 2008. doi: 10.1103/RevModPhys.80.517. URL `http://link.aps.org/doi/10.1103/RevModPhys.80.517`.

[7] T. J. G. Apollaro and F. Plastina. Entanglement localization by a single defect in a spin chain. *Physical Review A*, 74(6):062316, Dec. 2006. doi: 10.1103/PhysRevA.74.062316. URL `http://link.aps.org/doi/10.1103/PhysRevA.74.062316`.

Bibliography

[8] T. J. G. Apollaro and F. Plastina. Quantum information storage in the localized state of a spin chain. *Open Systems and Information Dynamics*, 14(1):41–51, Mar. 2007. ISSN 1230-1612. doi: 10. 1007/s11080-007-9027-5. URL `http://www.worldscinet.com/osid/14/1401/S123016120700005X.html`.

[9] L. Banchi, T. J. G. Apollaro, A. Cuccoli, R. Vaia, and P. Verrucchi. Optimal dynamics for quantum-state and entanglement transfer through homogeneous quantum systems. *Physical Review A*, 82:52321, Nov. 2010. URL `http://adsabs.harvard.edu/abs/2010PhRvA..82e2321B`.

[10] L. Banchi, T. J. G. Apollaro, A. Cuccoli, R. Vaia, and P. Verrucchi. Long quantum channels for high-quality entanglement transfer. *New Journal of Physics*, 13:3006, Dec. 2011. URL `http://adsabs.harvard.edu/abs/2011NJPh...13l3006B`.

[11] L. Banchi, A. Bayat, P. Verrucchi, and S. Bose. Nonperturbative entangling gates between distant qubits using uniform cold atom chains. *Physical Review Letters*, 106(14):140501, Apr. 2011. doi: 10.1103/ PhysRevLett.106.140501. URL `http://link.aps.org/doi/10.1103/PhysRevLett.106.140501`.

[12] C. H. Bennett and D. P. DiVincenzo. Quantum information and computation. *Nature*, 404(6775):247–255, Mar. 2000. ISSN 0028-0836. doi: 10.1038/35005001. URL `http://dx.doi.org/10.1038/35005001`.

[13] C. H. Bennett and S. J. Wiesner. Communication via one- and two-particle operators on Einstein-Podolsky-Rosen states. *Physical Review Letters*, 69(20):2881–2884, Nov. 1992. doi: 10.1103/PhysRevLett. 69.2881. URL `http://link.aps.org/doi/10.1103/PhysRevLett.69.2881`.

[14] C. H. Bennett, G. Brassard, C. Crépeau, R. Jozsa, A. Peres, and W. K. Wootters. Teleporting an unknown quantum state via dual classical and Einstein-Podolsky-Rosen channels. *Physical Review Letters*, 70(13): 1895–1899, Mar. 1993. doi: 10.1103/PhysRevLett.70.1895. URL `http://link.aps.org/doi/10.1103/PhysRevLett.70.1895`.

[15] S. Bose. Quantum communication through an unmodulated spin chain. *Physical Review Letters*, 91:207901, Nov. 2003. URL `http://adsabs.harvard.edu/abs/2003PhRvL..91t7901B`.

[16] S. Bose. Quantum communication through spin chain dynamics: an introductory overview. *Contemporary Physics*, 48:13–30, Jan. 2007. ISSN 0010-7514, 1366-5812. doi: 10.1080/00107510701342313. URL `http://www.tandfonline.com/doi/abs/10.1080/00107510701342313`.

[17] D. Bouwmeester, J. Pan, K. Mattle, M. Eibl, H. Weinfurter, and A. Zeilinger. Experimental quantum teleportation. *Nature*, 390(6660): 575–579, Dec. 1997. ISSN 0028-0836. doi: 10.1038/37539. URL `http://dx.doi.org/10.1038/37539`.

[18] D. Burgarth and S. Bose. Conclusive and arbitrarily perfect quantum-state transfer using parallel spin-chain channels. *Physical Review A*, 71 (5):052315, May 2005. doi: 10.1103/PhysRevA.71.052315. URL `http://link.aps.org/doi/10.1103/PhysRevA.71.052315`.

[19] D. Burgarth and S. Bose. Perfect quantum state transfer with randomly coupled quantum chains. *New Journal of Physics*, 7:135–135, May 2005. ISSN 1367-2630. doi: 10.1088/1367-2630/7/1/135. URL `http://iopscience.iop.org/1367-2630/7/1/135`.

[20] D. Burgarth, V. Giovannetti, and S. Bose. Efficient and perfect state transfer in quantum chains. *Journal of Physics A: Mathematical and General*, 38(30):6793–6802, July 2005. ISSN 0305-4470, 1361-6447. doi: 10.1088/0305-4470/38/30/013. URL `http://iopscience.iop.org/0305-4470/38/30/013`.

[21] D. Burgarth, V. Giovannetti, and S. Bose. Optimal quantum-chain communication by end gates. *Physical Review A*, 75(6):062327, June 2007. doi: 10.1103/PhysRevA.75.062327. URL `http://link.aps.org/doi/10.1103/PhysRevA.75.062327`.

[22] D. Burgarth, S. Bose, C. Bruder, and V. Giovannetti. Local controllability of quantum networks. *Physical Review A*, 79(6):060305, June 2009. doi: 10.1103/PhysRevA.79.060305. URL `http://link.aps.org/doi/10.1103/PhysRevA.79.060305`.

[23] D. Burgarth, K. Maruyama, M. Murphy, S. Montangero, T. Calarco, F. Nori, and M. B. Plenio. Scalable quantum computation via local control of only two qubits. *Physical Review A*, 81(4):040303, Apr. 2010. doi: 10.1103/PhysRevA.81.040303. URL `http://link.aps.org/doi/10.1103/PhysRevA.81.040303`.

Bibliography

[24] D. Burgarth, K. Maruyama, and F. Nori. Indirect quantum tomography of quadratic Hamiltonians. *New Journal of Physics*, 13(1):013019, Jan. 2011. ISSN 1367-2630. doi: 10.1088/1367-2630/13/1/013019. URL `http://iopscience.iop.org/1367-2630/13/1/013019`.

[25] C. K. Burrell and T. J. Osborne. Bounds on the speed of information propagation in disordered quantum spin chains. *Physical Review Letters*, 99(16):167201, Oct. 2007. doi: 10.1103/PhysRevLett.99.167201. URL `http://link.aps.org/doi/10.1103/PhysRevLett.99.167201`.

[26] P. Cappellaro, C. Ramanathan, and D. G. Cory. Dynamics and control of a quasi-one-dimensional spin system. *Physical Review A*, 76(3):032317, 2007. doi: 10.1103/PhysRevA.76.032317. URL `http://link.aps.org/doi/10.1103/PhysRevA.76.032317`.

[27] P. Cappellaro, L. Jiang, J. S. Hodges, and M. D. Lukin. Coherence and control of quantum registers based on electronic spin in a nuclear spin bath. *Physical Review Letters*, 102(21):210502, May 2009. doi: 10.1103/PhysRevLett.102.210502. URL `http://link.aps.org/doi/10.1103/PhysRevLett.102.210502`.

[28] G. D. Chiara, D. Rossini, S. Montangero, and R. Fazio. From perfect to fractal transmission in spin chains. *Physical Review A*, 72(1):012323, July 2005. doi: 10.1103/PhysRevA.72.012323. URL `http://link.aps.org/doi/10.1103/PhysRevA.72.012323`.

[29] M. Christandl, N. Datta, A. Ekert, and A. J. Landahl. Perfect state transfer in quantum spin networks. *Physical Review Letters*, 92(18): 187902, May 2004. doi: 10.1103/PhysRevLett.92.187902. URL `http://link.aps.org/doi/10.1103/PhysRevLett.92.187902`.

[30] M. Christandl, N. Datta, T. C. Dorlas, A. Ekert, A. Kay, and A. J. Landahl. Perfect transfer of arbitrary states in quantum spin networks. *Physical Review A*, 71(3):032312, Mar. 2005. doi: 10.1103/PhysRevA.71.032312. URL `http://link.aps.org/doi/10.1103/PhysRevA.71.032312`.

[31] R. J. Cook and B. W. Shore. Coherent dynamics of n-level atoms and molecules. III. an analytically soluble periodic case. *Physical Review A*, 20(2):539–544, 1979. doi: 10.1103/PhysRevA.20.539. URL `http://link.aps.org/doi/10.1103/PhysRevA.20.539`.

[32] F. M. Cucchietti, H. M. Pastawski, and D. A. Wisniacki. Decoherence as decay of the loschmidt echo in a lorentz gas. *Physical Review E*, 65 (4):045206, Apr. 2002. doi: 10.1103/PhysRevE.65.045206. URL `http://link.aps.org/doi/10.1103/PhysRevE.65.045206`.

[33] I. D'Amico. Quantum dot-based quantum buses for quantum computer hardware architecture. *Microelectronics Journal*, 37(12):1440–1441, Dec. 2006. ISSN 0026-2692. doi: 10.1016/j.mejo.2006.05.004. URL `http://www.sciencedirect.com/science/article/pii/S0026269206000929`.

[34] A. D. Dente, R. A. Bustos-Marún, and H. M. Pastawski. Dynamical regimes of a quantum SWAP gate beyond the Fermi golden rule. *Physical Review A*, 78(6):062116, Dec. 2008. doi: 10.1103/PhysRevA.78.062116. URL `http://link.aps.org/doi/10.1103/PhysRevA.78.062116`.

[35] D. Deutsch. Quantum computation. *Physics World*, 1/6/92.

[36] D. P. DiVincenzo. Quantum computation. *Science*, 270(5234):255 – 261, Oct. 1995. doi: 10.1126/science.270.5234.255. URL `http://www.sciencemag.org/content/270/5234/255.abstract`.

[37] D. P. DiVincenzo. The physical implementation of quantum computation. *Fortschritte der Physik*, 48(9):771, Sept. 2000. ISSN 1521-3978. doi: 10.1002/1521-3978(200009)48:9/11<771::AID-PROP771>3.0.CO;2-E. URL `http://onlinelibrary.wiley.com/doi/10.1002/1521-3978(200009)48:9/11<771::AID-PROP771>3.0.CO;2-E/abstract`.

[38] U. Dorner, P. Fedichev, D. Jaksch, M. Lewenstein, and P. Zoller. Entangling strings of neutral atoms in 1D atomic pipeline structures. *Physical Review Letters*, 91(7):073601, 2003. doi: 10.1103/PhysRevLett.91.073601. URL `http://link.aps.org/doi/10.1103/PhysRevLett.91.073601`.

[39] L. Duan, E. Demler, and M. D. Lukin. Controlling spin exchange interactions of ultracold atoms in optical lattices. *Physical Review Letters*, 91(9):090402, 2003. doi: 10.1103/PhysRevLett.91.090402. URL `http://link.aps.org/doi/10.1103/PhysRevLett.91.090402`.

[40] E. Fel'dman, R. Brüschweiler, and R. Ernst. From regular to erratic quantum dynamics in long spin1/2 chains with an XY Hamiltonian.

Chemical Physics Letters, 294(4-5):297–304, Sept. 1998. ISSN 0009-2614. doi: 16/S0009-2614(98)00887-2. URL `http://www.sciencedirect.com/science/article/pii/S0009261498008872`.

[41] E. B. Fel'dman, E. I. Kuznetsova, and A. I. Zenchuk. High-probability state transfer in spin-1/2 chains: Analytical and numerical approaches. *Physical Review A*, 82(2):022332, 2010. doi: 10.1103/PhysRevA.82.022332. URL `http://link.aps.org/doi/10.1103/PhysRevA.82.022332`.

[42] A. Ferrón, O. Osenda, and P. Serra. Entanglement in resonances of two-electron quantum dots. *Physical Review A*, 79(3):032509, Mar. 2009. doi: 10.1103/PhysRevA.79.032509. URL `http://link.aps.org/doi/10.1103/PhysRevA.79.032509`.

[43] R. Feynman. 'Classical talk' given in 1959 at the annual meeting of the american physical society at the caltech. *Caltech Engineering and Science*, 23:5(22), 1960.

[44] R. P. Feynman. Simulating physics with computers. *International Journal of Theoretical Physics*, 21(6-7):467–488, June 1982. ISSN 0020-7748, 1572-9575. doi: 10.1007/BF02650179. URL `http://www.springerlink.com/content/t2x8115127841630/`.

[45] J. Fitzsimons and J. Twamley. Globally controlled quantum wires for perfect qubit transport, mirroring, and computing. *Physical Review Letters*, 97(9):090502, 2006. doi: 10.1103/PhysRevLett.97.090502. URL `http://link.aps.org/doi/10.1103/PhysRevLett.97.090502`.

[46] J. Fitzsimons, L. Xiao, S. C. Benjamin, and J. A. Jones. Quantum information processing with delocalized qubits under global control. *Physical Review Letters*, 99(3):030501, July 2007. doi: 10.1103/PhysRevLett.99.030501. URL `http://link.aps.org/doi/10.1103/PhysRevLett.99.030501`.

[47] C. D. Franco, M. Paternostro, and M. S. Kim. Perfect state transfer on a spin chain without state initialization. *Physical Review Letters*, 101 (23):230502, Dec. 2008. doi: 10.1103/PhysRevLett.101.230502. URL `http://link.aps.org/doi/10.1103/PhysRevLett.101.230502`.

[48] A. Galindo and M. A. Martín-Delgado. Information and computation: Classical and quantum aspects. *Reviews of Modern Physics*, 74(2):347–

423, May 2002. doi: 10.1103/RevModPhys.74.347. URL `http://link.aps.org/doi/10.1103/RevModPhys.74.347`.

[49] B. Georgeot and D. L. Shepelyansky. Emergence of quantum chaos in the quantum computer core and how to manage it. *Physical Review E*, 62(5):6366, Nov. 2000. doi: 10.1103/PhysRevE.62.6366. URL `http://link.aps.org/doi/10.1103/PhysRevE.62.6366`.

[50] V. Giovannetti and D. Burgarth. Improved transfer of quantum information using a local memory. *Physical Review Letters*, 96(3):030501, Jan. 2006. doi: 10.1103/PhysRevLett.96.030501. URL `http://link.aps.org/doi/10.1103/PhysRevLett.96.030501`.

[51] O. Giraud, J. Martin, and B. Georgeot. Entanglement of localized states. *Physical Review A*, 76(4):042333, Oct. 2007. doi: 10.1103/PhysRevA.76.042333. URL `http://link.aps.org/doi/10.1103/PhysRevA.76.042333`.

[52] N. Gisin, G. Ribordy, W. Tittel, and H. Zbinden. Quantum cryptography. *Reviews of Modern Physics*, 74(1):145–195, Mar. 2002. doi: 10.1103/RevModPhys.74.145. URL `http://link.aps.org/doi/10.1103/RevModPhys.74.145`.

[53] G. M. L. Gladwell. Inverse problems in vibration, kluwer academic. *Boston*, 1986.

[54] M. Grajcar, A. Izmalkov, S. H. W. van der Ploeg, S. Linzen, T. Plecenik, T. Wagner, U. Hübner, E. Il'ichev, H. Meyer, A. Y. Smirnov, P. J. Love, A. M. van den Brink, M. H. S. Amin, S. Uchaikin, and A. M. Zagoskin. Four-Qubit device with mixed couplings. *Physical Review Letters*, 96(4):047006, Feb. 2006. doi: 10.1103/PhysRevLett.96.047006. URL `http://link.aps.org/doi/10.1103/PhysRevLett.96.047006`.

[55] G. Gualdi, V. Kostak, I. Marzoli, and P. Tombesi. Perfect state transfer in long-range interacting spin chains. *Physical Review A*, 78(2):022325, 2008. doi: 10.1103/PhysRevA.78.022325. URL `http://link.aps.org/doi/10.1103/PhysRevA.78.022325`.

[56] M. J. Hartmann, F. G. S. L. Brandão, and M. B. Plenio. Effective spin systems in coupled microcavities. *Physical Review Letters*, 99(16):160501, Oct. 2007. doi: 10.1103/PhysRevLett.99.160501. URL `http://link.aps.org/doi/10.1103/PhysRevLett.99.160501`.

Bibliography

[57] H. L. Haselgrove. Optimal state encoding for quantum walks and quantum communication over spin systems. *Physical Review A*, 72(6): 062326, Dec. 2005. doi: 10.1103/PhysRevA.72.062326. URL `http://link.aps.org/doi/10.1103/PhysRevA.72.062326`.

[58] M. Horodecki, P. Horodecki, and R. Horodecki. General teleportation channel, singlet fraction, and quasidistillation. *Physical Review A*, 60(3): 1888–1898, 1999. doi: 10.1103/PhysRevA.60.1888. URL `http://link.aps.org/doi/10.1103/PhysRevA.60.1888`.

[59] R. Jozsa. Fidelity for mixed quantum states. *J. Mod. Opt.*, 41:2315–2353, 1994.

[60] P. Karbach and J. Stolze. Spin chains as perfect quantum state mirrors. *Physical Review A*, 72:30301, Sept. 2005. URL `http://adsabs.harvard.edu/abs/2005PhRvA..72c0301K`.

[61] A. Kay. Perfect state transfer: Beyond nearest-neighbor couplings. *Physical Review A*, 73:32306, Mar. 2006. URL `http://adsabs.harvard.edu/abs/2006PhRvA..73c2306K`.

[62] A. Kay. Perfect, efficient, state transfer and its application as a constructive tool. *International Journal of Quantum Information*, 08(04):641, 2010. ISSN 0219-7499. doi: 10.1142/S0219749910006514. URL `http://www.worldscinet.com/ijqi/08/0804/S0219749910006514.html`.

[63] J. P. Keating, N. Linden, J. C. F. Matthews, and A. Winter. Localization and its consequences for quantum walk algorithms and quantum communication. *Physical Review A*, 76(1):012315, July 2007. doi: 10.1103/PhysRevA.76.012315. URL `http://link.aps.org/doi/10.1103/PhysRevA.76.012315`.

[64] T. D. Ladd, F. Jelezko, R. Laflamme, Y. Nakamura, C. Monroe, and J. L. O'Brien. Quantum computers. *Nature*, 464(7285):45–53, Mar. 2010. ISSN 0028-0836. doi: 10.1038/nature08812. URL `http://dx.doi.org/10.1038/nature08812`.

[65] L. B. Levitin and T. Toffoli. Fundamental limit on the rate of quantum dynamics: The unified bound is tight. *Physical Review Letters*, 103 (16):160502, Oct. 2009. doi: 10.1103/PhysRevLett.103.160502. URL `http://link.aps.org/doi/10.1103/PhysRevLett.103.160502`.

110

[66] M. Lewenstein, A. Sanpera, V. Ahufinger, B. Damski, A. Sen(De), and U. Sen. Ultracold atomic gases in optical lattices: mimicking condensed matter physics and beyond. *Advances in Physics*, 56(2):243–379, 2007. ISSN 0001-8732. doi: 10.1080/00018730701223200. URL `http://www.tandfonline.com/doi/abs/10.1080/00018730701223200`.

[67] E. H. Lieb and D. W. Robinson. The finite group velocity of quantum spin systems. *Communications in Mathematical Physics*, 28(3):251–257, Sept. 1972. ISSN 0010-3616. doi: 10.1007/BF01645779. URL `http://www.springerlink.com/content/xku2n1l2ml323515/`.

[68] T. Linneweber, J. Stolze, and G. S. Uhrig. Perfect state transfer in XX chains induced by boundary magnetic fields. *arXiv:1111.2686*, Nov. 2011. URL `http://arxiv.org/abs/1111.2686`.

[69] A. Lyakhov and C. Bruder. Quantum state transfer in arrays of flux qubits. *New Journal of Physics*, 7:181–181, Aug. 2005. ISSN 1367-2630. doi: 10.1088/1367-2630/7/1/181. URL `http://iopscience.iop.org/1367-2630/7/1/181`.

[70] A. O. Lyakhov and C. Bruder. Use of dynamical coupling for improved quantum state transfer. *Physical Review B*, 74(23):235303, Dec. 2006. doi: 10.1103/PhysRevB.74.235303. URL `http://link.aps.org/doi/10.1103/PhysRevB.74.235303`.

[71] Z. L. Mádi, B. Brutscher, T. Schulte-Herbrüggen, R. Brüschweiler, and R. R. Ernst. Time-resolved observation of spin waves in a linear chain of nuclear spins. *Chemical Physics Letters*, 268(3-4):300–305, Apr. 1997. ISSN 0009-2614. doi: 16/S0009-2614(97)00194-2. URL `http://www.sciencedirect.com/science/article/pii/S0009261497001942`.

[72] K. Maruyama, T. Iitaka, and F. Nori. Enhancement of entanglement transfer in a spin chain by phase-shift control. *Physical Review A*, 75 (1):012325, Jan. 2007. doi: 10.1103/PhysRevA.75.012325. URL `http://link.aps.org/doi/10.1103/PhysRevA.75.012325`.

[73] T. Michoel, J. Mulherkar, and B. Nachtergaele. Implementing quantum gates using the ferromagnetic spin XXZ chain with kink boundary conditions. *New Journal of Physics*, 12(2):025003, Feb. 2010. ISSN 1367-2630. doi: 10.1088/1367-2630/12/2/025003. URL `http://iopscience.iop.org/1367-2630/12/2/025003`.

Bibliography

[74] G. E. Moore. Cramming more components onto integrated circuits. *Electronics*, 38(8):114–117, Apr. 1965. ISSN 0018-9219. URL `http://dx.doi.org/10.1109/JPROC.1998.658762`.

[75] M. Murphy, S. Montangero, V. Giovannetti, and T. Calarco. Communication at the quantum speed limit along a spin chain. *Physical Review A*, 82(2):022318, 2010. doi: 10.1103/PhysRevA.82.022318. URL `http://link.aps.org/doi/10.1103/PhysRevA.82.022318`.

[76] P. Neumann, R. Kolesov, B. Naydenov, J. Beck, F. Rempp, M. Steiner, V. Jacques, G. Balasubramanian, M. L. Markham, D. J. Twitchen, S. Pezzagna, J. Meijer, J. Twamley, F. Jelezko, and J. Wrachtrup. Quantum register based on coupled electron spins in a room-temperature solid. *Nat Phys*, 6(4):249–253, Apr. 2010. ISSN 1745-2473. doi: 10.1038/nphys1536. URL `http://dx.doi.org/10.1038/nphys1536`.

[77] M. Nielsen and I. Chuang. *Quantum Computation and Quantum Information (Cambridge Series on Information and the Natural Sciences)*. Cambridge University Press, Jan. 2004. ISBN 0521635039.

[78] M. A. Nielsen, E. Knill, and R. Laflamme. Complete quantum teleportation using nuclear magnetic resonance. *Nature*, 396(6706):52–55, Nov. 1998. ISSN 0028-0836. doi: 10.1038/23891. URL `http://dx.doi.org/10.1038/23891`.

[79] G. M. Nikolopoulos, D. Petrosyan, and P. Lambropoulos. Coherent electron wavepacket propagation and entanglement in array of coupled quantum dots. *Europhysics Letters*, 65(3):297–303, 2004. doi: 10.1209/epl/i2003-10100-9.

[80] G. M. Nikolopoulos, D. Petrosyan, and P. Lambropoulos. Electron wavepacket propagation in a chain of coupled quantum dots. *Journal of Physics: Condensed Matter*, 16(28):4991–5002, July 2004. ISSN 0953-8984, 1361-648X. doi: 10.1088/0953-8984/16/28/019. URL `http://iopscience.iop.org/0953-8984/16/28/019`.

[81] S. Oh, L. Wu, Y. Shim, J. Fei, M. Friesen, and X. Hu. Heisenberg spin bus as a robust transmission line for quantum-state transfer. *Physical Review A*, 84(2):022330, 2011. doi: 10.1103/PhysRevA.84.022330. URL `http://link.aps.org/doi/10.1103/PhysRevA.84.022330`.

112

[82] T. J. Osborne and N. Linden. Propagation of quantum information through a spin system. *Physical Review A*, 69:52315, May 2004. URL `http://adsabs.harvard.edu/abs/2004PhRvA..69e2315O`.

[83] H. M. Pastawski, P. R. Levstein, and G. Usaj. Quantum dynamical echoes in the spin diffusion in mesoscopic systems. *Physical Review Letters*, 75(23):4310, Dec. 1995. doi: 10.1103/PhysRevLett.75.4310. URL `http://link.aps.org/doi/10.1103/PhysRevLett.75.4310`.

[84] H. M. Pastawski, G. Usaj, and P. R. Levstein. Quantum interference phenomena in the local polarization dynamics of mesoscopic systems: an NMR observation. *Chemical Physics Letters*, 261(3):329–334, Oct. 1996. ISSN 0009-2614. doi: 10.1016/0009-2614(96)00978-5. URL `http://www.sciencedirect.com/science/article/pii/0009261496009785`.

[85] D. Petrosyan and P. Lambropoulos. Coherent population transfer in a chain of tunnel coupled quantum dots. *Optics Communications*, 264(2): 419–425, Aug. 2006. ISSN 0030-4018. doi: 10.1016/j.optcom.2005.12. 082. URL `http://www.sciencedirect.com/science/article/pii/S0030401806005141`.

[86] D. Petrosyan, G. M. Nikolopoulos, and P. Lambropoulos. State transfer in static and dynamic spin chains with disorder. *Physical Review A*, 81: 42307, Apr. 2010. URL `http://adsabs.harvard.edu/abs/2010PhRvA..81d2307P`.

[87] F. Plastina and T. J. G. Apollaro. Local control of entanglement in a spin chain. *Physical Review Letters*, 99(17):177210, Oct. 2007. doi: 10.1103/PhysRevLett.99.177210. URL `http://link.aps.org/doi/10.1103/PhysRevLett.99.177210`.

[88] F. M. Pont, O. Osenda, J. H. Toloza, and P. Serra. Entropy, fidelity, and double orthogonality for resonance states in two-electron quantum dots. *Physical Review A*, 81(4):042518, Apr. 2010. doi: 10.1103/PhysRevA.81.042518. URL `http://link.aps.org/doi/10.1103/PhysRevA.81.042518`.

[89] J. Preskill. Lecture notes for physics: Quantum information and computation. *http://www.theory.caltech.edu/people/preskill/ph229/*, 1998.

[90] V. N. Prigodin, B. L. Altshuler, K. B. Efetov, and S. Iida. Mesoscopic dynamical echo in quantum dots. *Physical Review Letters*, 72(4):546,

Jan. 1994. doi: 10.1103/PhysRevLett.72.546. URL `http://link.aps.org/doi/10.1103/PhysRevLett.72.546`.

[91] R. Raussendorf. Quantum computation via translation-invariant operations on a chain of qubits. *Physical Review A*, 72(5):052301, Nov. 2005. doi: 10.1103/PhysRevA.72.052301. URL `http://link.aps.org/doi/10.1103/PhysRevA.72.052301`.

[92] A. Romito, R. Fazio, and C. Bruder. Solid-state quantum communication with josephson arrays. *Physical Review B*, 71(10):100501, Mar. 2005. doi: 10.1103/PhysRevB.71.100501. URL `http://link.aps.org/doi/10.1103/PhysRevB.71.100501`.

[93] R. Ronke, T. P. Spiller, and I. D'Amico. Effect of perturbations on information transfer in spin chains. *Physical Review A*, 83(1):012325, Jan. 2011. doi: 10.1103/PhysRevA.83.012325. URL `http://link.aps.org/doi/10.1103/PhysRevA.83.012325`.

[94] E. Rufeil-Fiori, C. M. Sánchez, F. Y. Oliva, H. M. Pastawski, and P. R. Levstein. Effective one-body dynamics in multiple-quantum NMR experiments. *Physical Review A*, 79(3):032324, Mar. 2009. doi: 10.1103/PhysRevA.79.032324. URL `http://link.aps.org/doi/10.1103/PhysRevA.79.032324`.

[95] L. F. Santos and M. I. Dykman. Two-particle localization and antiresonance in disordered spin and qubit chains. *Physical Review B*, 68(21):214410, Dec. 2003. doi: 10.1103/PhysRevB.68.214410. URL `http://link.aps.org/doi/10.1103/PhysRevB.68.214410`.

[96] T. Shi, Y. Li, Z. Song, and C. Sun. Quantum-state transfer via the ferromagnetic chain in a spatially modulated field. *Physical Review A*, 71 (3):032309, Mar. 2005. doi: 10.1103/PhysRevA.71.032309. URL `http://link.aps.org/doi/10.1103/PhysRevA.71.032309`.

[97] K. Shizume, K. Jacobs, D. Burgarth, and S. Bose. Quantum communication via a continuously monitored dual spin chain. *Physical Review A*, 75(6):062328, June 2007. doi: 10.1103/PhysRevA.75.062328. URL `http://link.aps.org/doi/10.1103/PhysRevA.75.062328`.

[98] T. P. Spiller, I. D'Amico, and B. W. Lovett. Entanglement distribution for a practical quantum-dot-based quantum processor architecture. *New Journal of Physics*, 9(1):20–20, Jan. 2007. ISSN 1367-2630. doi: 10.1088/

1367-2630/9/1/020. URL `http://iopscience.iop.org/1367-2630/9/1/020`.

[99] J. Stolze and D. Suter. *Quantum Computing: A Short Course from Theory to Experiment*. Wiley-VCH, 2008. ISBN 3527404384.

[100] J. Stolze and M. Vogel. Impurity spin relaxation in S=1/2 XX chains. *Physical Review B*, 61(6):4026, Feb. 2000. doi: 10.1103/PhysRevB.61.4026. URL `http://link.aps.org/doi/10.1103/PhysRevB.61.4026`.

[101] F. W. Strauch and C. J. Williams. Theoretical analysis of perfect quantum state transfer with superconducting qubits. *Physical Review B*, 78(9):094516, 2008. doi: 10.1103/PhysRevB.78.094516. URL `http://link.aps.org/doi/10.1103/PhysRevB.78.094516`.

[102] V. Subrahmanyam. Entanglement dynamics and quantum-state transport in spin chains. *Physical Review A*, 69(3):034304, Mar. 2004. doi: 10.1103/PhysRevA.69.034304. URL `http://link.aps.org/doi/10.1103/PhysRevA.69.034304`.

[103] D. I. Tsomokos, M. J. Hartmann, S. F. Huelga, and M. B. Plenio. Entanglement dynamics in chains of qubits with noise and disorder. *New Journal of Physics*, 9(3):79–79, Mar. 2007. ISSN 1367-2630. doi: 10.1088/1367-2630/9/3/079. URL `http://iopscience.iop.org/1367-2630/9/3/079`.

[104] A. Uhlmann. The 'transition probability'on the state space of a-algebra. *Rep. Math. Phys.*, 9:273–279, 1976.

[105] L. M. K. Vandersypen and I. L. Chuang. NMR techniques for quantum control and computation. *Reviews of Modern Physics*, 76(4):1037–1069, Jan. 2005. doi: 10.1103/RevModPhys.76.1037. URL `http://link.aps.org/doi/10.1103/RevModPhys.76.1037`.

[106] L. C. Venuti, C. D. E. Boschi, and M. Roncaglia. Qubit teleportation and transfer across antiferromagnetic spin chains. *Physical Review Letters*, 99(6):060401, 2007. doi: 10.1103/PhysRevLett.99.060401. URL `http://link.aps.org/doi/10.1103/PhysRevLett.99.060401`.

[107] R. F. Werner. Quantum information theory - an invitation. *arXiv:quant-ph/0101061*, Jan. 2001. URL `http://arxiv.org/abs/quant-ph/0101061`.

Bibliography

[108] M. Wieśniak and M. Markiewicz. Finding traps in nonlinear spin arrays. *Physical Review A*, 81(3):032340, Mar. 2010. doi: 10.1103/PhysRevA. 81.032340. URL `http://link.aps.org/doi/10.1103/PhysRevA.81.032340`.

[109] A. Wójcik, T. Łuczak, P. Kurzyński, A. Grudka, T. Gdala, and M. Bednarska. Unmodulated spin chains as universal quantum wires. *Physical Review A*, 72(3):034303, 2005. doi: 10.1103/PhysRevA.72.034303. URL `http://link.aps.org/doi/10.1103/PhysRevA.72.034303`.

[110] W. K. Wootters. Entanglement of formation of an arbitrary state of two qubits. *Physical Review Letters*, 80(10):2245, Mar. 1998. doi: 10.1103/PhysRevLett.80.2245. URL `http://link.aps.org/doi/10.1103/PhysRevLett.80.2245`.

[111] S. Yang, A. Bayat, and S. Bose. Entanglement-enhanced information transfer through strongly correlated systems and its application to optical lattices. *Physical Review A*, 84(2):020302, 2011. doi: 10.1103/PhysRevA.84.020302. URL `http://link.aps.org/doi/10.1103/PhysRevA.84.020302`.

[112] N. Y. Yao, L. Jiang, A. V. Gorshkov, P. C. Maurer, G. Giedke, J. I. Cirac, and M. D. Lukin. Scalable architecture for a room temperature Solid-State quantum information processor. *1012.2864*, Dec. 2010. URL `http://arxiv.org/abs/1012.2864`.

[113] N. Y. Yao, L. Jiang, A. V. Gorshkov, Z. Gong, A. Zhai, L. Duan, and M. D. Lukin. Robust quantum state transfer in random unpolarized spin chains. *Physical Review Letters*, 106:40505, Jan. 2011. URL `http://adsabs.harvard.edu/abs/2011PhRvL.106d0505Y`.

[114] M. Yung. Quantum speed limit for perfect state transfer in one dimension. *Physical Review A*, 74(3):030303, 2006. doi: 10.1103/PhysRevA. 74.030303. URL `http://link.aps.org/doi/10.1103/PhysRevA.74.030303`.

[115] M. Yung and S. Bose. Perfect state transfer, effective gates, and entanglement generation in engineered bosonic and fermionic networks. *Physical Review A*, 71(3):032310, Mar. 2005. doi: 10.1103/PhysRevA.71.032310. URL `http://link.aps.org/doi/10.1103/PhysRevA.71.032310`.

[116] J. Zhang, G. L. Long, W. Zhang, Z. Deng, W. Liu, and Z. Lu. Simulation of Heisenberg XY interactions and realization of a perfect state transfer

in spin chains using liquid nuclear magnetic resonance. *Physical Review A*, 72(1):012331, July 2005. doi: 10.1103/PhysRevA.72.012331. URL http://link.aps.org/doi/10.1103/PhysRevA.72.012331.

[117] J. Zhang, N. Rajendran, X. Peng, and D. Suter. Iterative quantum-state transfer along a chain of nuclear spin qubits. *Physical Review A*, 76(1):012317, July 2007. doi: 10.1103/PhysRevA.76.012317. URL http://link.aps.org/doi/10.1103/PhysRevA.76.012317.

[118] W. H. Zurek. Decoherence, einselection, and the quantum origins of the classical. *Reviews of Modern Physics*, 75(3):715, May 2003. doi: 10.1103/RevModPhys.75.715. URL http://link.aps.org/doi/10.1103/RevModPhys.75.715.

[119] A. Zwick and O. Osenda. Quantum state transfer in a XX chain with impurities. *Journal of Physics A Mathematical General*, 44:5302, Mar. 2011. URL http://adsabs.harvard.edu/abs/2011JPhA...44j5302Z.

[120] A. Zwick, G. A. Álvarez, J. Stolze, and O. Osenda. Robustness of spin-coupling distributions for perfect quantum state transfer. *Physical Review A*, 84:22311, Aug. 2011. URL http://adsabs.harvard.edu/abs/2011PhRvA..84b2311Z.

[121] A. Zwick, G. A. Álvarez, J. Stolze, and O. Osenda. Spin chains for robust state transfer: Modified boundary couplings versus completely engineered chains. *Physical Review A*, 85(1):012318, Jan. 2012. doi: 10.1103/PhysRevA.85.012318. URL http://link.aps.org/doi/10.1103/PhysRevA.85.012318.